RHODES UNIVERSITY

Where leaders learn

Lateral and vertical mineral-chemical variation in high-grade ores of the Kalahari Manganese Field, and implications for ore genesis and geometallurgy

Donald Motilaodi

Thesis submitted in fulfilment of the requirements for degree of

MASTER OF SCIENCE

In the Department of Geology, Rhodes University.

March 2021

Supervised by: Prof. Harilaos Tsikos

DECLARATION

I declare that this thesis, titled: "**Lateral and vertical mineral-chemical variation in high-grade ores of the Kalahari Manganese Field, and implications for ore genesis and geometallurgy**" is my own work, and information from other publications is adequately referenced. This thesis is being submitted in fulfilment for the Master of Science degree in the Department of Geology, Rhodes University.

Name and signature of candidate:

D.Motilaodi

Donald Motilaodi

TABLE OF CONTENTS

ACKNOWLEDGEMENTS

I would first like to thank my thesis advisor Prof. Hari Tsikos of the Geology Department at Rhodes University and head of research unit PRIMOR. The door to Prof. Tsikos' office was always open whenever I ran into a trouble spot or had a question about my research or my writing. He consistently allowed this paper to be my own work but steered me in the right direction whenever he thought I needed it. His patience and guidance throughout the years were nothing short of amazing and have helped me blossom in my current career field.

I would also like to thank my research colleagues who were involved in the validation of data for this research project, namely Dr Xolane Mhlanga and the entire PRIMOR team of the last few years. Without their passionate participation and input, the data collection and thesis write-up could not have been successfully conducted.

I would also like to acknowledge ASSMANG Ltd. and Rhodes University in large for funding this project and allowing me to conduct this research at the highest possible.

Finally, I must express my very profound gratitude to my parents and to my partner for providing me with unfailing support and continuous encouragement throughout my years of study and through the process of researching and writing this thesis. This accomplishment would not have been possible without them. Thank you.

Author

Donald Motilaodi

ABSTRACT

The Kalahari Manganese Field (KMF) is a world-class resource of manganese ore hosted by the Paleoproterozoic Hotazel banded iron formation. KMF ores are categorised into two main types, i.e., low-grade, carbonate rich, braunitic ore (Mn≤40wt%) and carbonate-free, high-grade, Ca-braunite+hausmannite ore (Mn≥44wt%). High-grade ores, also known as Wessels type from the homonymous mine in the northernmost KMF, are thought to have formed from variable degrees of hydrothermal carbonate and silica leaching from a low-grade ore precursor, termed Mamatwan-type after the homonymous mine in the southernmost KMF. This project aims to conduct a mineralogical and mineral-chemical study of representative manganese ore samples from a suite of drillcores intersecting both the upper and the lower layers in the northern KMF, covering the areas of Wessels, N'chwaning and Gloria mines.

Petrographically, the high-grade Mn ore displays great variability in three-dimensional space. Texturally, the ores exhibit a great variety of textures which may or may not show preservation of the laminated and ovoidal textures that typify the postulated low-grade protore. There is also significant variation in the mineralogical and geochemical characteristics of the high-grade Mn ores both vertically and laterally. Vertical variation includes, probably for the first time, variability between the upper and lower ore layers within individual drillcores of the Hotazel sequence. Mineralogically, the ores contain variable modal abundances of the ore-forming minerals braunite (I, II, "new") and hausmannite, and much less so of bixbyite, marokite and manganite. Common accessories include andradite, barite and low-Mn carbonate minerals.

Chemically, the dominant ore minerals braunite and hausmannite, contain Fe up to 22 and 15wt% respectively, which accounts for the bulk of the iron contained in the ores. Braunite compositions also exhibit a large range with respect to their ratio of Ca/Si. Mineral-specific trace element concentrations for the same minerals measured by LA-ICP-MS, reveal generally large variations from one element to the other. When normalized against the trace element composition of bulk low-grade precursor ore, strong enrichments are recorded for both hausmannite and braunite in selected alkali/alkali earth elements, transition metals and lanthanides, such as Sc, Co, Zn, Cu, Pb, La, and Ce. These are akin to enrichments recorded in average high-grade ore. Although there is also no obvious relationship between Fe content in both hausmannite and braunite and their trace element abundances, the drillcore that captures

high-grade ore with the highest trace element concentrations appears to be located most proximal to a major fault.

Results collectively suggest that high-grade Mn ores of the KMF have undergone a complex hydrothermal history with a clear and significant metasomatic addition of trace elements into ore-forming minerals. First order trends in the mineralogical and mineral-chemical distribution of the ores in space, suggest hausmannite-dominated ores near the Hotazel suboutcrop, and an apparent decline in ore quality with braunite II-andradite-barite-calcite ores as the major graben fault is approached in a southwesterly direction. The latter trend appears to be at odds with prevailing fault-controlled alteration models. Elucidating that hydrothermal history of the Wessels-type high grade Mn ores of the KMF, will be crucial to understanding the compositional controls of these ores in space, and the potential impact thereof in terms of geometallurgy.

1. INTRODUCTION

1.1. General

Manganese (Mn) is the 12th most abundant element in the Earth's crust and the third most abundant transition metal. It has multiple oxidation states and occurs predominantly as an oxide in nature (Armstrong, 2008). Manganese oxides are excellent proxies for environments rich in free molecular oxygen and are highly favorable electron acceptors in the absence of it (Johnson *et al*, 2016). In various igneous minerals found across ultrabasic, basaltic and syenitic rocks, manganese is present exclusively in its divalent form (Mn^{2+}) and accounts for a low abundance generally not exceeding 0.1 wt.% in bulk rock (Johnson *et al*, 2016). In surface and ground-waters, manganese is present in the soluble Mn^{2+} state as it is sourced through silicate weathering, eventually joining the hydrological cycle. In the oceanic environment, the main source of Mn^{2+} is hydrothermal fluids (Von Damm, 1990). In order to concentrate manganese into significant sedimentary deposits, multiple redox conversions must occur resulting in the oxidation of the divalent manganese (Mn^{2+}) to Mn^{3+} and Mn^{4+}.

Manganese was first recognized and isolated as a separate chemical element in 1774 by Carl Wilhelm Scheele and Johan Gottlieb Gahn. It is a black, brittle metal predominantly used in metallurgical applications as a component in alloys, particularly in steel and cast-iron production, which together provide the largest market for manganese (Cairncross and Beukes, 2013). Manganese is therefore one of the most important metals known to mankind, particularly since the industrial revolution, continuing to modern day. The Spartans, in ancient Greece, used manganese in their steel weapons to give superior strength, whereas the Romans and Egyptians used manganese compounds to remove or add color to their glass during glassmaking (Olsen et al., 2007), as is still done today.

Manganese is alloyed with non-ferrous metals such as aluminium and copper in steel production thus having major economic importance. By virtue of its indispensable role in steel production, a continued supply of manganese raw materials is vital to any defence effort as well as to maintenance and growth of an industrial economy (Cairncross and Beukes, 2013). Non-metallurgical applications of manganese include battery cathodes, soft ferrite magnets used in electronics, micronutrients found in fertilizers and animal feed, water treatment chemicals, and a colorant for bricks and ceramics (Cairncross and Beukes, 2013).

In terms of the natural economic resources of manganese, Park (1956) and Kuleshov (2016) classify all known manganese deposits into three classic genetic types namely: (1) sedimentary and volcano-sedimentary deposits, including all deposits formed as chemical sediments, irrespective of source (Figure 1.1). In these deposits, the manganese may be derived from both volcanogenic and non-volcanogenic sources; (2) lateritic and other weathering-type deposits; and (3) magmatic/hydrothermal and metamorphic/metasomatic deposits. The economically significant deposits are often exclusively confined to sedimentary or volcano-sedimentary units that are formed in diverse sedimentary basins, and are represented by manganese carbonate, and less so oxide and hydroxide assemblages. Transformation and upgrade of these units from uneconomic manganiferous rocks to a viable manganese resource of economic significance, can occur under supergene conditions or through interaction with hydrothermal fluids, which result in breakdown of manganese carbonates and development of oxide-dominated assemblages (Kuleshov, 2016). Percolation of such fluids through structural discontinuities in the rocks can lead to the formation of high-grade manganese oxide ores. Examples include supergiant deposits such as the Proterozoic Kalahari Manganese Field in South Africa (Tsikos and Moore, 1997; Tsikos et al, 2003, 2010), which is the focus of this study, or smaller deposits of predominantly Phanerozoic age such as those in Molango, Mexico and Taojiang, China (Okita and Shanks, 1992; Fig. 1.1).

1.2. Geological framework

Situated about 60 km northwest of the town of Kuruman in the Northern Cape Province, South Africa, lies the Kalahari Manganese Field (KMF), the largest known land-based manganese

deposit in the world (Gutzmer and Beukes, 1995; Tsikos et al., 2003; Cairncross and Beukes, 2013). It is host to over 13 billion metric tons of ore varying in grade from 20 to over 50 wt.% in some areas (Cairncross and Beukes, 2013). The ores are hosted in the Hotazel Formation, which is a succession of chemical sedimentary rocks dominated by banded iron formation (BIF) and three intercalated manganese rich layers (De Villiers, 1986; Tsikos and Moore 1997; Tsikos et al., 2003, 2010). The KMF is essentially the largest erosional relic of an original sedimentary basin of Paleoproterozoic age (~2.4 Ga; Schier et al., 2020). The following sections elaborate on the general geology of the KMF, with emphasis on its northernmost margin containing high-grade Mn ores.

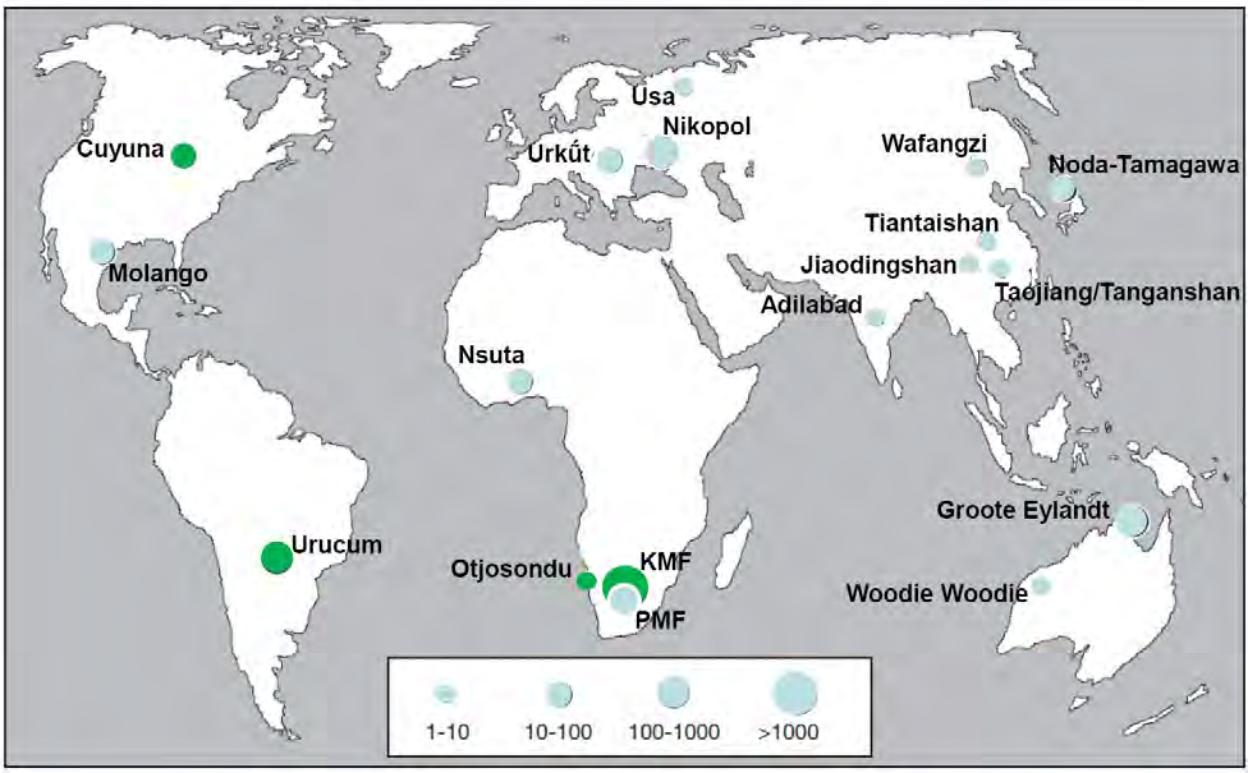

Figure 1.1: Map showing the geographic localities of major land-based manganese deposits around the world. Green circles represent major iron formation-hosted deposits, whereas the light grey circles indicate Mn deposits in association with black shale/carbonate sequences. Diameter of individual circles are proportional to the size of the corresponding deposits (modified after Maynard, 2010).

1.3. Regional stratigraphy

The Transvaal Supergroup of South Africa was deposited during the end of the Archean to the earliest Proterozoic (2.6 – 2.2 Ga) and is geographically separated into two basins namely the eastern Transvaal Basin, and the western Griqualand West Basin (Beukes, 1983; Moore et al, 2001). The Transvaal Basin is located on the northeastern margin of the Vryburg arch where it encloses the Bushveld Complex, whereas the Griqualand West Basin is located on the western margin of the Kaapvaal Craton, and it extends into southern Botswana below the Kalahari cover as the Kanye Basin (Moore et al, 2001).

The Griqualand West Basin (Fig. 1.2) consists of two stratigraphic groups, namely the Ghaap and Postmasburg Groups (Beukes, 1983). The Ghaap Group, which makes up the lower part of the Transvaal Supergroup, is made up of a thick succession of dolomitic carbonates at the base (Campbellrand Subgroup), overlain by a thick succession of BIF of the Kuruman and Griquatown Formations (Beukes and Klein, 1990; Beukes et al., 1990). Stratigraphically above the latter BIF is a glacial diamictite unit known as the Makganyene Formation which marks the base of the Postmasburg Group. The Postmasburg Group consists of three formations overlying the Makganyene Formation, namely the volcanic Ongeluk Formation, the Hotazel Fe/Mn Formation and the Mooidraai carbonate Formation. The Hotazel and Mooidraai Formations together constitute the so-called Voelwater Subgroup. (Tsikos and Moore, 1997; Bau et al., 1998; Tsikos et al., 2001; Fairey et al., 2013).

The 2.43Ga Ongeluk Formation (Gumsley et al., 2017) is a thick continental volcanic succession that consists of basaltic-andesite flows with characteristic pillow structures at the upper portions (Tsikos and Moore, 1997). The age of the Ongeluk Formation has been controversial: earlier age constraints placed the Ongeluk volcanic event at approximately 2.22Ga (Cornell et al, 1996) but recent work by Gumsley et al (2017) have provided a revised age for the Ongeluk lavas at 2.43Ga, This age agrees well with other available age constraints for the overlying Hotazel and Mooidraai Formations (Bau et al., 1998; Fairey et al., 2013; Schier et al., 2020.)

The Ongeluk Formation is overlain by the Hotazel Formation, which reaches a maximum thickness of no more than 200 meters. The succession comprises banded iron formation that hosts three distinct manganese ore layers. Each manganese ore layer forms the centre of one of three symmetrical, chemical sedimentary lithological cycles. Each cycle consists of a sequence of iron formation – hematite lutite – braunite/carbonate lutite layers, whereby hematite lutite

constitutes the gradational contact between the BIF and manganese layers dominated by very fine-grained hematite and Mn-carbonate (Tsikos and Moore, 1997; Tsikos et al., 2003, 2010). The collective stratigraphic thickness of the manganese layers alone is known to range between 15 and 80m (Gutzmer and Beukes, 1995, 1996; Tsikos et al., 2003).

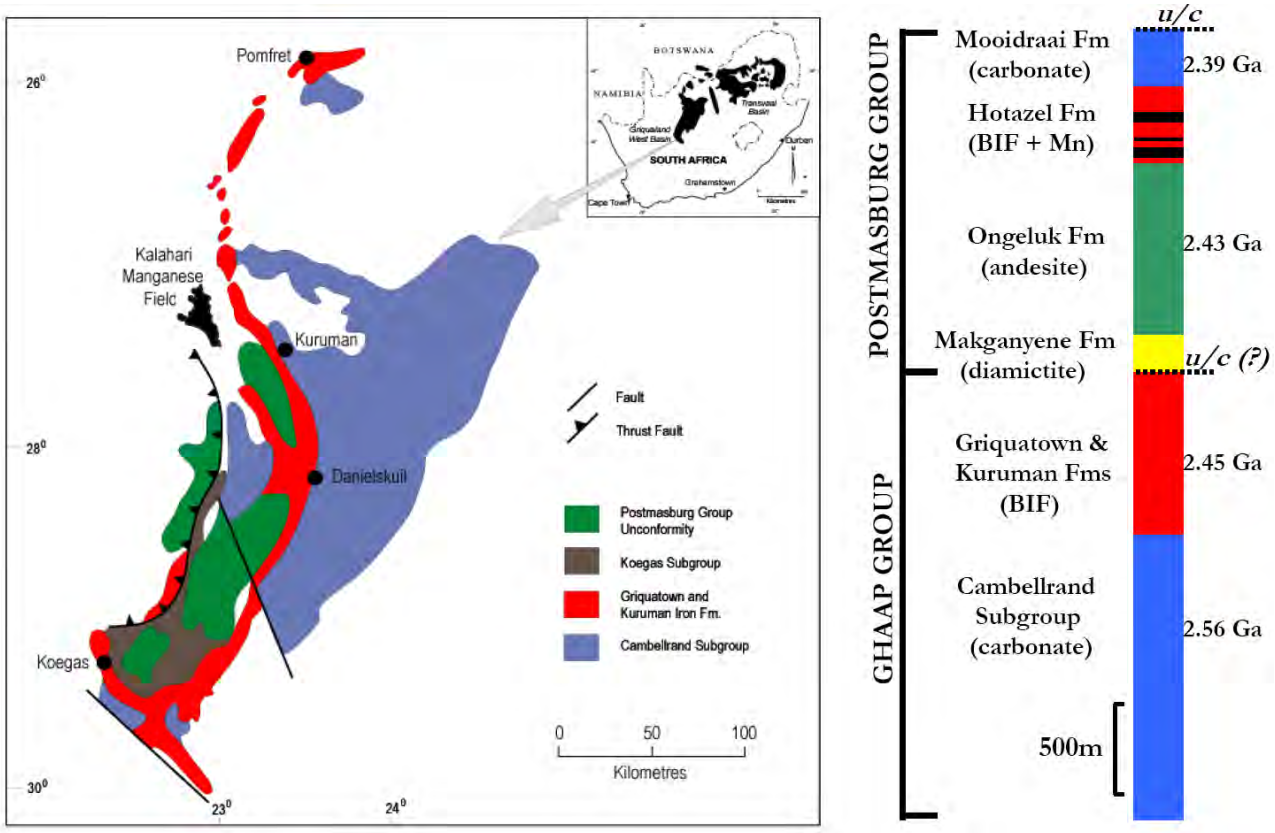

Figure 1.2: Simplified map showing the geographical distribution, regional stratigraphic framework of and age relationships in the Transvaal Supergroup in Griqualand West, South Africa. (Modified after Siahi et al., 2020).

The bulk of the manganese ore produced through mining in the KMF comes from the lowermost of the three cycles, due to the fact that it is the thickest of the three layers and has the highest manganese content (Cairncross and Beukes, 2013; Tsikos and Moore, 1997; Tsikos et al., 2003). However, the uppermost layer has recently drawn economic interest in its own right, whereas the

middle layer locally referred to as the “manganese marker” is very thin and therefore is not being exploited.

In terms of manganese content, the KMF ores have been variously subdivided in the literature into two ore types, namely low-grade, carbonate-rich, braunite ore of a grade generally ≤40wt% Mn; and carbonate-poor, high-grade, braunite II-hausmannite ore with a bulk Mn content ≥44wt% (Cairncross and Beukes, 2013). The same ores are often referred to in the literature as “Mamatwan”- and “Wessels”-type respectively, from the two homonymous mine areas located in the southernmost and northernmost parts of the Kalahari Manganese Field (Gutzmer and Beukes, 1996). Additional background information on the mineralogy and geochemistry of these two ore types is presented in the next section.

1.4. Diverse Mn ore types in the KMF

The KMF is an area of much geological and economic significance alike, which has led to varied research of both academic and applied interest. Outcrops of the Hotazel Formation are restricted to one locality in the northernmost KMF at Black Rock, where an overthrust of the Hotazel Formation through the Cenozoic Kalahari Formation, results in the localised development of a small hillock (*koppie)* (Tsikos, 1999; Cairncross and Beukes, 2013). The lack of outcrop in the KMF invariably poses challenges in the study of these ores across space, that is remedied by the availability of numerous drill cores obtained in the area by a number of mining companies.

As noted earlier, the KMF hosts two major types of manganese ore, namely the low-grade Mamatwan-type ore in the southern KMF and hydrothermally altered, Wessels type ore in the northernmost part of the KMF (Gutzmer and Beukes, 1995, 1996; see Figure 1.3). The Mamatwan-type ore is described as diagenetic to very low metamorphic in origin, carbonate-rich braunitic ore (Gutzmer and Beukes, 1996; Schneiderhahn et al., 2006). The overall manganese content of this ore type ranges between 25-40 wt.% Mn. Texturally, the Mamatwan type ore is known to be microcrystalline and distinctly laminated, with braunite, hematite, Mn-rich calcite and kutnohorite being the dominant mineral phases occurring as fine intergrowths (Gutzmer and Beukes, 1996). Microscopic, ooid-like features known as *ovoids* as well as micro-laminations of manganese-bearing calcite, are omnipresent in the Mamatwan type ore (Figure 1.4).

The high grade Wessels type ore is mineralogically and texturally much different from the Mamatwan type ore. It occurs in the northern part of the KMF and is said to be derived from the hydrothermal alteration of Mamatwan-type ore (Gutzmer and Beukes, 1996). The ore is therefore relatively carbonate poor, oxide rich, and coarser grained, at Mn grades generally between 44 and 50 wt.%. Dominant ore minerals include Ca-braunite (braunite II), hausmannite, and lesser bixbyite and marokite. Preservation of low-grade precursor sedimentary structures such as laminations and ovoids ranges from well preserved to totally obliterated through apparent recrystallization. The Wessels type ore appears to be restricted to the northwestern part of the KMF in an area which is characterized by intense structural deformation in the form of thrust duplication and normal faulting. This has historically led previous authors to the conclusion that the faults may have had a big role to the hydrothermal enrichment of the KMF ores (De Villiers, 1970; Beukes and Gutzmer, 1995). The next section presents an account of ore-genetic models for the northernmost KMF and their structural controls.

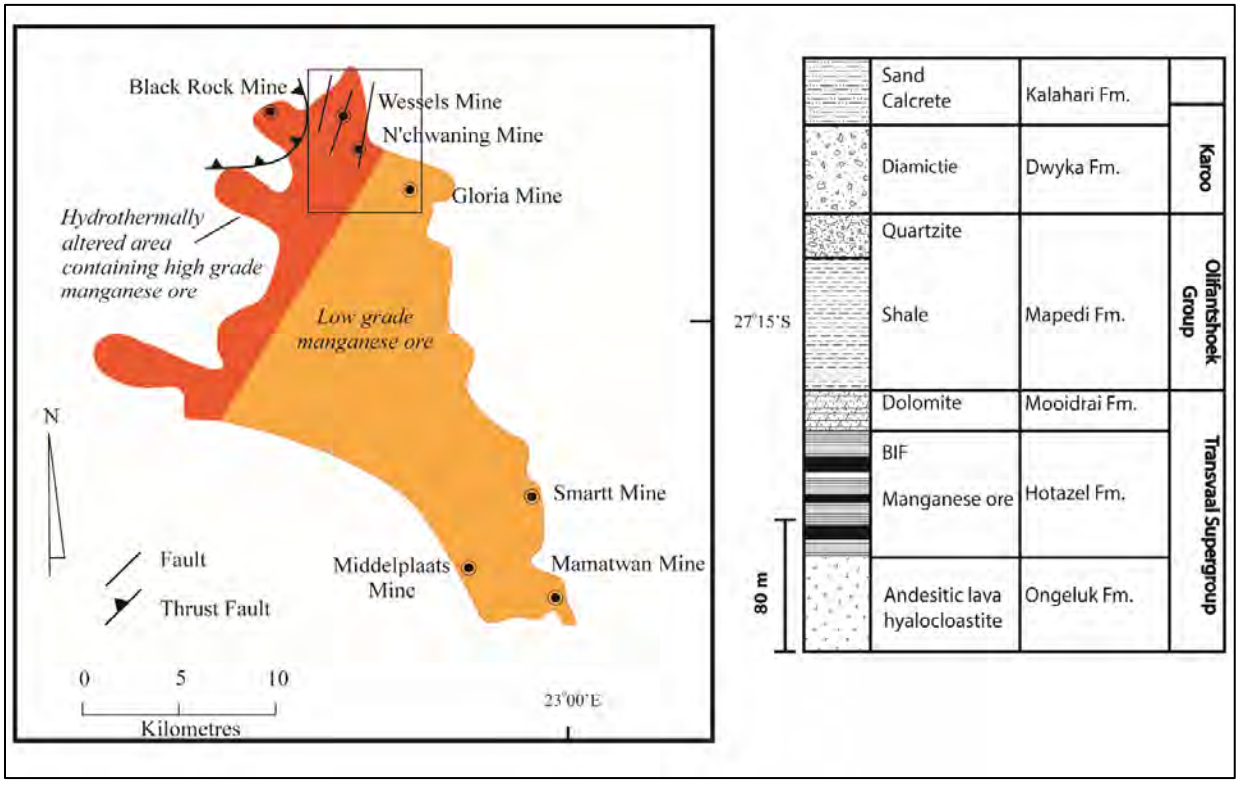

Figure 1.3. Map of the Kalahari Manganese Field illustrating the distribution of high versus low-grade Mn ore in space, key structural features and the regional stratigraphic placement of the Hotazel Formation. Insert: study area (adapted from Gutzmer and Beukes, 1995, 1996).

1.5. Genetic modelling for high-grade KMF ores

According to Beukes and Gutzmer (1996), there are multiple post-depositional alteration events that have affected the KMF ores. Three alteration events are specifically credited for the enrichment of the respective ore types and include the Wessels, Mamatwan and Smartt alteration events (Gutzmer and Beukes, 1996). From these three, the Wessels event is considered as the most important in terms of producing economic high grade ores in the northernmost KMF, the area of focus in this study.

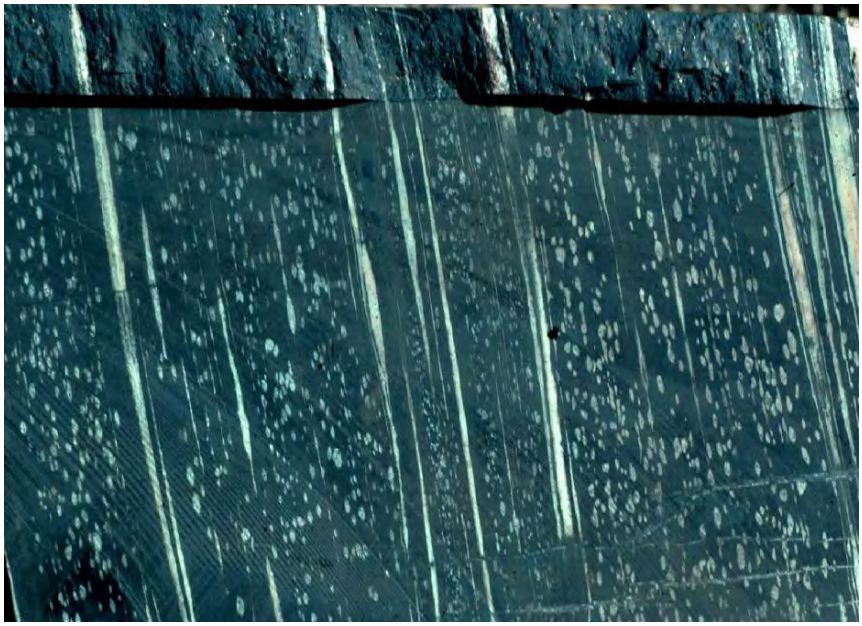

Figure 1.4. Photographic image of a halved drillcore intersection of typical Mamatwan-type, low-grade manganese ore in the Kalahari Manganese Filed. Note the characteristic laminae and ovoids of Mn carbonate in a matrix of very fine-grained braunite(+hematite). Width of field of view: 8cm. (Insert reference here)

1.6. The Wessels alteration event

The Wessels hydrothermal alteration event is thought to have affected Mamatwan type ore along major N-S-striking and minor E-W-striking faults. The model states that fluid circulation would have transformed the precursor low-grade, carbonate-rich Mamatwan-type Mn ore into oxide-

rich, carbonate-poor, high-grade Wessels-type manganese ore (Gutzmer and Beukes, 1995; Beukes et al., 1995). This reported overall transformation of Mamatwan-type ore would have primarily involved the breakdown of earlier sedimentary carbonate minerals. This would have resulted in considerable bulk leaching of Ca, Mg and CO_2 accompanied by at least some redistribution of Fe, Mn and Si in space. The geochemistry of the Wessels manganese ores and adjacent Hotazel BIF also suggests that minor amounts of alkalis such as Na and Ba must have been introduced into the system by the percolating fluids (Gutzmer and Beukes, 1996; Tsikos and Moore, 2005).

Gutzmer and Beukes (1995, 1996) note that the degree of alteration is at its highest immediately adjacent to abundant N-S fault structures, which they consider to have been key feeder channels. Texturally, the Wessels-type high grade Mn ore is coarse crystalline and massive with abundant secondary porosity and small vugs lined by euhedral crystals of ore and gangue minerals alike. However, locally finer-grained ore types also occur, seemingly preserving primary textures with minimal secondary porosity development (Gutzmer and Beukes, 1996). To the naked eye, the physical appearance of the ores resulting from the enrichment process is typically black or brownish-black with submetallic sheen. Upon the enrichment processes, the mineral assemblage of typical Wessels-type ore comprises combinations of the minerals hausmannite, Ca-braunite, bixbyite, manganite, marokite, minor hematite, and accessory andradite garnet, barite and carbonates, depending on the apparent degree and style of alteration in relation to faults and distances from them.

The Wessels alteration event has been further broken down into two mineralisation styles, on the basis of overall mineralogy and structural control, namely (Gutzmer and Beukes, 1996); (1) tabular, high-grade braunite/hausmannite Wessels type ore developed at the expense of precursor Mamatwan type ore, with clear lateral zonation relative to normal faults; and (2) Vein- and vug-hosted mineral associations, which manifest in the form of massive alkali-rich, calc-silicate assemblages in and around faults and veins and as isolated bodies on the margins of the manganese ore beds (Gutzmer and Beukes, 1996). In terms of spatial distribution of tabular, Wessels type ore, two different end-members can be further identified by the metasomatic zoning reported from around the feeder faults. These styles are referred to as the ferruginous and siliceous types of alteration and are illustrated in Figure 1.5 (Gutzmer and Beukes, 1996).

The ferruginous style of ore is characterized by massive braunite ore located around a zone of intense ferruginization directly adjacent to the feeder fault. Away from the fault zone towards the centre of the faulted blocks, the braunite becomes less massive and gradually grades into zones of relatively coarser crystalline, hausmannite-rich ore, giving way laterally outwards into medium grained hausmannite-rich ore. The ores then grade further away into bixbyite-braunite and ultimately braunite-rich ore, with a corresponding decline in hausmannite abundance. Traces of the original Mamatwan type ore can be seen in the distal braunite rich assemblages mentioned above (Burger et al., 1994; Gutzmer and Beukes, 1995; Gutzmer, 1996).

The siliceous style of alteration is represented by coarse-crystalline, high-grade hausmannite ore in proximity to the feeder channels. Moving further away from the fault structures, the hausmannite becomes less abundant and, texturally, the grain size declines (Gutzmer and Beukes, 1995, 1996). At the same time, braunite becomes progressively more abundant with distance from the faults, whereas andradite prevails across the entire lateral profile. The same authors argue that a fluid convection system caused by temperature gradients circulated dissolved Si, Ca and CO_2 back into the main feeder channel. These components would have reprecipitated in proximity to the main feeder channels as secondary braunite-rich zones, as well as quartz and other silicates, resulting in the variability in zonal assemblages from one fault to the next.

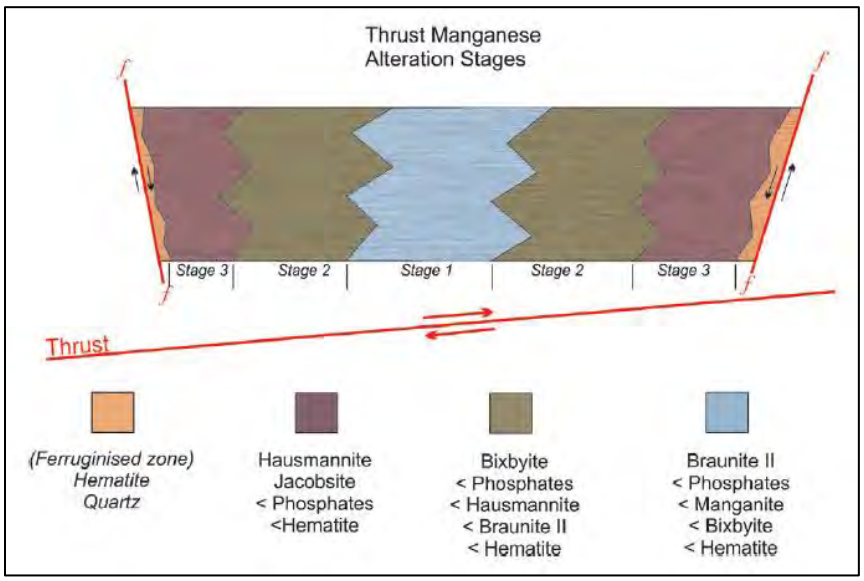

Figure 1.5: Mineralogical zonation found around faults that would acted as fluid feeders during ferruginous and siliceous style of alteration in the northernmost KMF (modified after Gutzmer and Beukes, 1996).

The age constraints for the Wessels alteration event have so far come from dating of alkali rich minerals that are found in vugs and fissures in association with Wessels-type ore. One such age was derived from Ar-Ar dating of norrishite and yielded 1048.1±5.9 Ma (Gnos *et al*, 2003). The latter age agrees broadly with similar age constraints by Dixon (1989), and suggests a major Neoproterozoic fluid event producing Wessels-type Mn ore. It should be noted however, that the age of the Wessels alteration event may not necessarily be reflected in the ages of the transgressive calc-silicate assemblages that have been previously targeted for dating, if the fluid circulation process producing these metasomatic assemblages are not the same for the larger scale transformation of Mamatwan type to Wessels type ore.

1.7. Other alteration events

1.7.1. Mamatwan alteration event

The Mamatwan alteration event is characterized by the development of carbonate-sulphide-hematite mineral associations along joints and minor faults in the southernmost KMF where the Mamatwan mine is located. It is the second oldest of the three events and has been linked to the Gariep/Damara Orogeny, thus postdating the Wessels event and predating the deposition of the Phanerozoic Karoo Supergroup around 0.55 to 0.6 Ga (Gutzmer, 1996). This event involved the alteration of carbonate-rich braunite lutite that typifies Mamatwan-type ore (Fig. 1.4) along fauts and fractures. This can be observed through the reduction of manganese and iron oxides and the formation of jacobsite, pyrite, and quartz at the expense of braunite and hematite (Gutzmer and Beukes, 1996).

The Mamatwan alteration event had an overall impact on the physical appearance of the ores: the originally dark brown to grey, carbonate-rich manganese ore interacted with the percolating fluids, changing its appearance through leaching (carbonate breakdown) into black, porous manganese ore. Formation of quartz and pyrite represents the highest degree of alteration (Gutzmer and Beukes, 1996). Red discolouration of the manganese ore can be attributed to the

reduction and leaching of manganese and iron oxides. Recrystallization/reprecipitation of carbonates and the dissolution of braunite would have resulted in secondary quartz formation along with secondary manganese oxides and small amounts of clinochlore. Through such mineralogical transformations, the primary sedimentary textures of Mamatwan type ore are largely preserved in microscopic detail (Gutzmer and Beukes, 1995, 1996).

1.7.2. Smartt alteration event

Gutzmer and Beukes (1996) recognized the presence of altered, brecciated ore in the fault zones of the Smartt mining area in the south-eastern area of the KMF. This has been fittingly termed the Smartt hydrothermal alteration event, and is marked by the formation of todorokite and manganomelane through the replacement of Mn-carbonates and braunite in the low-grade precursor ore of the Mamatwan type. A typical alteration zone is said to be over 15 m wide and is closely associated with intensely brecciated normal faults (Gutzmer and Beukes, 1995, 1996). The altered ore is greenish to brownish black with little to no primary sedimentary features preserved. The fault breccia zones consist of altered manganese ore and iron formation fragments cemented by a vuggy matrix of chalcedony, calcite (or locally dolomite) and microcrystalline quartz. Calcite crystals range in habit from simple to complex rhombohedral shapes to lens-shaped crystals.

A characteristic of the Smartt alteration event is the development of several generations of asbestiform manganese oxides in successive banded occurrences. The mineral todorokite is a major component of these asbestiform assemblages (Cairncross and Beukes, 2013). Calcite and rose-coloured chalcedony, associated with the manganomelane/todorokite fibres appear somewhat younger than the asbestiform Mn-oxides themselves (Gutzmer and Beukes, 1995, 1996). Coarse crystalline calcspar fills vugs between fibre bundles. Bands of massive sparitic calcite occur that enclose fragments of todorokite/manganomelane fibres, indicating renewed opening of the bedding-parallel fractures. Similar occurrences of todorokite are also known to occur in high grade ore at Hotazel and Langdon mines on the eastern margin of the KMF.

The Smartt alteration event is a classic example of supergene alteration along the Kalahari unconformity (Gutzmer and Beukes, 1996); these supergene processes are thought to be ongoing. Meteoric fluids are thought to have infiltrated the Hotazel Formation through the unconformity,

ultimately causing further enrichment of the Mn ores through carbonate leaching and manganese oxidation (Gutzmer and Beukes, 1996; Du Plooy, 2002; Blignaut, 2017). The result is the development of oxides and hydroxide mineral assemblages (todorokite, cryptomelane, pyrolusite and goethite) replacing braunite and Mn-carbonate which make up the bulk of the primary ore. Ongoing supergene alteration processes is also observed at the Black Rock *koppie* where high-grade manganese ore outcrops and is exposed to weathering.

1.8. Review of Wessels-type high-grade Mn ore

1.8.1. Mineral endowment in the northern KMF

Despite its remoteness, the KMF has become an important site for mineral collectors and economic geologists alike. The economic geologist is attracted to the astonishing size of the deposit, which is said to contain more than 13 billion tons of manganese ore, corresponding to about 80 percent of the world's resources of minable manganese ore (Cairncross and Beukes, 2013). The mineral collector, by contrast, is attracted to a host of spectacular and rare minerals, including many of the world's finest specimens of sugilite, rhodochrosite, hematite, olmiite, sturmanite and other rare species. This apparent dichotomy is reflective of the two different styles of mineralisation seen in the northern KMF in terms of structural control, namely tabular and vug/vein hosted, as defined earlier in this chapter. It is important to emphasise two points in this respect: firstly, it is not considered imperative by the author that the above two styles of mineralisation are synchronous and therefore genetically linked. Secondly, the present study does not deal with the vug/vein assemblages but only with the ore forming ones in the tabular high-grade deposits of the Wessels type.

As mentioned earlier, several systematic geological and mineralogical studies have been conducted to obtain a detailed understanding of the mineralogy of the different types of manganese assemblages present in the Kalahari Manganese Field Gutzmer and Beukes, 1995, 1996). It is not the aim of this study to present a detailed review and analysis of the very complex mineralogy of the northern KMF. Instead, the focus is on the ore-forming minerals, and particularly the mineral chemical variability thereof in 3D space that have been established to represent the high-grade Wessels type ore assemblage.

1.8.2. Comparisons between Mamatwan- and Wessels-type ore mineralogy

Over the largest part of the KMF lies Mamatwan type ore. Mineralogically, this low-grade precursor ore is relatively "unattractive" to mineral collectors as it is typically microcrystalline and composed of only a few finely intergrown minerals, namely braunite, hematite and carbonates (de Villiers, 1945; Kleyenstuber, 1984; Gutzmer and Beukes, 1995, 1996; Tsikos and Moore, 1997). By contrast, high grade assemblages of Wessels type ore in the northernmost KMF are, as indicated earlier, both far more diverse and coarser crystalline. This has been attributed to the presence of intense brittle deformation around the area where normal faults have displaced a west-verging thrust, thus initializing and facilitating hydrothermal activity at the expense of Mamatwan-type precursor ore. As indicated earlier (Gutzmer and Beukes, 1995) as the hydrothermal fluids made their way through the Hotazel Fe-Mn succession, they leached calcium, magnesium, and carbon dioxide, redistributed iron, manganese and silicon, and produced coarse-crystalline, porous, and massive Wessels type ore. This recrystallized and higher-grade manganese ore mineral assemblage is now dominated by braunite and hausmannite assemblages, which is the most sought-after resource at present and constitutes the subject of this thesis.

1.9. Key ore minerals in Wessels-type Mn ore

Wessels type manganese ore *sensu lato* comprises a combination of oxides/hydroxides, carbonates and silicates namely; braunite, hausmannite, bixbyite, manganite, marokite, hematite, andradite, calcite/dolomite and barite (de Villiers, 1945; Kleyenstuber, 1984, Gutzmer and Beukes, 1995 and 1996; Tsikos and Moore, 1997). The first five of the above-mentioned minerals will be reviewed in the following paragraphs, whereas some mention will also be made to the accessory phases that typically characterize the ore but do not contain Mn (e.g. andradite).

1.9.1. Braunite

Braunite is reported to be both an ore-forming mineral and precursor of supergene oxide ores in stratabound manganese deposits worldwide (e.g. Ostwald, 1992; Robie et al, 1995). Examples of economically important braunite deposits include the metamorphosed Sausar Group in India (Robie et al, 1995) and the Hotazel Formation of the KMF (Gutzmer and Beukes, 1995 and

1996; Tsikos and Moore, 1997). According to several authors, braunite is the most common and most abundant manganese mineral in the Hotazel Formation (Kleyenstuber, 1984; Gutzmer and Beukes, 1995 and 1996). Minerals commonly associated with braunite in the KMF include kutnahorite, hausmannite, jacobsite, bixbyite, calcite and hematite; several mineral associations involving braunite are comprehensively reported by Gutzmer and Beukes (1996).

Braunite is strictly a manganese silicate mineral with the general formula: $Mn^{2+}6Mn^{3+}SiO_2$ and typically contains an average of 10 wt.%. SiO_2. There are however, three known compositional varieties of braunite in an apparent solid solution with one another, and they are all present in the KMF deposits. The main variable across these different braunite types is the calcium-silica ratio, resulting in different chemical forms belonging to the braunite group (Gutzmer and Beukes, 1996).

Early published work on braunite by J.E. de Villiers (1945), reported a type of braunite containing half the amount of silica required by the ideal formula indicated above, along with significant increases in iron content. This mineral is now known and referred to as "braunite II" (de Villiers, 1945; Kleyenstuber, 1984, 1993; Gutzmer and Beukes, 1995, 1996). The structural and chemical formula for braunite II is expressed as: $Ca_{0.5}(Mn,Fe)_7Si_{0.5}O_{12}$. In the structure of braunite II, Ca replaces Si and the resultant charge imbalance is made up by a changing ratio of Mn^{2+}/Mn^{3+}. The third member of the braunite group is often referred to as braunite "new": it was detected through electron microprobe analysis and was reported to be similar to braunite II both structurally and chemically (Kleyenstuber, 1984, 1993). What sets the two calcic braunites apart is a ratio of Ca:Si that is lower than one in braunite "new" as shown in Table 1.1 below. From a metallogenic point of view, the formation of calcic braunite species in the Hotazel high-grade ores would have resulted from reaction of braunite with Ca-rich alkali hydrothermal fluids, whereby the Ca may have been sourced largely from carbonate breakdown against Mamatwan type precursor ore.

1.9.2. Hausmannite

Hausmannite is widespread in manganese deposits globally. The internet site *Mindat.org* (accessed in October 2018) lists forty-one countries with 338 individual localities that are reported to have ores containing hausmannite. Hausmannite, $(Mn^{2+}Mn^{3+})_2O_4$, crystallizes in the

tetragonal system and can be considered a tetragonally-deformed spinel type (Jarosch, 1987). Hausmannite from the KMF occurs both as an ore-forming mineral and as one of the phases present in vug-hosted hydrothermal assemblages. In the latter case, it is present as spectacular, coarse-grained tetrahedral crystals forming twinned arrangements resembling "pagodas" (Cairncross and Beukes, 2013), Associated minerals include about a dozen other mineral species such as andradite, barite, brucite, calcite, celestine, clinochlore, diopside, gageite, gaudefroyite, hematite, henritermierite, kutnohorite, leucophoenicite, manganvesuvianite, rhodochrosite, and sturmanite (von Bezing et al. 1991; Cairncross and Beukes, 2013). The most common associations of the above include those with andradite, calcite, and barite (Gutzmer and Beukes, 1996).

Table 1.1: Comparative chemical analysis of the three braunite-group minerals in the KMF (Kleyenstuber, 1984; Gutzmer and Beukes, 1996). Note the increase in Fe content from braunite to braunite "new", and the corresponding decrease in Si.

Element oxides (wt%)	Braunite I	Braunite II	Braunite "new"
Mn_2O_3	80.54	75.53	77.70
Fe_2O_3	5.82	13.73	15.91
Al_2O_3	0.18	0.07	0.30
SiO_2	10.39	5.48	3.02
CaO	1.83	5.90	3.04
MgO	0.77	0.04	0.04
BaO	0.03	0.10	0.05
K_2O	0.02	bd	bd
Na_2O	0.01	bd	bd
Total	99.56	100.04	99.97

According to Kleyenstuber (1984), hausmannite in the KMF can occur in three different modes (Table 1.2): the first is in the form of early secondary hausmannite forming by the oxidation of primary manganese carbonate according to the following reaction:

$$3CaMnCO_3 + 2O_2 = Mn_3O_4 + 3CaCO_3$$

The above type of hausmannite occurs locally in the Hotazel Formation as irregular patches replacing carbonate ooids. The second type of hausmannite is as massive, thick bands of early-grown hausmannite associated with carbonate bands of similar thickness in braunitic ore of the Mamatwan type (Kleyenstuber, 1984). This type of hausmannite is reported to have also crystallized locally where reducing conditions and low silica availability precluded formation of braunite instead (Gutzmer and Beukes, 1995, 1996). The third type of hausmannite according to Kleyenstuber (1984), appears as late secondary, coarse euhedral crystals and crosscutting veins in Wessels type ore. This type of hausmannite is typical of transgressive hydrothermal origin and is associated closely with the presence of barite and andradite. As mentioned earlier, the crystals are larger and euhedral compared to the two previous hausmannite types synonymous with Mamatwan type ore.

Table 1.2: Mineral chemistry of different types of hausmannite as encountered in the KMF ores (adapted from Kleyenstuber, 1984).

Element oxides (wt%)	Oxidation-related	Primary	Hydrotheral
K_2O	bd	0.01	0.01
Na_2O	0.03	bd	0.04
BaO	bd	0.01	0.04
SiO_2	bd	0.07	0.06
Mn_2O_3	66.29	64.58	59.98
MnO	33.15	32.22	31.56
MgO	0.06	0.05	1.03
CaO	0.03	0.89	0.06
Fe_2O_3	0.39	2.26	7.46
Al_2O_3	0.07	nd	0.03
Total	100.02	100.10	100.27

The following ore forming hausmannite associations have been observed in the Wessels type ore (Gutzmer and Beukes, 1995):

- Hausmannite + braunite II + calcite + barite + andradite + (trace) hematite
- Braunite II + hausmannite + hematite + andradite

- Hausmannite + marokite + portlandite + braunite “new” + manganite + hematite
- Gaudefroyite + hausmannite + braunite II + bixbyite + braunite “new”.

Depending upon the amount of iron present, some of the ore forming hausmannite in the KMF can show magnetic properties as reported by several authors (Baron et al. 1998).

1.9.3. Other manganese minerals (bixbyite, manganite, marokite)

Other, less common ore-forming minerals found in the Wessels type ore include bixbyite, manganite and marokite. Bixbyite $(Mn,Fe)_2O_3$ is a sesquioxide and is a common manganese mineral amongst other abundant manganese minerals associated with hydrothermal environments, such as hausmannite and braunite (Kleyenstuber, 1984; de Villiers and Buseck, 1989). Bixbyite is expected to form in environments where the availability of Fe is high enough to exceed the capacity of more common phases like hausmannite to accommodate it.

In the northern KMF, the oxy-hydroxide manganite (MnO.OH) is also reportedly found in small amounts in the lower manganese ore layer (Kleyenstuber, 1984; Gutzmer and Beukes, 1996). Manganite is reported to occur with several other manganese oxides in a variety of manganese deposits which have been affected by circulating meteoric water in the weathering environment (Hewett, 1972). Typical associated mineralogy therefore includes minerals such as pyrolusite, cryptomelane, braunite, hausmannite and goethite, along with calcite, barite and siderite in the form of low temperature hydrothermal and other similar space-filling textures (Golden et al., 1987).

Finally, marokite ($CaMnO_4$) is a relatively uncommon manganese phase which has been reported to occur occasionally in the Wessels type ore (de Villiers and Herbstein, 1968; Kleyenstuber, 1984; Gutzmer and Beukes, 1996). It generally shows a fibrous appearance in the form of densely packed slender crystals and occurs as remnants associated with pyrolusite and cryptomelane in the form of possibly vug fillings and veins. It therefore has a probable association with low-temperature fluid circulation, whereby the abundance of calcium must have been high enough to permit incorporation into a manganese oxide structure.

1.10. Accessory mineralogy in Wessels-type Mn ores

1.10.1. Andradite

Two types of garnet species have been identified in the Hotazel manganese ores, namely andradite and grossularite. The former is reported to be by far the most abundant of the two (de Villiers, 1945; Kleyenstuber, 1984, Gutzmer and Beukes, 1995 and 1996). Andradite is mainly found in hydrothermal environments and, in the case of the Hotazel Formation, it exhibits a close relationship with recrystallized hausmannite, braunite II, bixbyite and hematite (Kleyenstuber, 1984; Gutzmer and Caincross, 2002). The average chemical composition of andradite (in wt.%) as reported by Gutzmer and Beukes (1995) is CaO = 32.3, BaO = 0.1, MgO = 0.2, Al_2O_3 = 0.8, Fe_2O_3 = 28.8, SiO_2 = 34.9 and Mn_2O_3 = 2.9. The andradite in the Wessels type is reported to be typical of a low temperature hydrothermal origin and may have formed through the following reaction:

$$Fe_2O_3 + 3CaCO_3 + SiO_2 \longrightarrow Ca_3Fe_2Si_3O_{12} + 3CO_2$$

It is thought that the above reaction would have utilized available Fe, Ca and Si in solution that were largely mobilized during the transformation of Mamatwan-type to Wessels-type manganese ore.

1.10.2. Carbonates

Most of the carbonates in the KMF are thought to be primary or diagenetic in orgin, and this is typically observed in the largest part of the KMF where Mamatwan-type Mn ore is found. Calcite ($CaCO_3$) is the most common carbonate mineral found in the Wessels type ore, though dolomite has also been reported (Gutzmer and Beukes, 1996). Here, calcite occurs in different paragenetic associations that are related to diverse geological processes. The finest crystalline specimens such as up to 30-cm groups of clear crystals with a complex, stubby habit, are again hosted in vugs and fissures and are related to the hydrothermal circulation process/es producing and/or overprinting high-grade Wessels-type ores. Within massive high-grade ores, fine-grained interstitial calcite is also a common paragenetic component. Unlike the Mamatwan type ore where calcite is typically manganiferous and very fine grained, calcite in the Wessels type ore is most commonly manganese free (Kleyenstuber, 1984; Gutzmer and Beukes, 1996). Frequent calcite veins are also reported to cut across the high-grade ore zones, in association with hausmannite, andradite, braunite II, hematite and barite.

1.10.3. Barite

Barite is a generally white or colourless mineral and is the main source of barium. It is a very common mineral in a variety of hydrothermal environments and associated mineral deposits, such as felsic VMS systems, MVT and SEDEX environments (Robb, 2005). It belongs to a group of sulphate minerals that include barite itself, celestine (strontium sulphate), anglesite (lead sulphate), and anhydrite (calcium sulphate). From the above, barite and celestine form a solid solution $(Ba,Sr)SO_4$ which is known to dominate in the KMF (Kleyenstuber, 1984; Gutzmer and Beukes, 1996). In the KMF, barite occurs mainly as vug fillings in association with various exotic mineral phases, and in veinlets that postdate the formation of the oxides.

1.11. Research rationale

One of the first systematic studies undertaken on the mineralogy of the manganese ores of the KMF was by De Villiers (1970), followed by more detailed work by the same author in 1983. Soon thereafter, similar mineralogical work was carried out by Kleyenstuber (1984) and then by Nel et al (1986). However, arguably the most comprehensive accounts of the mineralogy of the KMF with particular emphasis on the highly diverse and exotic assemblages of Wessels type ore, comes from the papers of researchers from the University of Johannesburg (e.g. Gutzmer & Beukes, 1995, 1996). Practically all of the mineralogical work that was carried out by previous researchers, has concentrated on the most economically important lowermost manganese ore layer in the Hotazel Formation, either stratigraphically on drillcore, or laterally on underground exposures.

As mentioned earlier, the virtual absence of outcrop in the KMF poses a challenge when one wants to examine the ore in 3D space. Therefore, one must rely on systematic and detailed mineralogy utilizing drillcore material, in order to reconstruct compositional relationships and their causes in space. This study, for the first time, will attempt to elucidate the origin of compositional variability in the Wessels type ores, by exploring the mineralogy of not only the lower manganese layer but also the upper one. The primary motivation for that approach is two-fold: firstly, if the prevailing fault-controlled models are correct, then one would reasonably expect that each ore layer will record comparable mineralogical associations in space, given that

the postulated faults are essentially vertical and dissect the entire Hotazel Formation. Secondly, there is increasing interest in the upper ore layer making up an important additional resource of manganese, and therefore it is crucial for mine geologists involved to be able to ascertain whether the same model of mineralogical and geochemical variability – and thus grade distribution – can be applied to both ore layers. If it cannot, then either the existing fault-controlled model requires revision, or other controls of mineralogical variability will additionally need to be considered. More specifically structured objectives of this study will be presented in the section that follows.

1.12. Project outline and objectives

The present study on the manganese ores from the northernmost KMF was preceded by another one at Honours level by the author, which involved examination of two suites of samples across the upper and lower ore layers from the N'chwaning high grade manganese mine to the immediate south of Wessels manganese mine. The results of this work revealed stark differences in mineralogy between the two ore layers from the given locality, which sparked a personal interest on the causes for these differences and their possible implications for exploration, exploitation and geometallurgy.

The following years saw the initiation of the present MSc study. It was launched in parallel with another two MSc studies currently still in progress, dealing with a detailed geochemical account of both the upper and the lower manganese layer and interbedded iron formation at N'chwaning mine and at Wessels mine. This study complements the geochemically intensive character of these two MSc studies with a more detailed mineralogical and particularly mineral-chemical emphasis of the same manganese ores across space. All three projects are therefore naturally linked and thus occasional mention of the other two works will be made in this thesis. In the case where unpublished data from these parallel projects is used to draw comparisons, the said data will be included in the Appendix of this thesis.

In light of the foregoing, the specific objectives of the current MSc thesis are to:

- Conduct a mineralogical and mineral-chemical study of representative manganese ore samples from 12 drillcores intersecting both the upper and the lower layers in the northern KMF, covering the areas of Wessels, N'chwaning and Gloria mines;
- Present and assess mineral-chemical variability within specific mineral species (e.g. braunite) across vertical (i.e. in the upper and lower ore layers of a given drillcore) and lateral (within the upper or lower ore layer) space, as well as among different mineral hosts with respect to commonly contained elements such as Fe, Ca and Si;
- Discuss the possible factors that may control the aforementioned variabilities and distribution controls in the various ore-forming manganese minerals present in the ore;
- Interpret the results and discuss their implications in terms of distribution controls, ore- genetic models, mining, and where possible the geometallurgy of the high-grade Wessels type manganese ore, with emphasis on whether current models can satisfactorily explain these results or calls for possible refinement or revision.

1.13. Sample selection and methodology

Manganese ore samples were collected from a selection of 12 drillcores from the northern KMF containing high grade Mn mineralization. Seven of these come from the Wessels mine (operated by the company SOUTH32) and the other five from the N'chwaning and Gloria mines (operated by the company ASSMANG Ltd). The reader is referred to Figure 1.6 below, for the overall geographical and geological context.

Both the upper and lower Mn ore layers of the Hotazel Formation have thicknesses ranging between 4-8 m and were sampled through 4 to 6 samples taken broadly equidistantly from each other, across each intersected layer. The third Mn layer (the so-called Mn "marker") was not targeted for analysis, as it is generally very thin and thus of very low economic potential.

The drillcores were logged and sampled together by the author and another two MSc candidates involved in the bulk geochemical aspects of parallel study of Wessels-type ore, as also indicated earlier. Attention in all studies was placed in selecting drillcores from areas that represent different geological contexts on a local scale, specifically with respect to proximity to known structures and/or igneous intrusions. The northernmost KMF is known to contain abundant

vertical faults on predominantly a N-S strike, and NE-SW-trending mafic dykes intersecting the Hotazel strata (Fig. 1.6). The former also intersect the unconformably overlying Olifantshoek sequence and therefore postdate its deposition, whereas the latter do not (Grobbelaar et al, 1995).

Drillcores were also selected on the basis of diverse ore geochemistry as revealed by standard assay results obtained by the two companies operating the Wessels and N'chwaning/Gloria mines. This specifically pertains to the variable bulk Mn/Ca, Mn/Fe and Mn/Si ratios of Mn ore in space. Low Si ores, for example, are expected to be braunite-poor and hausmannite-rich, whereas the opposite would apply for ores containing relatively higher bulk Si. The situation would be mineralogically more complex for variable bulk Fe and Ca content in the ores, as both elements can be hosted in a variety of mineral species, namely hematite, andradite and Mn minerals for Fe; and carbonate, andradite and/or braunite II for Ca. The sections that follow provide such spatial geochemical information as it was used for the sample selection. Actual compositional maps for high-grade ore at the N'chwaning mine, have been included in the Appendix.

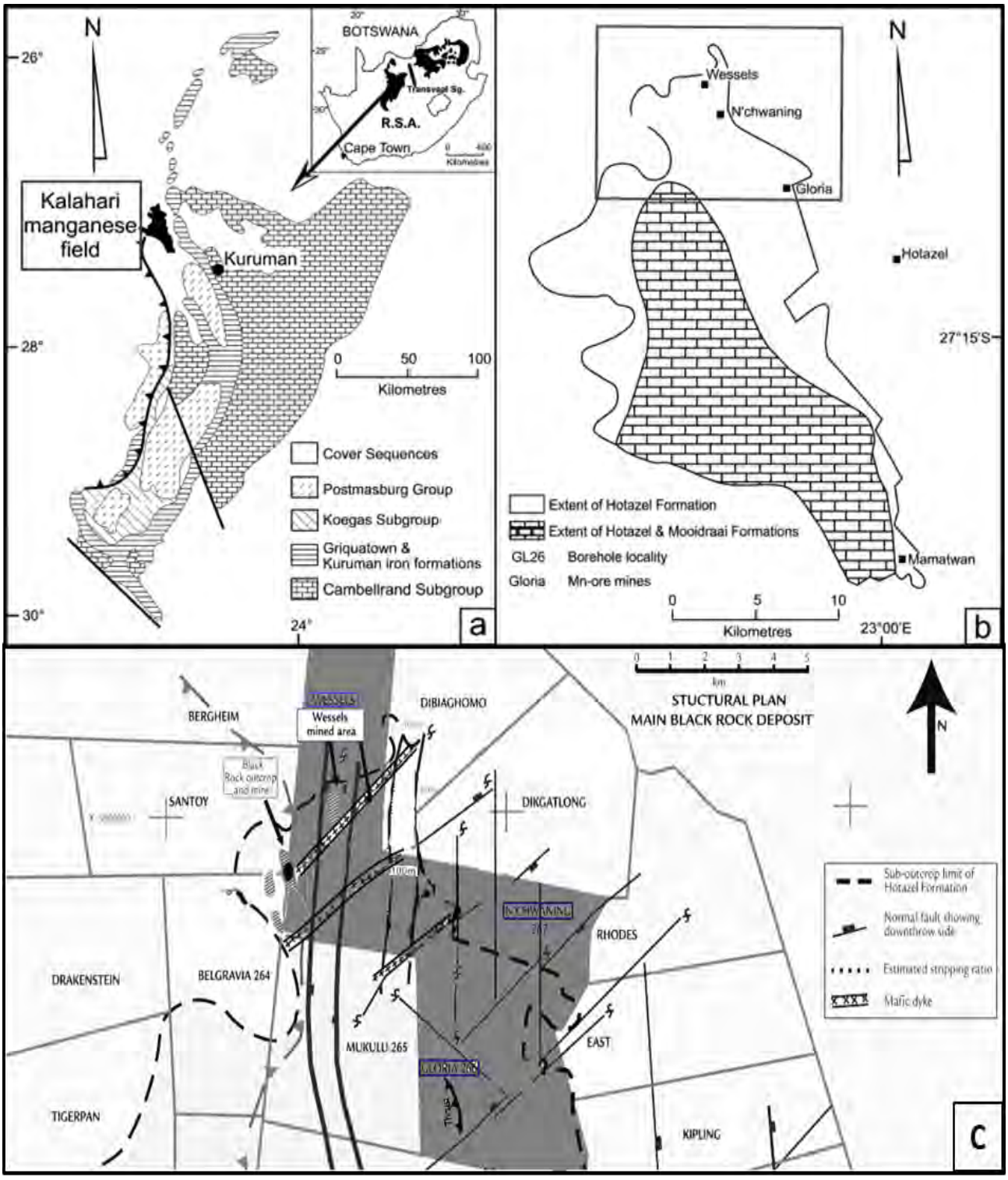

Figure 1.6: a) Geological map of the Griqualand West sequence of the Transvaal Supergroup showing the location of the KMF. b) Geological map of the KMF with inset of the northern part of the KMF (this study). c) Enlarged image of the northern KMF showing the Wessels, Gloria and N'chwaning farms

(highlighted in grey) and structures as typically encountered in the area (after Cairncross and Beukes, 2013).

1.13.1. N'chwaning mining area

As mentioned earlier, five drillcore intersections were obtained from the N'chwaning Mn mine in the greater N'chwaning/Black Rock area (Figure 1.6). Of these, four were drilled in the N'chwaning Farm *sensu stricto*, while one drillcore was obtained from the adjacent Gloria Farm and will be discussed separately later on. The four drillcores selected were N95E, N92I, N95A and N94J (see Figure 1.7 below). All four drillcores from the N'chwaning Farm area were selected and sampled based on the different criteria indicated in the previous section, namely the compositional ratios of each intersection obtained from analytical ore assays conducted by the company, as well as their location with respect to significant structural features in the area. Maps showing the compositional ratio distributions for both ore layers as provided by ASSMANG Ltd, are shown in the Appendix.

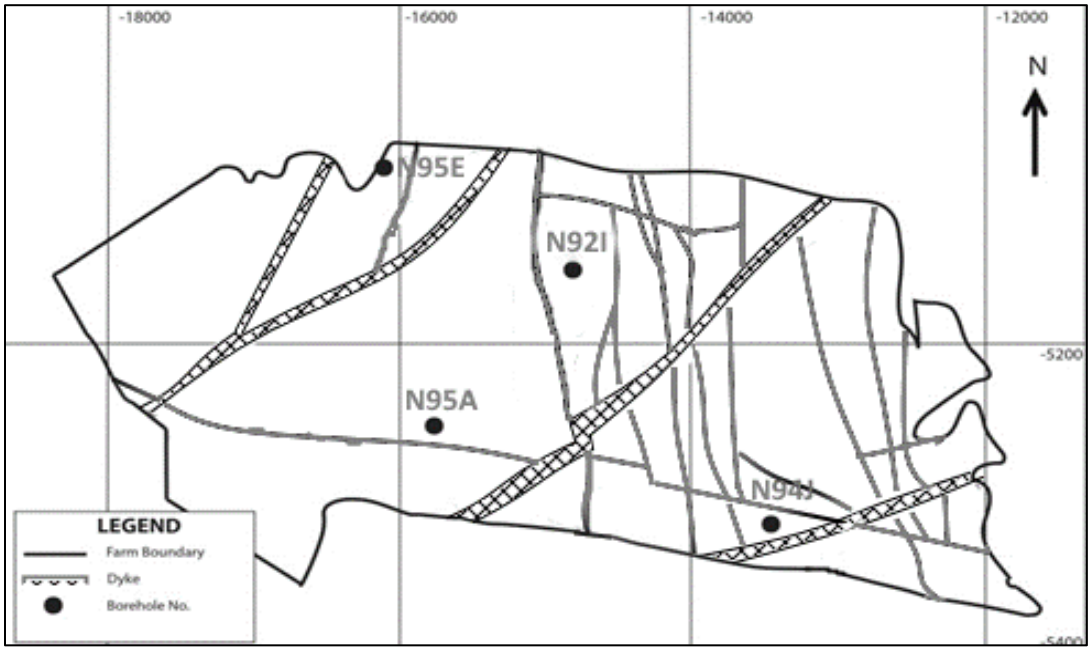

Figure 1.7: Map illustrating the N'chwaning Farm along with recognised and inferred structural features (N-S faults and NE-SW dykes) and the location of the individual cores selected for this study.

- Drillcore N95E is located in the north-westernmost section of the N'chwaning area. It lies between two splices of a major mafic dyke and shows close proximity to a fault. The selection of this drillcore was based in large part on its geochemical fingerprint in terms

of the intersected ore layers: the lower ore layer here has a high Mn/Si ratio but the top ore layer has a significantly lower Mn/Si ratio (see also Appendix).

- Drillcore N95A is located in the south-western part of the N'chwaning area and lies on the western block of the most major graben fault recognised in the area in terms of vertical displacement (Grobbelaar et al., 1995), while adjacent to an E-W trending fault. Geochemically, both ore layers here exhibit relatively high Mn/Fe ratio, therefore selection of this drillcore was based primarily on its proximity to the E-W and graben faults.
- Drillcore N92I was drilled in the central area of the N'chwaning farm and is also located to the immediate east of the major graben fault (downthrown block). In addition, this drillcore records a higher Mn/Si ratio in the upper ore layer relative to the lower ore layer.
- Finally, drillcore N94J is from the south-eastern region of the N'chwaning area and lies close to the easternmost dyke that runs throughout the N'chwaning area. It is also located near N-S vertical faults and was selected due to the very high Mn/Ca ratio exhibited in the upper ore layer by comparison to the lower ore layer that has a much lower Mn/Ca ratio.

1.13.2. Wessels mining area

A total of 7 (seven) drillcores were selected from the Wessels Farm. Similar with the drillcores from the N'chwaning area, these cores were selected based on geochemical variations as illustrated directly on the maps of Figure 1.8 below, and their location in relation to structural features (faults and dykes).

- Drillcore W162 is located to the north of the central Wessels mine area and lies very close to a major NE-SW dyke in an area of otherwise relatively low faulting density. Geochemically, W162 is enriched in Fe in the upper ore layer compared to the lower ore layer which records substantially less Fe relative to Mn.
- Drillcore W125 contains some of the highest-grade ore in the area with bulk Mn reaching 52 and 48 wt.% in both the upper and lower ore layer respectively. The said drillcore was obtained in the western area of the Wessels Farm and lies close to the same (north side) dyke as with drillcore W162, but also to the east of the major N-S graben fault.

- The third drillcore, W136, is also located just east of the major graben fault and south of the major dyke, but unlike drillcore W125, the lower ore layer in drillcore W136 is relatively richer in Mn by comparison to the upper ore layer, which in turn has very high Fe content.

The remaining four drillcores come from the eastern margin of the Wessels Mine area:

- Drillcore DB7 is located centrally and lies proximal to minor N-S faults in the area but relatively distal to two splices of the major dyke running through the area.
- Drillcores DB50 and DK21 are located on the far east of the area, near the actual farm border. Both drillcores are located practically along a N-S trajectory but are compositionally very dissimilar, with DK21 being relatively rich in Mn whilst DB50 is relatively rich in CaO and thus of much lower manganese grade.
- Finally, drillcore DB38 is located in the north-eastermost margin near the farm boundary, where the two major dykes appear to conferge. It is situated near faults and the so-called "suboutcrop" of the Hotazel Formation (dotted red line), that is, the northernmost extent of the Hotazel Formation in the region. Compositionally, drillcore DB38 records the highest Fe content of all 12 drillcores sampled.

1.13.3. Gloria mining area

Drillcore GL57 is the only drillcore sampled from the Gloria Mine area where the company ASSMANG Ltd exploit low-grade manganese ore. Indeed, classic drillcore intersections in the Gloria area contain low-grade, carbonate-rich, classic Mamatwan-type ore. Yet, drillcore GL57 exhibits in the upper ore layer, a high Mn ore grade akin to that seen typically in Wessels type ore, while the lower ore layer shows low-grade (Mamatwan-type) manganese ore. Furthermore, the same drillcore lies relatively proximally to a broadly E-W trending fault, and is also situated close to a pair of NE-SW trending dykes (Fig. 1.9).

1.13.4. Methods and analytical techniques

Polished sections were made from all collected samples for standard reflected light petrography, SEM, EPMA for mineral chemical analyses, and LA-ICP-MS for trace element analyses on a sub-selection of samples. Analytical instrumentation used includes a JEOL electron microprobe at Rhodes University; a CAMECA electron microprobe at the University of Johannesburg; and

LA-ICP-MS (Perkins *et al*, 1993) instrumentation also at the University of Johannesburg. Details on instrument specifications, analytical conditions used and the analytical results themselves, are included in the forthcoming chapters and the Appendix.

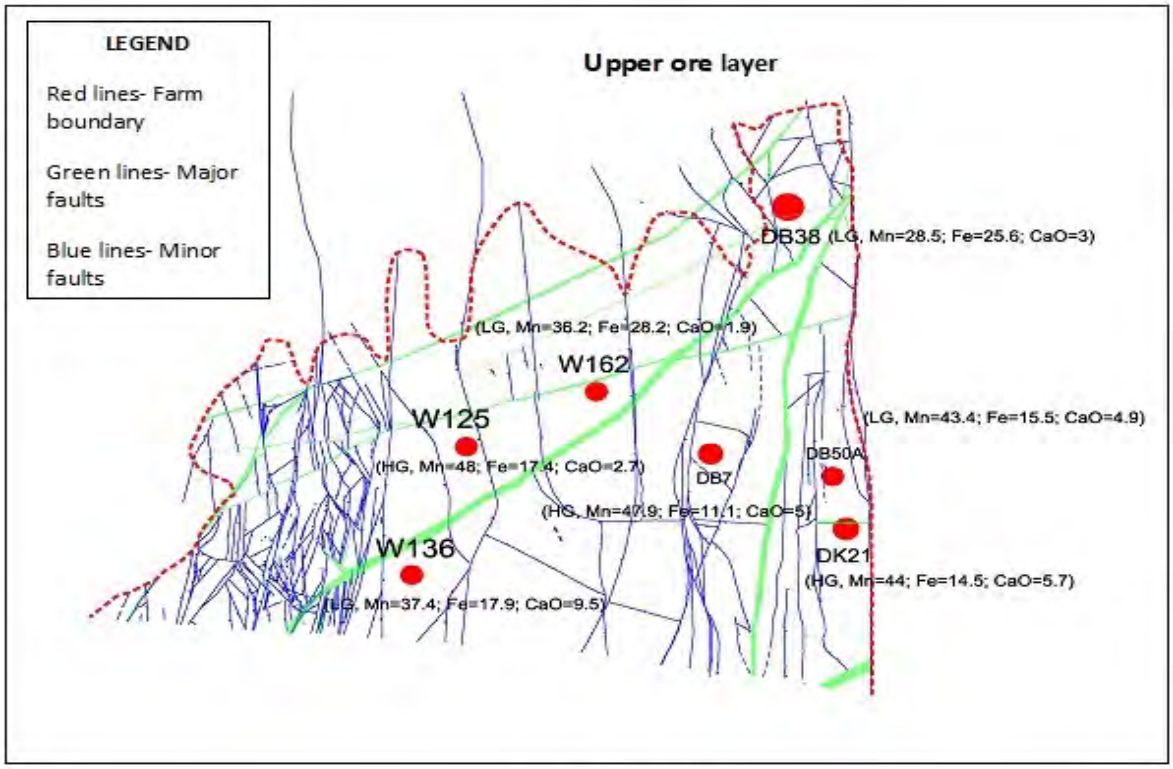

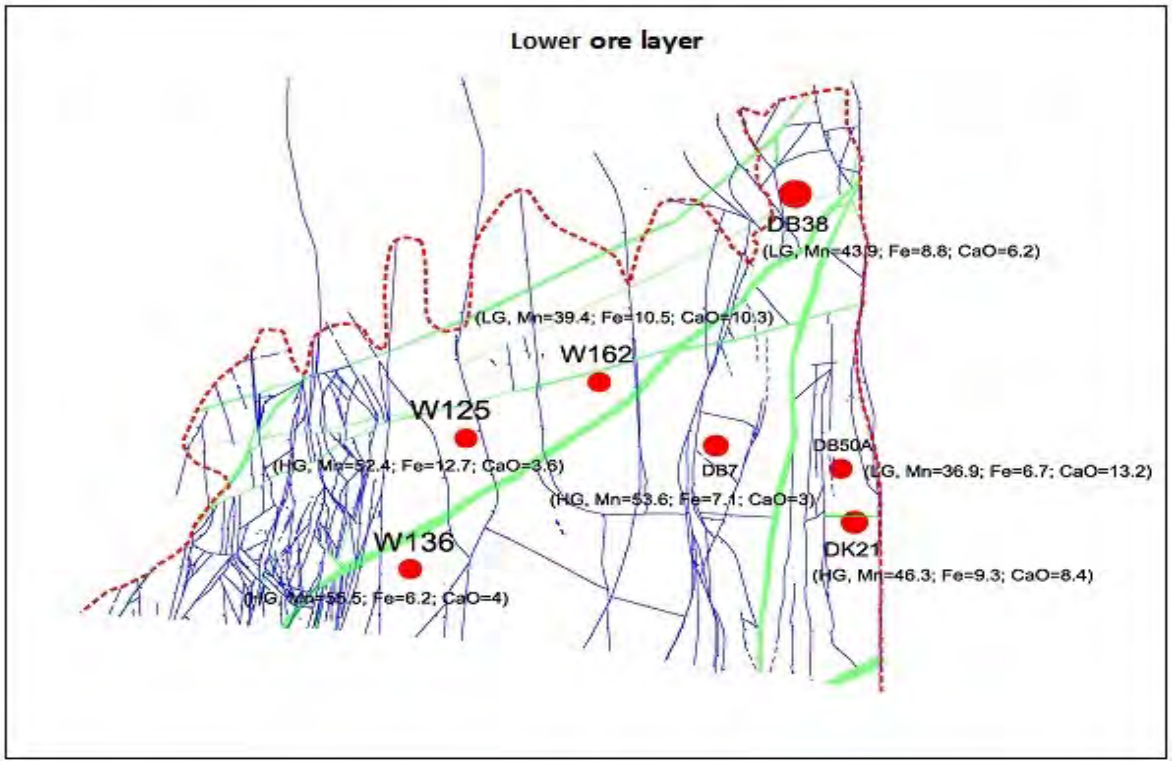

Figure 1.8: Map illustrating the Wessels Mn mine area, structural features (faults in blue; dykes in green, suboutcrop in red) as well as location of the individual cores in relation to the various structural elements**.**

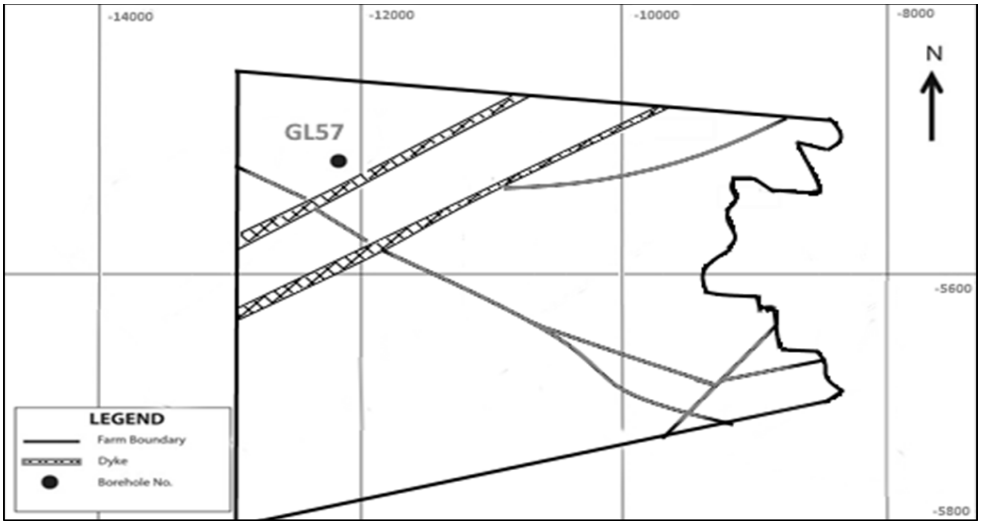

Figure 1.9: Plan view of the Gloria mine area illustrating structural features (faults and dykes) as well as the location of drillcore GL57.

2. MINERALOGY AND TEXTURAL OBSERVATIONS

2.1. Introduction

As mentioned in the introductory chapter, whereas there are a number of previous studies dealing with the complex mineralogy and mineral assemblages of the KMF manganese ores, few attempts have been made to showcase and compare the mineralogy of the upper ore layer and the lower ore layer in a single drillcore and within a given ore layer across space in the northernmost parts of the KMF (Gutzmer and Beukes, 1995, 1996; Tsikos, 1999; Tsikos et al., 2003, 2010; Mhlanga, 2020). This study is thus aimed at achieving primarily that very objective, namely to examine, report and assess the mineralogical characteristics and mineral-chemical variation in space of the upper and lower ore layers in a parallel fashion.

This chapter aims to provide a comprehensive petrographic description of manganese ore in the northern part of the KMF using Mn ore samples from all 12 (twelve) drillcores from the three mine localities selected, namely Wessels, N'chwaning and Gloria (Figure 4). Although between 4 and 6 samples representing each ore layer from each drillcore were collected and prepared for petrographic analysis, only a representative selection of these were the focus of this study. As previously stated, original samples were selected at an approximately 1-meter interval from the inferred contact of the ore with the overlying and underlying hematite-rich lutitic zones bordering the ores. It should be noted that those contacts are extremely difficult to define, as they are highly gradational and obscured further during the hydrothermal processes leading to Wessels-type ore formation. Therefore, the collection of samples was also aided by available geochemical assays from each respective mine.

The following sections will serve to illustrate the diverse mineralogical and textural relationships exhibited by both Mn ore layers in a given drillcore and across different drillcores. The petrographic characteristics of the high-grade Mn ores were studied first on polished thin sections under a standard Zeiss reflected light microscope. Minerals were identified where possible under the petrographic microscope using their optical properties. When grain size hindered identification, the use of energy dispersive spectrometry (EDS) on a scanning electron

microscope (SEM) was employed at the Electron Microscopy Unit of Rhodes University. Spot analyses of specific mineral grains were performed using this technique, in order to determine qualitatively the different mineral constituents encountered. SEM studies formed an extremely useful tool due to the fact that manganese oxide minerals are quite difficult to identify from one another when intergrown in complex fine-grained assemblages as those typically seen in the KMF ores. Following the use of SEM-EDS instrumentation, quantitative electron probe micro-analyses were obtained from the same assemblages using an EPMA facility in the Geology Department at Rhodes University, the EPMA results will be comprehensively presented in the chapter following the petrographic descriptions. Instrument and analytical conditions are provided in the Appendix.

2.2. Petrography

In the forthcoming sections, petrographic results will be presented in a systematic fashion as follows: each section will deal with all drillcores and their contained ores from each mine area selected for study. Representative petrographic descriptions and results will be shown in parallel from the upper and lower ore layer from each drillcore, using SEM imagery at increasing resolution in a top-down sense. Images on all scales will permit adequate viewing of the prevailing textures and mineral intergrowths for each section, but annotations and labels illustrating the dominant mineralogy in each case, will be shown in the higher resolution images at the lower sections of each page.

2.3. Wessels mine

2.3.1. Drillcore DB50

Figure 2.1 illustrates representative images obtained from samples from drillcore DB50A; the upper ore layer (left) and lower ore layer (right) are shown next to each other at similar magnification for comparative purposes. (The same convention will be used for each drillcore hereon). Mineralogically, the two ore layers display slight variability in textures and mineralogy. The upper ore layer comprises the minerals hausmannite and braunite II as the key ore-forming phases, and calcite with barite as non-manganiferous accessory phases. Modally, the dominant

mineral in the sample is braunite II along with calcite, with hausmannite occurring mainly as veins or apparent replacement features together with barite. Texturally, the top ore layer appears to preserve primary textures from the low-grade ore protolith. These manifest as discontinuous lenticular calcite bands whereby some of the calcite appears to be replaced by hausmannite. In association with these calcite bands is relics of fine-grained braunite, possibly from the original protolith. Cross-cutting these calcite bands are veins rich in barite and hausmannite.

The lower ore layer differs texturally by comparison to the upper ore layer but shares a similar mineral assemblage. It consists of braunite, calcite, hausmannite and minor barite, with braunite and calcite being the modally dominant phases. The braunite is Ca-poor (see mineral chemistry section later), it occurs as subhedral grains in a calcite matrix, and contains occasional patches of barite occurring in a texturally rather irregular fashion.

The hausmannite occurs in lesser amounts as apparent inclusions and overgrowths within and at the expense of braunite II. The main textural difference between the lower and upper ore layers is that the former appears coarser-grained relative to the upper ore layer, and primary textures of precursor ore seem to be completely absent, hence the ore has a recrystallized, annealed texture.

2.3.2. Drillcore DB38

Drillcore DB38 is located on the eastern border of the Wessels Farm area. Figure 2.2 illustrates BSE images of the upper (left) and lower (right) ore layers alongside one another, allowing direct comparison of their contrasting mineralogical and textural attributes. Specifically, the upper ore layer shows little evidence of texture preservation from the assumed low-grade precursor. The ore is dominated by hausmannite and braunite II along with carbonate minerals and subordinate barite. The textural arrangement of these phases is generally as recrystallized masses with little evidence of primary laminated textures being preserved. A characteristic textural feature here is sub-spherical dolomite-rich clusters with minor inclusions of Fe-Mn oxides and occasional patches of anhedral barite. The ore matrix is predominantly made up of hausmannite with hematite becoming more abundant in association with the carbonates and barite.

The lower ore layer shows a dominantly braunite II-rich assemblage with apparent development of compositional banding which may be a relic feature of primary textures in precursor Mn ore. Mineralogically, this ore layer comprises both braunite II and hausmannite as the main ore-

forming phases and contains andradite, calcite and barite as non-manganiferous minerals. Hausmannite is less abundant than braunite II and seems to grow within calcite-rich bands mimicking the orientation of banding. The braunite II along with calcite make up the microcrystalline matrix.

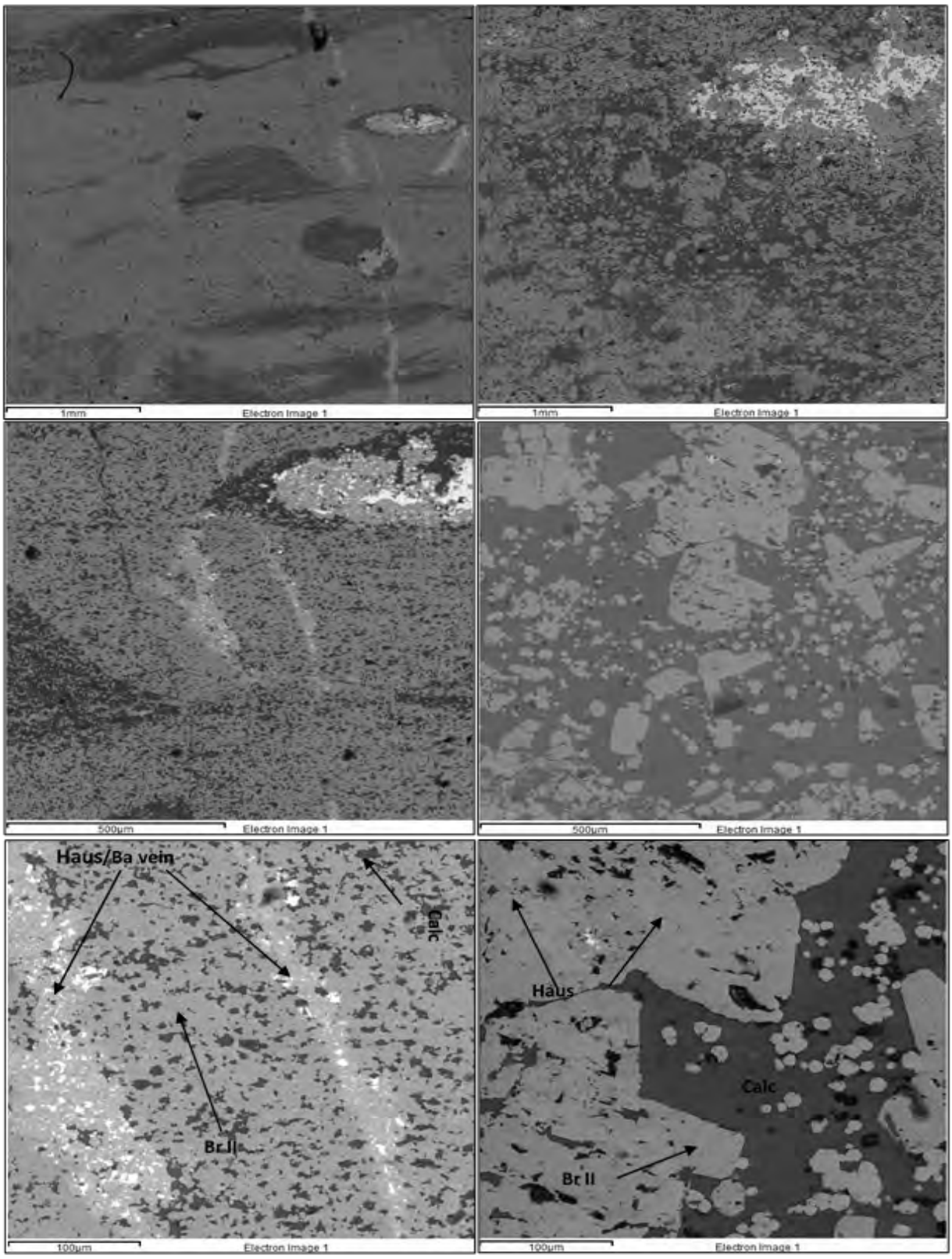

Figure 2.1: Backscatter electron images of drillcore DB50A at increasing magnification from top to bottom. The left side represents the upper ore layer while the right shows the lower ore layer.

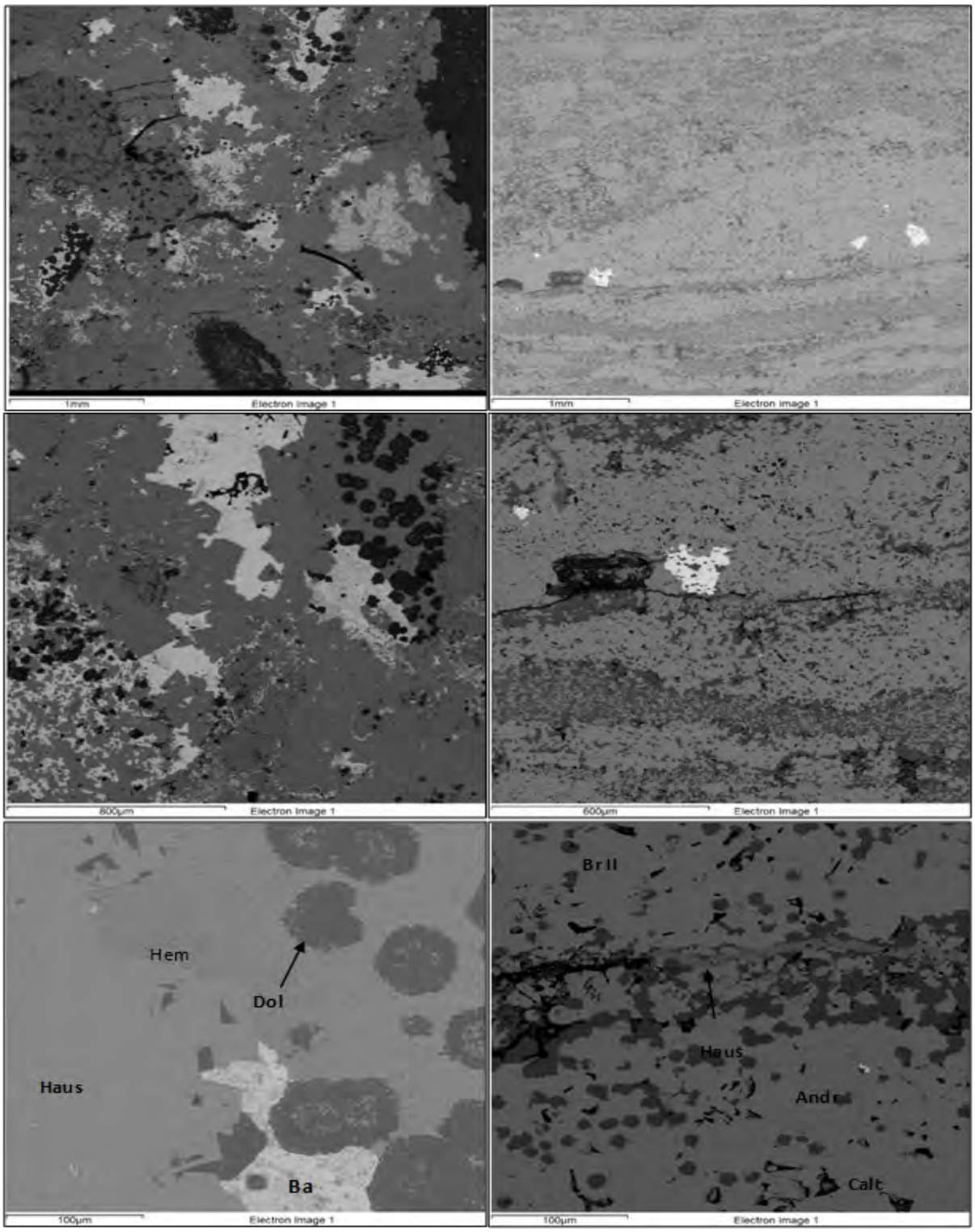

Figure 2.2: Backscatter electron images of drillcore DB38 showing ore textures and mineralogy for the upper ore layer (left) and the lower ore layer (right). Images increase in magnification in a top-down sense.

In summary, drillcore DB38 has a hausmannite- and dolomite-rich upper ore layer and a braunite II rich lower ore layer. Texturally, both ore layers are also different, with the lower ore layer seemingly preserving primary laminations in the form of calcite/hausmannite-rich bands whereas the upper ore layer displays curious textures of spherical dolomite that are difficult to attribute to primary textures, both mineralogically and texturally.

2.3.3. Drillcore DB7

Drillcore DB7 illustrates comparable mineralogy across both ore layers but variable ore textures within each layer (Fig. 2.3, 2.4). Textural variability is particularly prominent in the top ore layer and provides a very fitting illustration of the effect of scale in observation. On a large scale, a crude lamination pattern is observed which is locally obscured by mineral recrystallization. The bottom ore layer does not seem to preserve such banding/laminations on a single sample scale.

Mineralogically, the upper ore layer is enriched in hausmannite, which appears to be overgrowing/replacing an assemblage of braunite and andradite. On a small scale, the hausmannite shows subhedral habit with apparently euhedral grain terminations into populations of braunite and andradite. The latter exhibit a poikiloblastic-like texture with hausmannite inclusions. On a larger scale, the hausmannite-rich subhedral masses map out discrete bands which are sub-paralleled by the distribution of andradite-rich patches. Occasionally, the latter truncate the hausmannite banding.

The lower ore layer exhibits a more recrystallized, coarser-grained texture relative to what is observed in the upper ore layer. Mineralogically, it also contains an assemblage comprising braunite II and hausmannite, along with hematite, but calcite here is the dominant accessory phase instead of andradite. On a larger scale, the textural arrangement of braunite displays a characteristics and curious globular development, whereby apparent globules of braunite II and hematite are randomly dispersed in a matrix of microcrystalline braunite II and calcite, and minor hausmannite. In terms of the fine scale relationship between hausmannite and braunite II, the former occurs mainly as irregular patches and pseudo-veinlettes, and also as patchy fibrous aggregates containing small inclusions of braunite.

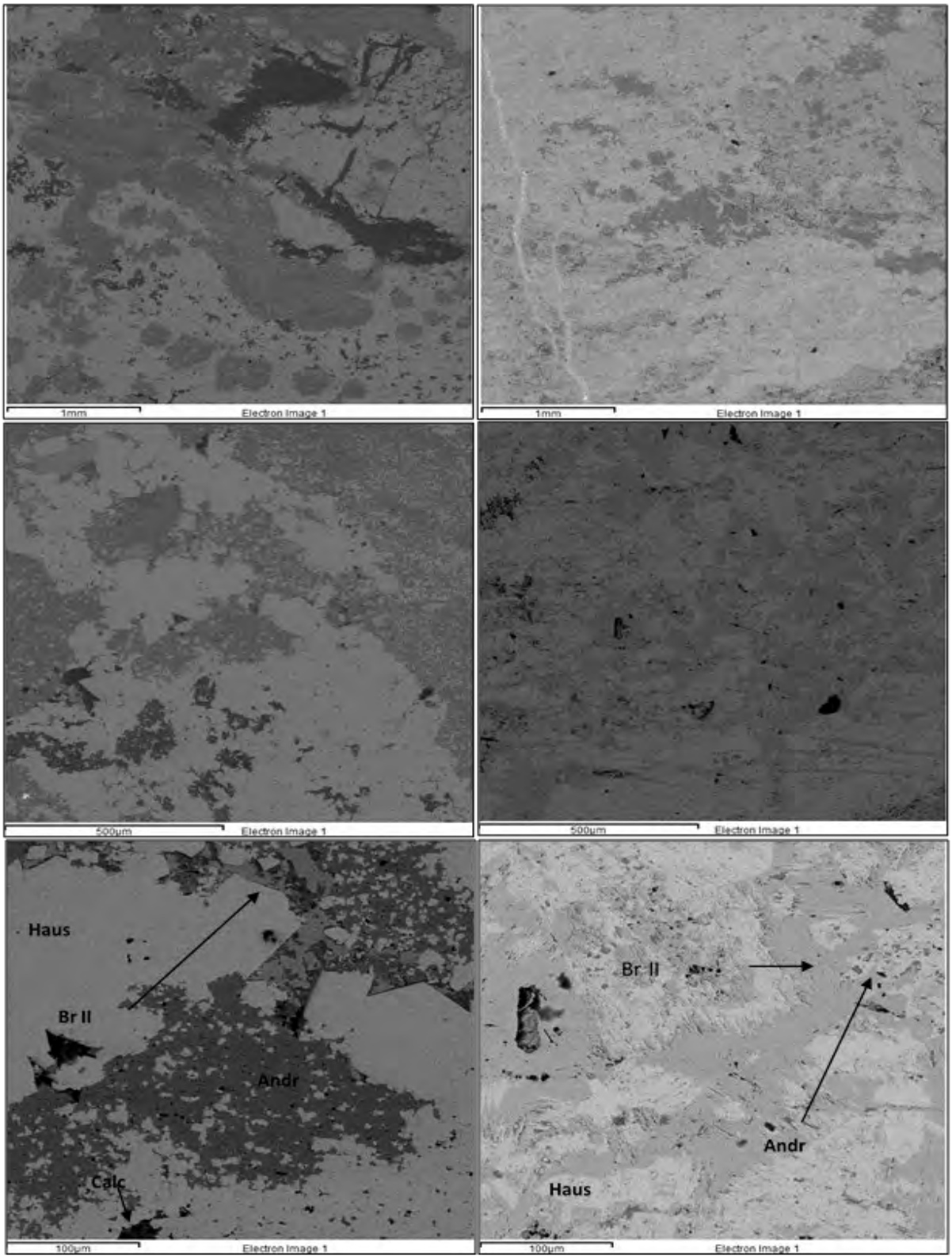

Figure 2.3: Backscattered electron images of drillcore DB7 textures and mineralogy for the upper ore layer (left) and the lower ore layer (right). Scale of images increases in a top-down sense.

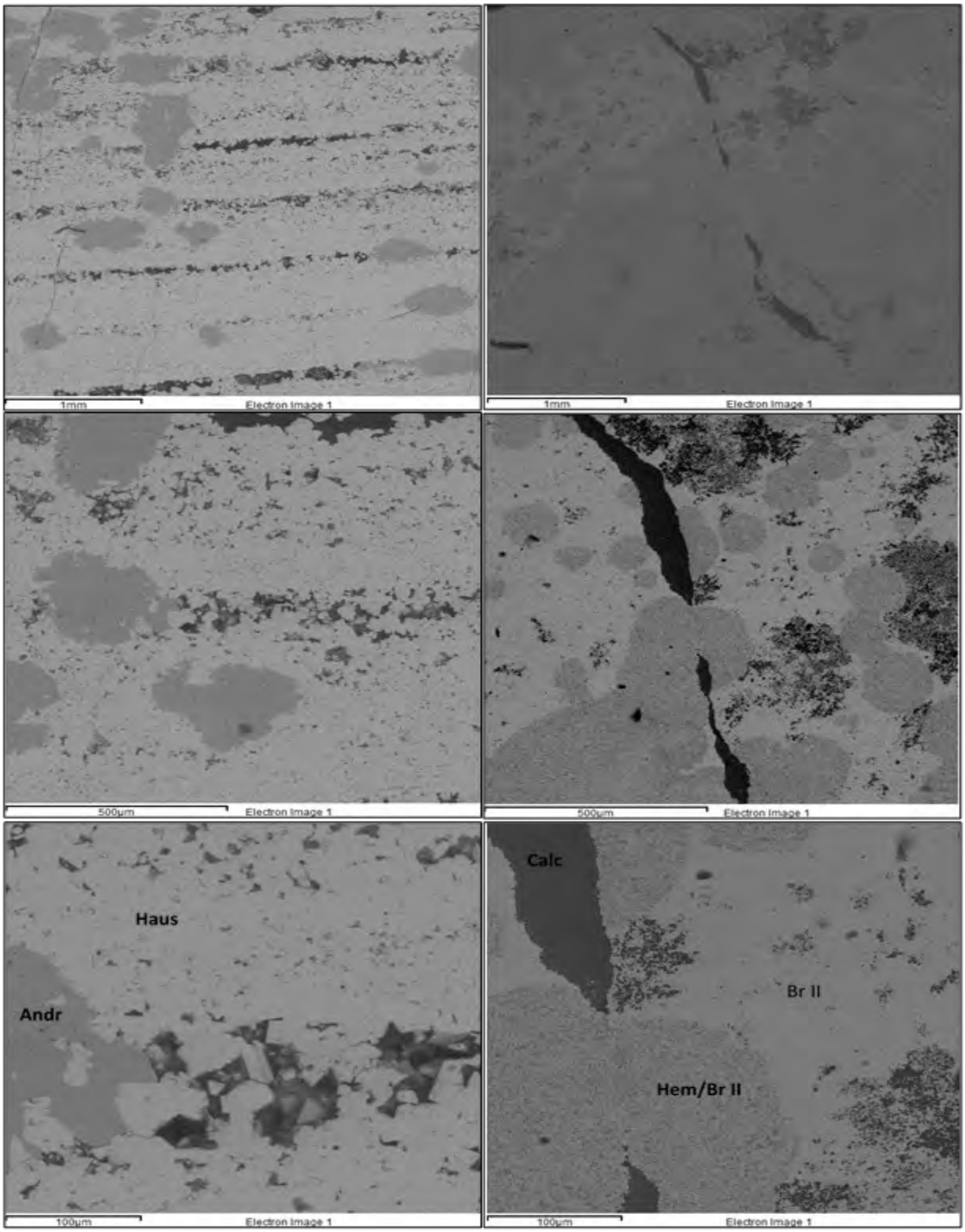

Figure 9: Further backscattered electron images of Mn ore from drillcore DB7, showing textures and mineralogy for the upper ore layer (left) and the lower ore layer (right).

2.3.4. Drillcore DK21

Figure 2.5 shows representative BSE images of mangaese ore from drillcore DK21. The upper ore layer is predominantly made up of braunite II and hausmannite as the main ore phases. Other minerals present in the upper ore layer include calcite, barite, strontianite ($SrCO_3$) and apatite in minor amounts. Primary texture preservation is not seen in the upper ore layer. Braunite II makes up the ore matrix as microcrystalline subhedral grains. Barite occurs as random fine-grained patches whereas all accessory minerals (calcite, strontianite, apatite) occur interstitially to braunite II.

Contrary to the upper ore layer, the lower ore layer consists of both hausmannite and braunite II as the main ore minerals, with minor marokite. Again, there is no evidence of primary ore textures being preserved in the samples; rather, there is a recrystallized, massive coarser-grained texture associated with the ore. The braunite II is developed as patchy, subhedral fine-grained aggregates floating in an equally massive, fine-grained hausmannite matrix. Accessory minerals include both calcite and andradite with barite occurring as a minor occasional phase. In stark contrast to the top ore layer, no strontianite is observed in the lower ore layer.

2.3.5. Drillcore W136

Drillcore W136 (Figure 2.6) lies in the south-eastern area of the Wessels farm boundary, in close proximity to the main graben fault documented from the area. The lower ore layer here is mainly made up of two major phases in terms of modal abundance, namely hausmannite and andradite with subordinate calcite present in the matrix. There is evidence of primary textures is the form of laminae being preserved. It is inferred that calcite previously defined these laminae and is now replaced by hausmannite in a solid state. Relic calcite is not observed except as minor interstitial grains; interstitial andradite is relatively more abundant within the hausmannite matrix.

The upper ore layer has a similar mineralogy to the upper ore layer with exception being the presence of the mineral marokite. Hausmannite occurs as irregular blobs throughout the ore layer, which is otherwise dominated by a marokite/calcite matrix. Crude laminations in the ore layer is interpreted to represent original calcite replaced by the braunite/marokite pair. Minor andradite and traces of chlorite are present in close textural association with the hausmannite. In summary, samples in the lower ore layer of drillcore W136 display a dominance of hausmannite

and andradite, whereas the upper layer is broadly defined by a marokite and hausmannite assemblage.

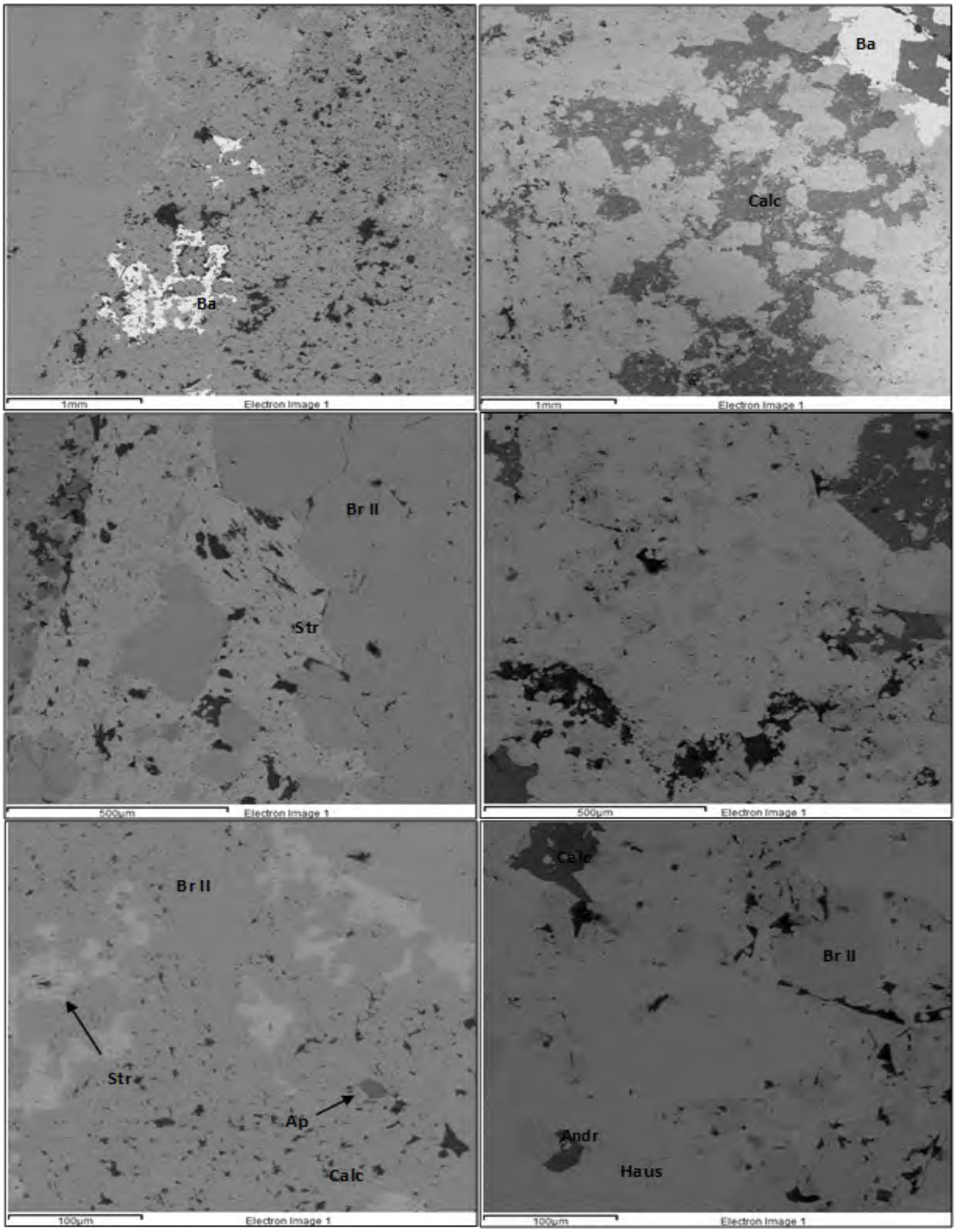

Figure 2.5: Backscattered images of drillcore DK21 showing the upper ore layer (left) and the lower ore layer (right). Increased magnification in a top down sense illustrates textural and mineralogical characteristics for the two ore layers.

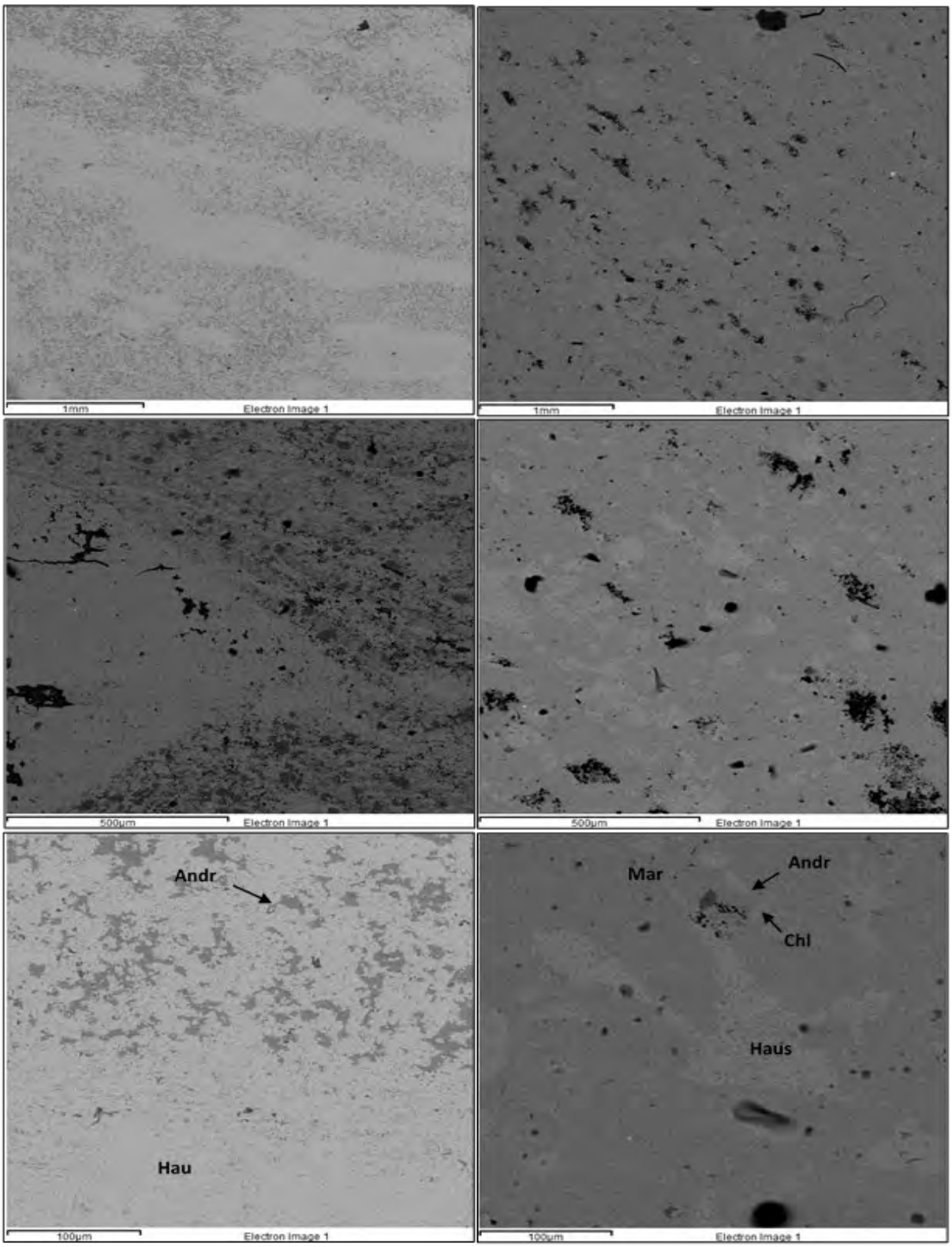

Figure 2.6: Backscattered electron images of drillcore W136 showing textural and mineralogical attributes for the upper ore layer (right) and the lower ore layer (left). Image magnification increases from top to bottom.

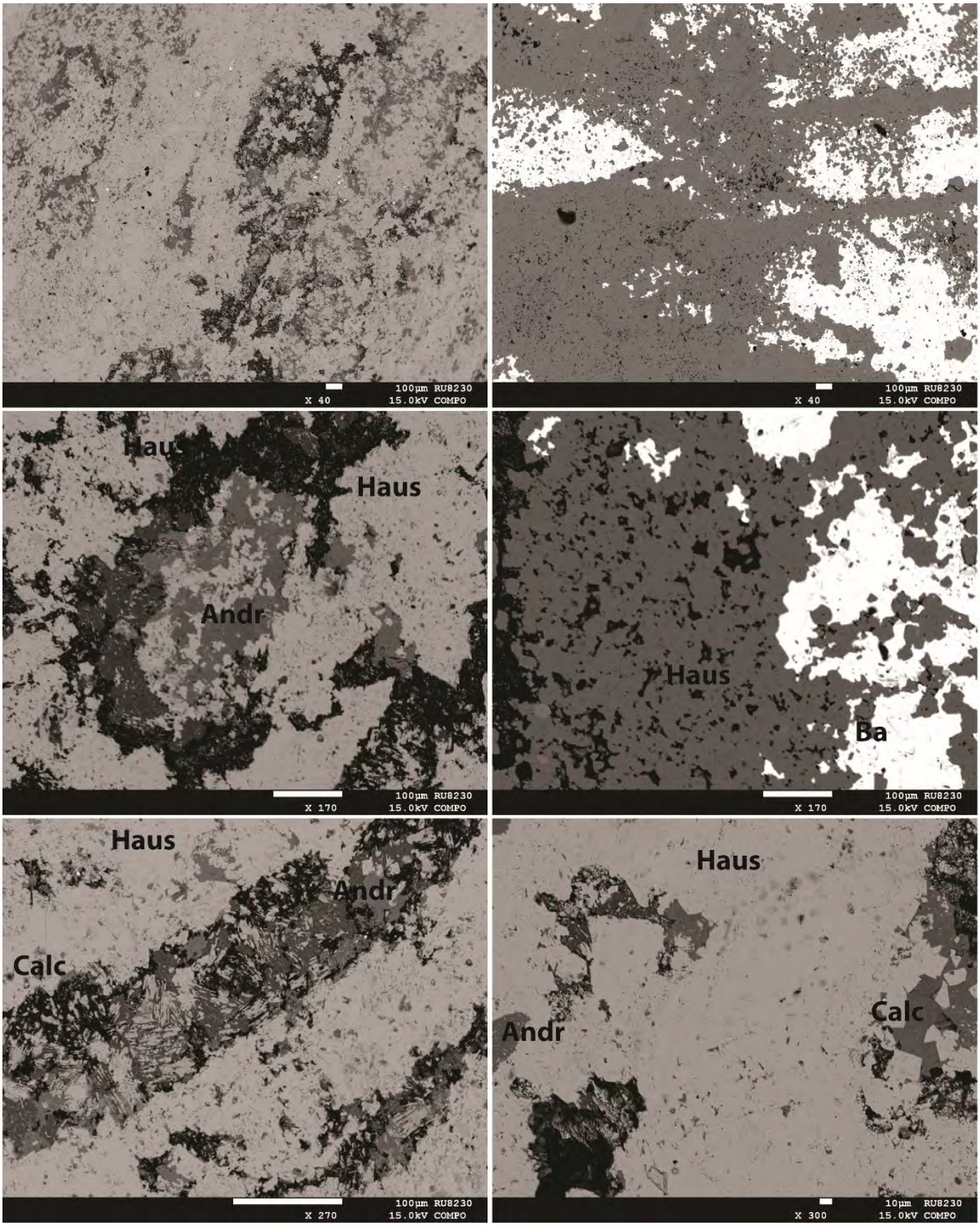

Figure 2.7: Further backscattered electron images for drillcore W136 showing the upper ore layer (left) and the lower ore layer (right). Increased image magnification from top to bottom helps to illustrate textural and mineralogical characteristics between the two ore layers.

2.3.6. Drillcore W162

This drillcore was selected in the north-central are of the Wessels farm. Both the upper and the lower ore layers display textural variability on varying scales (Fig. 2.8). In the upper ore layer, apparently primary inherited textures in the form of ovoids of carbonate minerals are present, whilst they are absent in the lower ore layer. These lenticular, ovoid-like features in the upper ore layer are tentatively interpreted to be residual from primary carbonate ovoids in precursor Mamatwan-type ore. These are now filled with hausmannite and carbonates (calcite and dolomite) in micro-crystalline aggregates without any clear pattern in mineral distribution. The main manganese minerals present in the ovoid-hosting matrix of the upper ore layer is braunite II, with hausmannite occurring in lesser amounts. Accessory phases include barite and hematite.

By contrast, the lower ore layer is rather different both texturally and mineralogically. The main textural difference is the lack of primary texture preservation: it is generally a microcrystalline mineral assemblage comprising predominantly hausmannite and braunite as the main Mn hosts, along with andradite, barite and calcite as accessory phases of the assemblage. This hausmannite-bearing assemblage also shows a second textural forms in the form of micro-veins that crosscut the groundmass; in both instances, calcite and barite are common accessory minerals. In summarising, the key difference between the two ore layers in this drillcore is the presence of apparent ovoids in the upper ore layer and the resultant dominance of carbonate minerals in its assemblage, by comparison to the more massive, carbonate-poor lower ore layer.

2.4. N’chwaning Mine

2.4.1. Drillcore N92I

In this core (Fig. 2.9), both ore layers exhibit a coarse-grained texture indicating recrystallization and destruction of any primary textures. The upper ore layer consists predominantly of a braunite II and hausmannite-rich matrix with minor hematite, calcite and andradite. Hematite exists mainly as veinlets crosscutting the matrix. Modally, the most abundant mineral phase is braunite II, with a microcrystalline texture containing subordinate calcite. Hausmannite on the other hand, is relatively coarser-grained, has a patchy distribution in the braunite dominated matrix, and shows an association with grains of andradite and fine braunite+calcite in its outer margins.

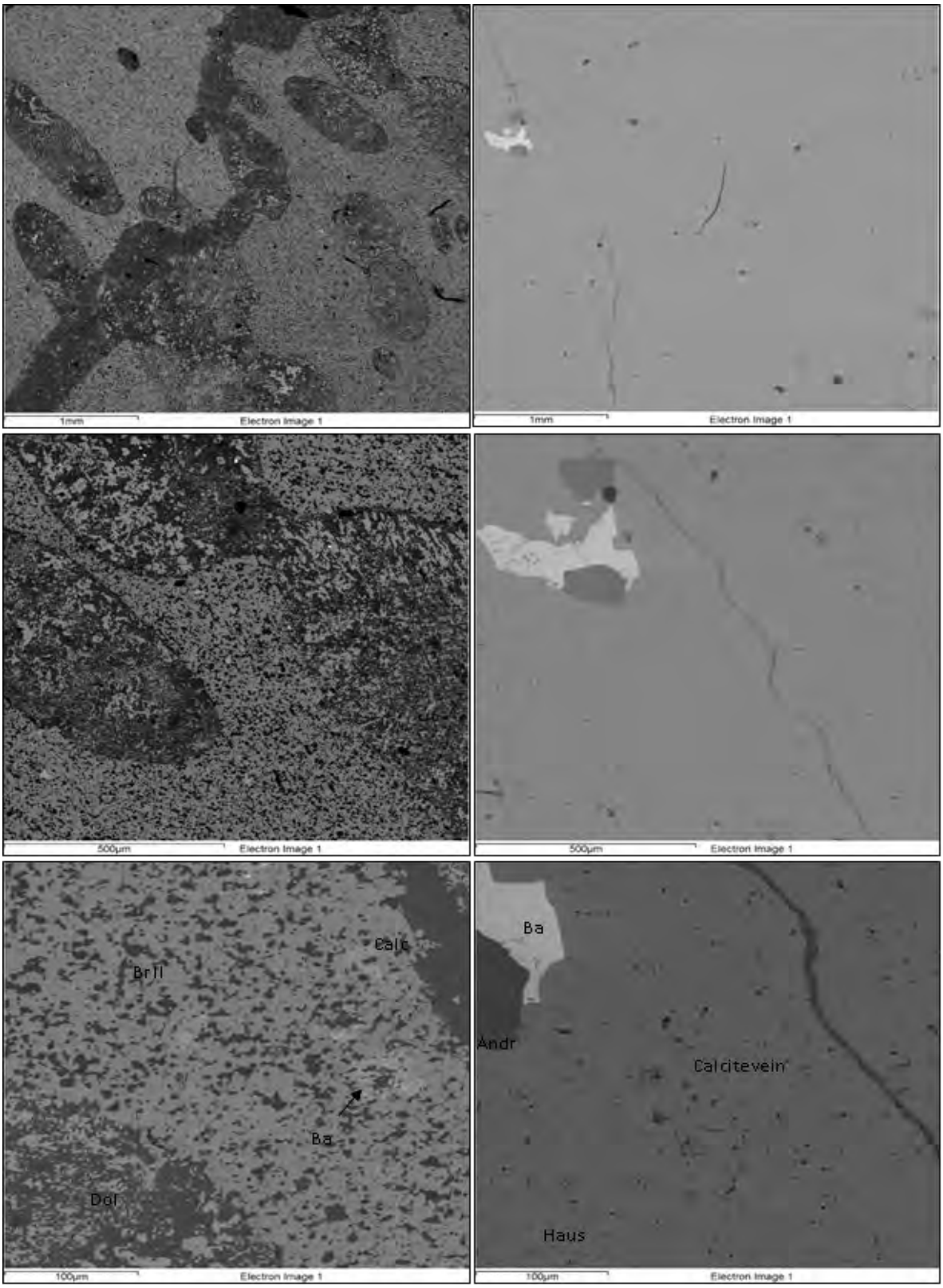
1mm
Electron Image 1
1mm
Electron Image 1
500µm
Electron Image 1
500µm
Electron Image 1
Calc
Brll
Ba
Dol
100µm
Electron Image 1
Ba
Andr
Calcitevein
Haus
100µm
Electron Image 1

Figure 2.8: Backscattered electron images of Mn ore from drillcore W162 showing textures and mineralogy for the upper ore layer (left) and the lower ore layer (right). Image magnification increases top-down.

The lower ore layer consists predominantly of hausmannite, andradite and calcite, with much lesser braunite. The hausmannite has a massive microcrystalline texture and is the most common mineral phase in this layer. Evidence of brittle deformation and development of micro-brecciation and micro-faulting is visible in the groundmass of this ore layer. On a finer scale, apparent pseudo-ovoidal structures develop that are mineralogically characterized by the assemblage andradite-carbonate-hausmannite, floating in the hausmannite-dominated matrix. The contacts between these features and the matrix are very diffuse as though the two assemblages blend in with one another. It is possible that these characteristic "clumps" of high andradite-calcite dominance versus the hausmannite matrix, represent possibly earlier carbonate ovoids that have been replaced by silicate-carbonate material during decarbonation reactions (see introductory sections for relevant mineral reactions). If this interpretation is correct, then the andradite dominated "clumps" above may in fact represent evidence of at least partial primary textural preservation.

2.4.2. Drillcore N94J

This drillcore lies in the south-eastern region of the N'chwaning Farm area and it is in close proximity with a NE-SW dike that cuts through the Hotazel Formation. The upper ore layer exhibits a fined-grained groundmass with abundant veins crosscutting it. The veins are effectively fracture-fills in an evidently overall brittle texture of this layer. Mineralogically, the groundmass is made up of mainly hausmannite with minor marokite and very occasional braunite II. The veins, on the other hand, contain small and variable abundances in barite, marokite, hematite and/or calcite; distribution of each of these minerals within these veins is very irregular, with specific subdomains containing no more than one of these minerals at any given instance.

Conversely, the lower ore layer appears coarser-grained by comparison to the top ore layer, with grains ranging in size from sub-mm to over a mm across. Mineral species identified in this ore layer are hausmannite, braunite, marokite and calcite in order of relative modal abundance. The hausmannite forms a crystalline groundmass in which the other minerals occur. The dominant

texture is in the form of microcrystalline crack- and vug-fills, suggesting that they probably formed later than the hausmannite that hosts them. In particular, the marokite locally shows a textural relationship with adjacent braunite and calcite grains suggesting that it could have formed through a chemical reaction between these phases through net loss of Si and CO_2. From a Mn content point of view, the above assemblage is one of the highest-grade assemblages of this study.

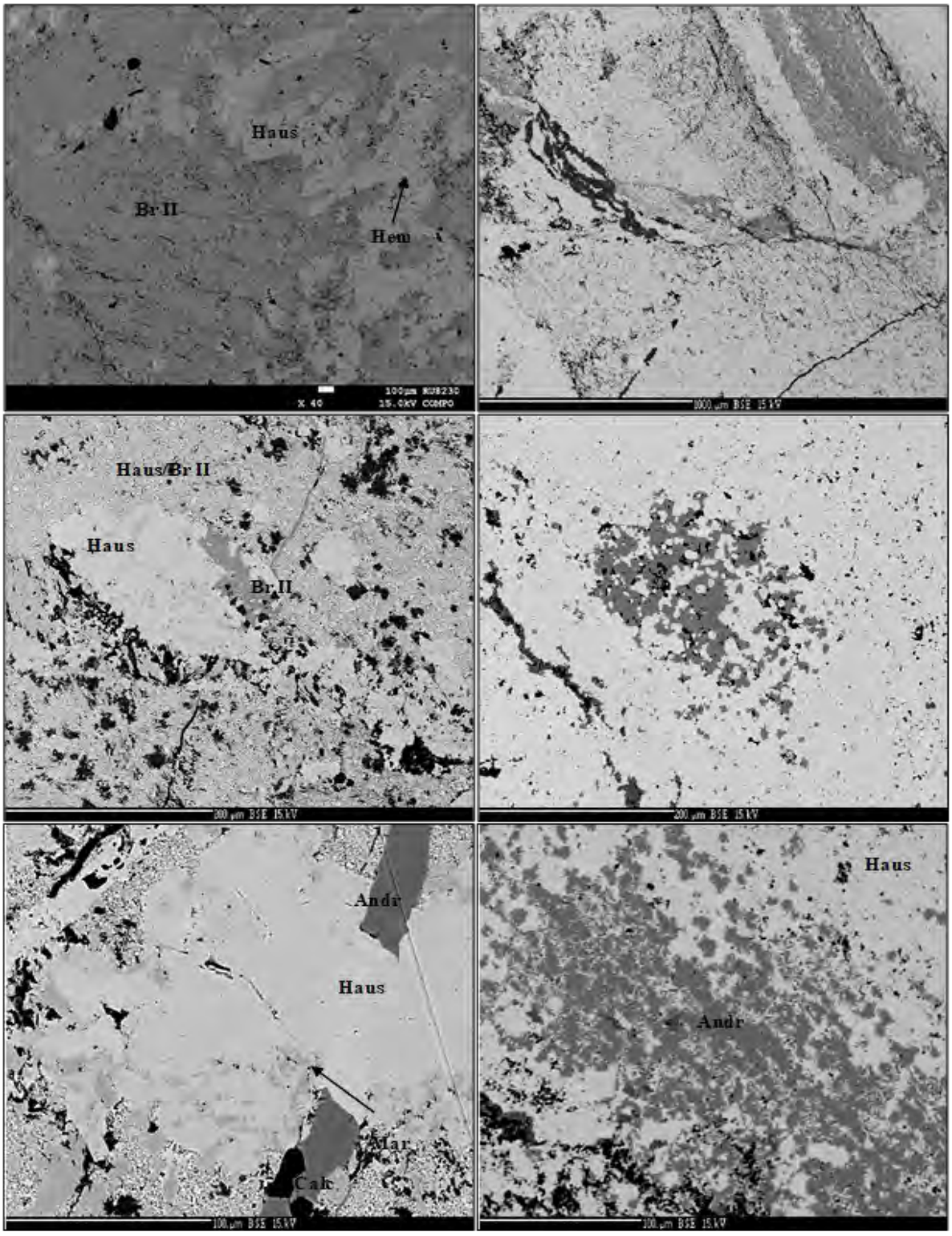

Figure 2.9: Backscattered electron images of drillcore N92I showing Mn ore from the upper ore layer (left) and the lower ore layer (right). Increasing magnifications top-down illustrate respective textural and mineralogical attributes and comparisons between them.

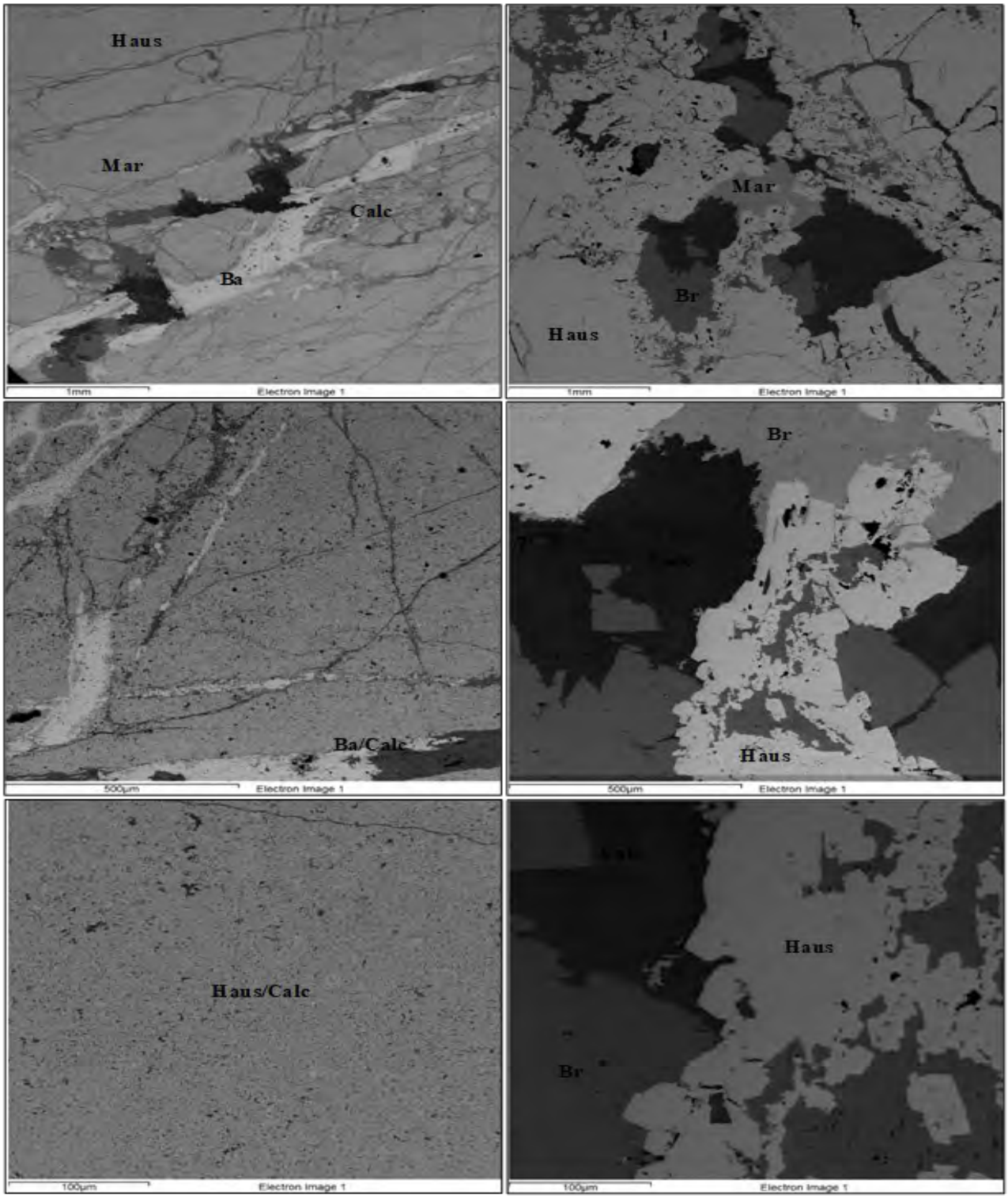

Figure 2.10: Backscattered electron images for Mn ore from the upper (left) and lower ore bodies (right) of drillcore N94J. Image magnification increases in a top down sense.

2.4.3. Drillcore N95A

Drillcore N95A (Fig. 2.11) comes from the central area in the N'chwaning Farm and lies adjacent to minor faults and between two dikes. The upper ore layer shows textures that appear to represent preserved pre-existing ovoids within a braunitic matrix. These features have a predominantly hausmannitic and andraditic composition; the former seems to dominate in the core of the ovoids whereas andradite is found at the rim. However, variants of that can also be seen on small scales whereby some ovoids may be dominantly hausmannitic whereas others nearby may be dominantly andraditic. Also, associated with the ovoids is calcite that can be observed as filling empty pores and cracks within the ore groundmass, but also as part of the andradite-hausmannite assemblage.

Similar with the upper ore layer, the lower ore layer is also predominantly made up of braunite. Texturally, the two ore layers show some clear differences, the main one being the evident absence of ovoid-like features from the lower ore layer. Instead, there appears to be a development of crude banding in the lower ore layer which may represent the relic of primary bedding/lamination. The mineral assemblage in the lower ore layer comprises braunite, hematite, minor hausmannite and calcite. The banding manifests itself as essentially pure braunite bands alternating with ones that contain an intricate assemblage of hematite- -braunite(+hausmannite+calcite). Calcite veinlettes cut through both of the aforementioned banded assemblages and therefore appear to be clearly secondary in origin.

2.4.4. Drillcore N95E

This drillcore lies in the north-eastern part of the N'chwaning Farm area. Here, both ore layers exhibit a coarse-grained, evidently recrystallized texture with practically no sign of any primary texture preservation observed in the form of ovoids or laminae (Fig. 2.12). The upper ore layer is comparatively coarser-grained than the lower one, with individual grains ranging from 1mm to as large as 10mm across. The mineral assemblage comprises braunite, hausmannite and some marokite as the key manganese minerals, with andradite and calcite contributing as gangue phases. The hausmannite takes the form of subhedral to euhedral grains and usually it is associated in space with calcite. Braunite and marokite exhibit characteristics textural intergrowths suggesting that they grew largely simultaneously. In terms of chemical controls for the formation of these two phases, it is thought that the relative abundance of Ca and Si at the

time of formation was such (i.e. excess Ca compared to Si) that the above two minerals would have formed largely in equilibrium.

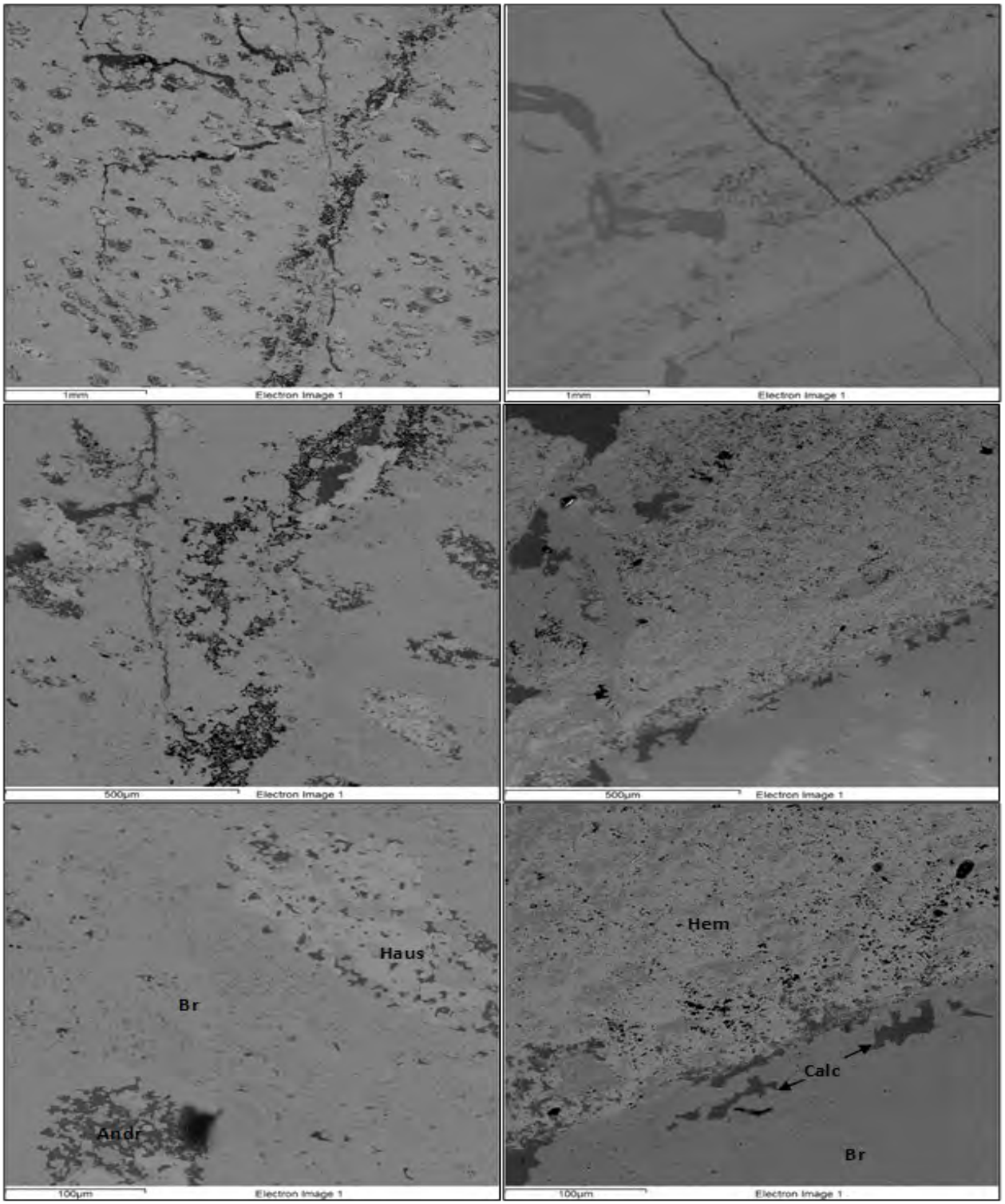

Figure 2.11: Backscattered electron images illustrating mineralogical and textural associations of the upper (left) and lower ore bodies (right) of drillcore N95A. Image magnification increases top-down.

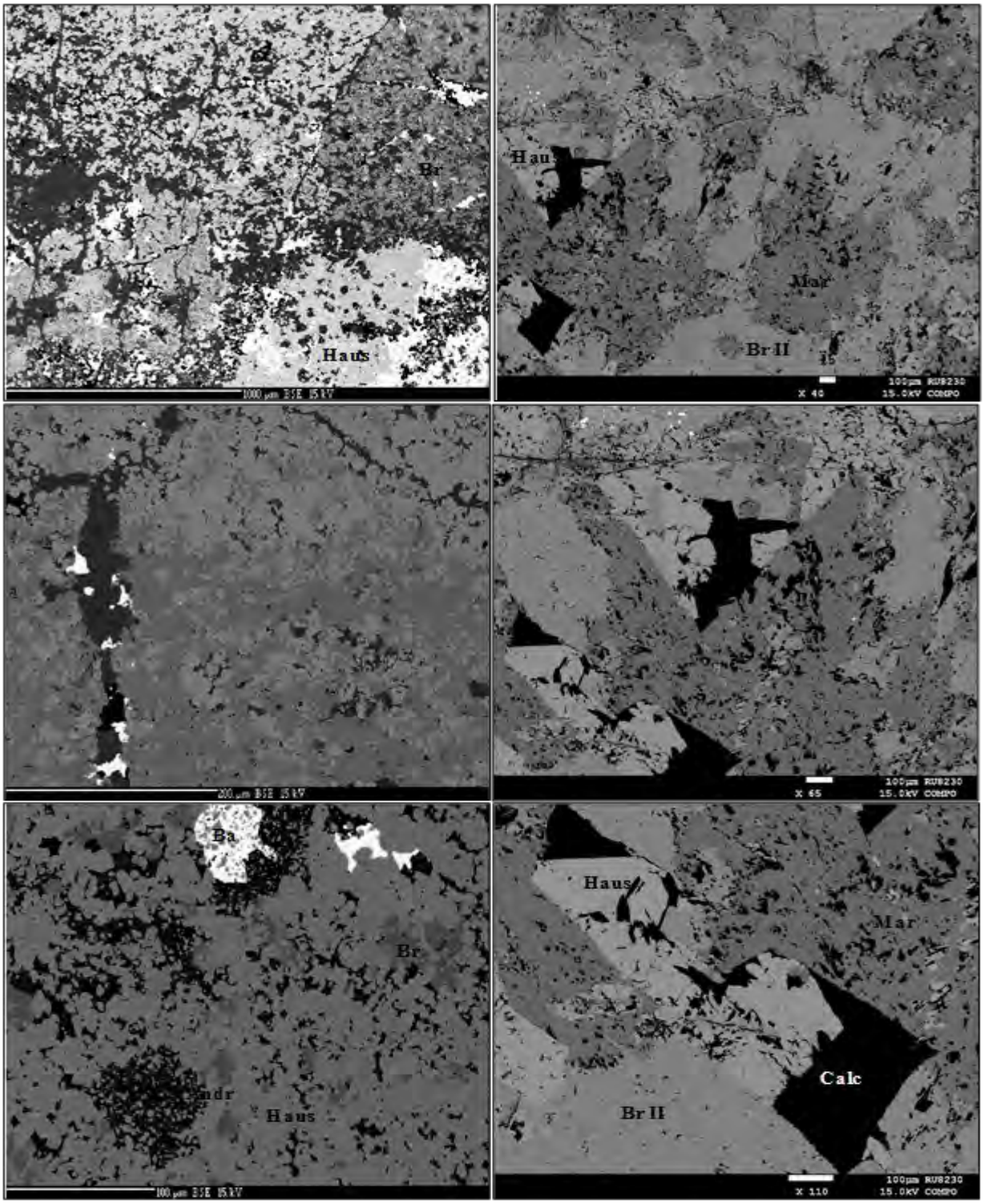

Figure 2.12: Backscattered electron images displaying textural and mineralogical associations for the upper (right) and lower (left) ore layers of drillcore N95E. Image magnification increases from top to bottom.

The lower ore layer in drillcore N95E (Fig. 2.12), consists predominantly of hausmannite. The ore here also contains common but rather patchy and irregular clusters of barite as an accessory phase, which occasionally takes the form of veins as well. The assemblage also includes andradite with abundant hausmannite inclusions. Small amounts of braunite are ocasionally present as anhedral interstitial phase within the hausmannitic groundmass, which otherwise makes up the bulk of ore.

2.5. Gloria area – drillcore GL57

Drillcore GL57 was the only drillcore selected from the Gloria Farm area. As indicated in the introduction, the Gloria area is characterized by low-grade braunite-carbonate rich manganese ore of the so-called Mamatwan type. However, locally at the margins of the low-grade manganese area as one approaches the N'chwaning farm northwards, high grade manganese ore may be intersected through drilling. Drillcore GL57 represents exactly that kind of drillcore intersection. In both ore layers, primary textures are preserved especially in the lower ore layer which looks a lot like low-grade, Mamatwan-type laminated Mn ore. Importantly, the top ore layer in this drillcore appears to be substantially higher grade than the lower ore layer. This is reflected through the mineralogy of the two ore layers: the upper ore layer has a mineral assemblage consisting of hausmannite, braunite and (mainly) dolomite, whist the lower ore layer comprises the classic braunite, carbonate and lesser hematite assemblage that typifies Mamatwan-type ore.

From a textural point of view (Fig. 2.13), the upper ore layer shows a crystalline texture with apparent preservation of primary lamination and ovoids. Hausmannite is the main manganese phase as microcrystalline aggregates with braunite only present as inclusions. The carbonate minerals are present chiefly as dolomite and much less so calcite, develop as relic ovoid-like features, and are expected to have formed from the original low-grade assemblage through a general loss of silica. Manganese from the original precursor carbonates (e.g. kutnahorite) would have partitioned, partly or wholly, into the hausmannite. In sharp contrast, the lower ore layer shows a typically very fine-grained, laminated texture of braunite-carbonate ore that typifies the Mamatwan type precursor. Preservation of abundant, pristine carbonate ovoids suggest no secondary mineral formation or texture destruction. As expected, the laminae and ovoids are

defined by carbonate minerals (Mn-calcite and kutnahorite) in a very fine-grained braunite matrix.

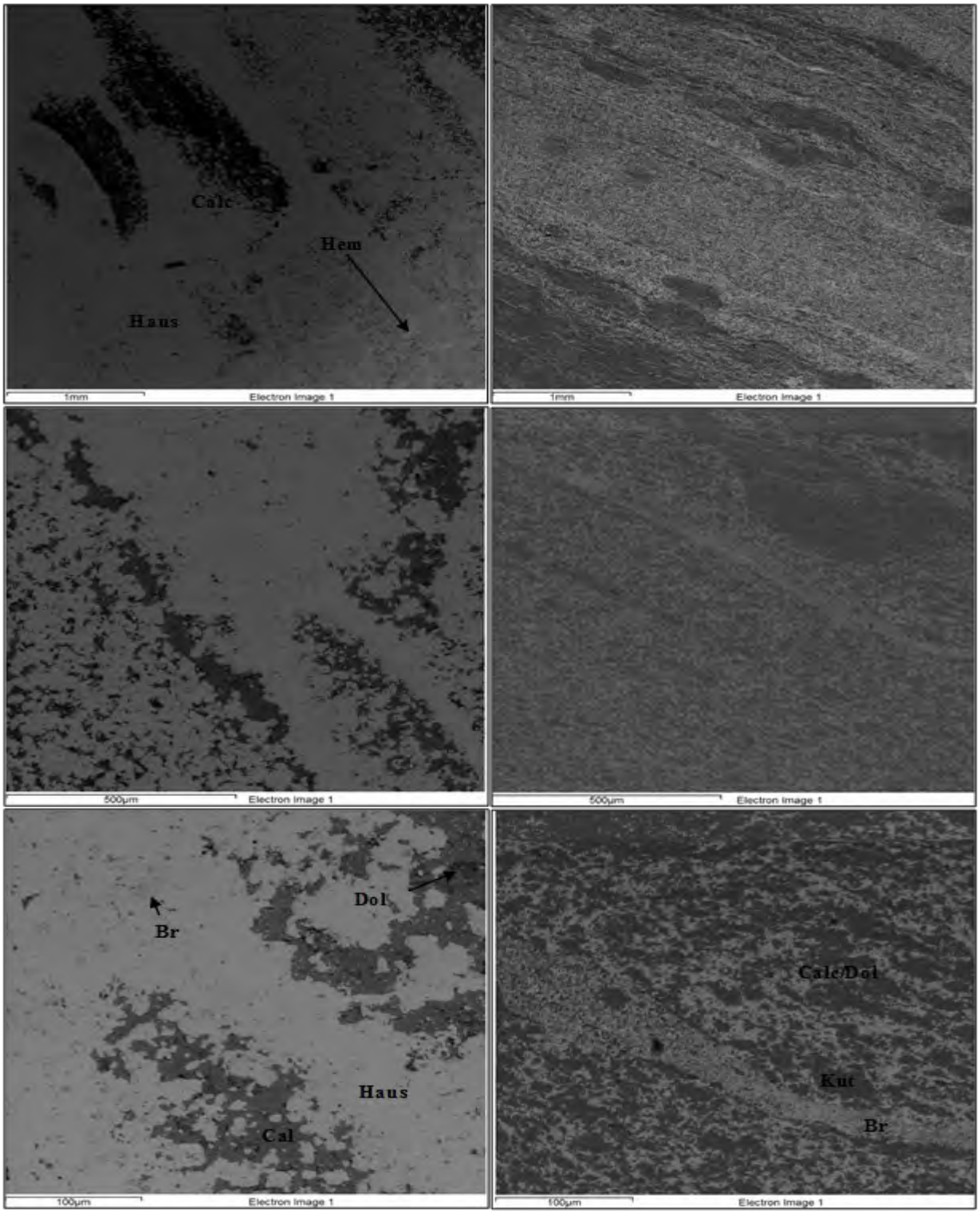

Figure 2.13: Backscattered electron images showing contrasting mineralogical and textural associations for the upper (left) and lower ore bodies (right) of drillcore GL57 from the Gloria Mn mine. Image magnification increases top-down.

3. MINERAL-SPECIFIC GEOCHEMISTRY

Following the detailed petrographic work using first a reflected light microscope and mainly the SEM facility at Rhodes University, samples were selected for mineral-specific analyses. A total of 48 polished section were specifically selected for detailed mineral chemical analyses using the electron-probe microanalytical facility (EPMA) at Rhodes University. These represent – on average, two samples per ore layer per drillcore. The above analyses permitted valuable insights into mineral chemical variability for every ore-forming manganese mineral as described in the previous chapter across all drillcores selected. Emphasis was placed, understandably, on the mineral-chemical signatures of the main ore minerals in terms of modal abundance, namely braunite and hausmannite. Since these minerals are chemically quite simple, as they contain essentially only five chemical elements (Mn, Fe, Si, Ca and Mg), the focus of this chapter will be on the variability of these species within each drillcore and across drillcores for each ore layer.

The common elements that would permit correlation and comparison between drillcores but also between individual mineral phases are expectedly those of manganese and iron. Iron in particular, is an element that appears in practically every ore-forming phase of the manganese ores of the KMF but is also a constituent of two other accessory minerals in the ores, namely hematite and andradite. Therefore, the partitioning and distribution of Fe has the potential to provide very useful information about its behavior during hydrothermal upgrading of the manganese ores in the northern KMF. Furthermore, the speciation of Fe, in other words the association of it with specific minerals, can yield insights into the metallurgy and economic character of the ores, and specifically how much of it is hosted in ore-forming *versus* accessory phases, and the possible reasons why.

The EPMA analyses were complemented by additional analyses of a small sub-selection of seven samples using a laser ablation inductively coupled plasma mass spectrometry (LA ICP-MS) facility. The laser ablation analyses were performed on a selection of hausmannite and braunite grains from diverse ore assemblages, and permitted comparative considerations using – possibly for the first time hitherto for the Kalahari Mn ores – trace element abundances in such minerals. Comparisons were also possible to be made between the trace element mineral chemistry of braunite and hausmannite with that of bulk high-grade ores that contain these

minerals. These bulk ore compositions were derived from analytical results on the same ores as obtained from the other thesis projects conducted in parallel with this study, as mentioned in earlier chapters.

3.1. Sample preparation and EPMA instrument settings

After examination under the optical microscope, samples on which EPMA analyses were conducted were carbon-coated (20nm). EPMA data acquisition was performed at the University of Johannesburg and Rhodes University, on a Cameca SX-100 Microprobe and a JEOL JXA 8320 Superprobe, respectively. Analytical conditions employed were as follows: acceleration voltage 15kv, probe current 20nA, counting time 10sec on peak and 5 sec on background, and beam spot size less than 1 micron. Natural standards were used for measuring the characteristic X-rays. ZAF matrix correction method was employed for quantification. Additional qualitative data for mineral identification were obtained using a TESCAN Vega TS 5136LM SEM coupled with an Oxford Instruments EDS for spot analysis, housed in the department of Biology at Rhodes University. The obtained spectra were evaluated using the INCA software by Oxford Instruments.

3.2. Chemical variability in minerals of the braunite group

Based on the petrographic descriptions as reported in the previous chapter and in conjunction with existing information form the literature (Kleyenstuber, 1984; Gutzmer and Beukes, 1995), braunite was confirmed to be one of the most abundant ore-forming mineral species in the manganese ores of the KMF. As indicated in the introductory sections, a variety of chemically different braunite compositions are encountered in the KMF, ranging from standard Ca-free braunite in low-grade ores of the Mamatwan type, to calcic and less silica-rich varieties (braunite II and braunite “new”) which are found in abundance in high-grade Wessels type ores. However, little is known or reported on the iron abundance and distribution in braunite across space. An important aspect that will be exploited in the forthcoming sections concerns how much iron is contained in braunite grains from the different ore assemblages that were described

petrographically in the previous chapter, compared to other co-existing manganese minerals (mainly hausmannite) or accessory minerals (e.g. andradite).

Braunite grains were therefore targeted for EPMA analysis to further understand the compositional variability across space, with special emphasis on iron and its possible controls. Figure 3.1 is a ternary diagram that depicts the compositions of braunite in the Wessels and N'chwaning mine areas, including the single drillcore from Gloria mine (GL57). The oxide components used for the construction of the ternary diagram are those for CaO, SiO_2 and Fe_2O_3, that is, the main oxide components of braunite other than Mn.

The ternary diagram illustrates the dominance of two end-member types of braunite, namely braunite and braunite II: the first is illustrated as a cluster of datapoints corresponding to little or no calcium (i.e. very close to the Fe-Si tie-line) whereas the other is represented by a cluster close to the centre-top of the ternary diagram corresponding to a ratio of Ca-Si of 1:1 (braunite II). Notable on this diagram is a population of datapoints which diverge from these two end-members by showing a more erratic variability in the Ca- and Si content and the ratio thereof. These compositions are thought to represent intermediate compositional members of braunite such as the braunite "new" species as reported by Gutzmer and Beukes (1995, 1996).

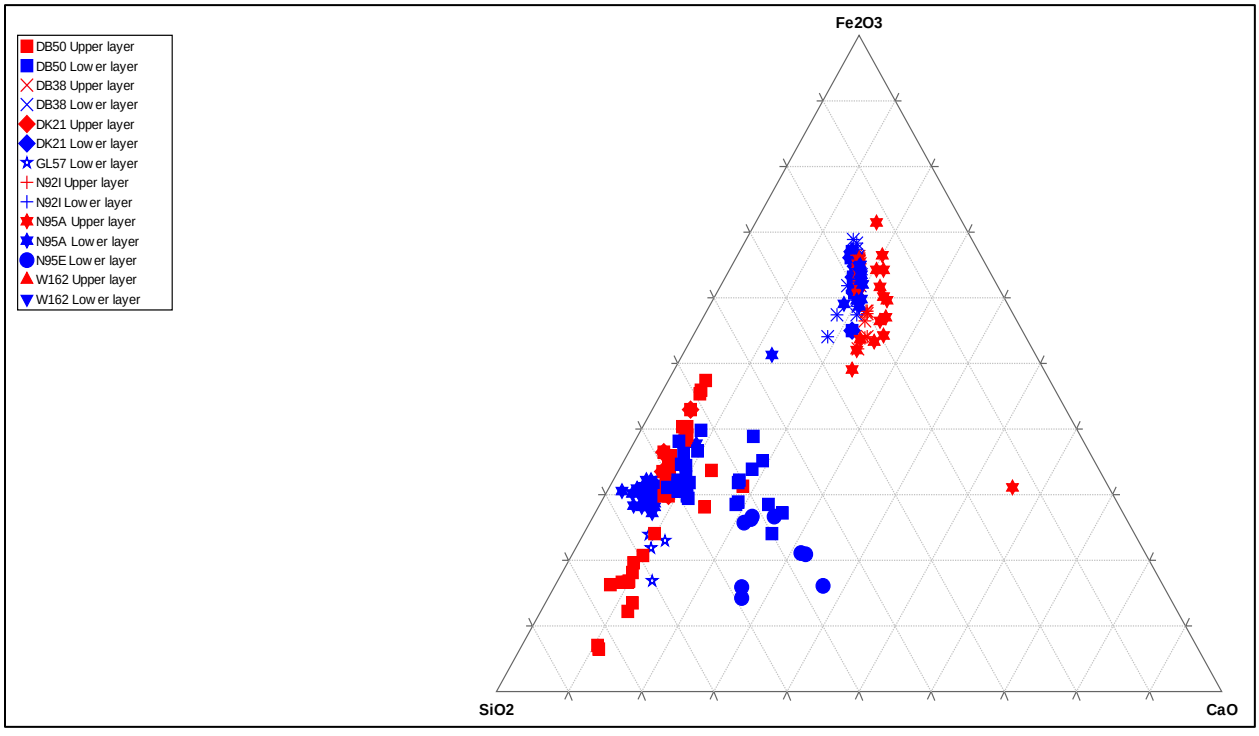

Figure 3.1: Ternary diagram that depicts the compositions of braunite in the Wessels and N'chwaning

mine areas, including a single drillcore from Gloria mine (GL57). Red symbols correspond to analyses from the upper ore-layer, whereas blue symbols represent analyses from the lower ore layer.

Table 3.1: Average EPMA data for braunite for both Mn ore layers from all drillcores where braunite is an ore-forming constituent

Drillcore	SiO_2	Al_2O_3	MgO	Fe_2O_3	Mn_2O_3	CaO	Total
W162up	9.24	0.18	0.11	5.60	80.72	2.46	98.32
W162Low	9.15	0.34	0.19	4.51	82.10	1.32	97.61
N92I up	4.30	0.18	0.01	12.13	76.94	4.74	98.31
N92I low	3.42	0.18	0.08	14.23	76.37	3.56	97.83
DK21 up	7.75	0.05	0.09	7.38	81.86	1.90	99.03
DK21 low	3.66	0.50	0.13	11.77	76.65	4.55	97.29
N95A up	9.18	0.27	0.40	6.03	76.40	5.78	98.06
N95A low	9.44	0.28	0.22	1.85	83.24	3.20	98.23
DB50 up	4.72	0.20	0.05	15.16	74.03	4.34	98.50
DB50 low	9.49	0.36	0.08	5.74	82.17	1.03	98.85
N95E up	10.94	0.32	0.04	4.64	75.87	5.79	97.60
DB38 up	4.62	0.45	0.04	15.63	74.26	4.39	99.39
DB38 low	4.59	0.21	0.05	15.59	74.45	4.66	99.55
GL57 up	7.23	0.01	0.09	2.31	86.55	1.19	97.37

3.3. Drillcore-specific braunite compositions

The collection of binary diagrams of Figure 3.2 below, presents a summary compilation of braunite-hosted iron (Fe_2O_3) plotted against manganese (expressed as Mn_2O_3) for all drillcores where braunite is a dominant ore-forming component of the ores. This figure also permits a broad overview of the control that braunite has on iron abundances in the ores. In order to contextualize that control, the average iron oxide content of the presumed Mamatwan type low-grade ore precursor is plotted on both diagrams for the upper and lower ore layer, as sourced from the recent PhD study on Gloria mine by Mhlanga (2020). It should be noted that the Fe

content in bulk precursor ore is predominantly in the form of hematite, whereas braunite from that ore is in fact Fe-poor (Mhlanga, 2020).

There are three important first-order conclusions that can be drawn from these diagrams: (1) there is a clear antithetic relationship between the two components indicating that Fe substitutes for Mn in braunite mainly in the trivalent state. (2) Maximum Fe content in braunite can reach values over 20 wt.%, suggesting that braunite on its own can accommodate Fe contents available in the original protolith. (3) The range of Fe-oxide content is overall also quite high (0-20 wt.%) but individual ore layers in individual drillcores record narrow ranges (clusters) in terms of iron oxide content. More detailed description of braunite chemistry is presented in the text that follows.

Drillcores from the Wessels mine area exhibit significant variability in braunite iron content for both ore layers. Standard Ca-poor braunite is the type found in drillcore W162 in both ore layers. It has an average CaO content close to 2 wt. % (Table 4) whereas the average SiO_2 content is at around 9 wt.%. This composition is comparable to that of standard braunite in terms of Si, suggesting that perhaps the little Ca contained substitutes mainly for the component of Mn^{2+} in the structure of braunite. In terms of average Fe content, the substitution of Mn by Fe seems to be relatively limited, which makes the braunite contained in both ore layers of this drillcore to be amongst the richest in Mn from the entire dataset of this study. The upper ore layer has relatively higher average iron content with specific analyses going as high as 10 wt.%, whereas data from the lower ore layer vary somewhat more widely: whereby maximum values are also close to 10 wt.%, standard deviation is higher resulting in a lower average than the upper ore layer.

Drillcore DB50 shows a wider range of braunite compositions. Specifically, three compositional types of braunite with varying Fe_2O_3 can be identified. The upper ore layer is dominated by braunite II but also contains some occasional, apparently relic braunite from precursor low-grade ore (see the Petrography chapter earlier). This earlier braunite is however extremely fine-grained and was not targeted for EPMA analyses. Braunite II from the upper ore layer has average Fe_2O_3 content of *circa* 15 wt.% at a range of compositions consistently exceeding 10 wt.%. By contrast, braunite from the lower ore layer is essentially calcium-free and thus more similar to standard braunite. With regards to Fe-oxide content, the two braunite variants from the upper and lower

ore layers have contrasting signatures, with braunite from the lower ore layer being substantially less iron rich (average around 5 wt.%) and at a relatively narrower range of Fe concentrations.

Braunite analyses from drillcore DB38 show significant enrichment in Fe_2O_3 at a range of values that is comparable for both ore layers together (10-20 wt.%). In both instances, the dominant type of braunite is braunite II. There is no clear distinction between the two ore layers in terms of iron abundance in braunite II. However, notable is the apparent behaviour of Al between the two braunite populations: specifically, braunite from the upper ore layer has twice as much Al on average than that from the lower ore layer. It appears as though where the Al-content is highest, that corresponding Fe-content is lowest. This suggests that Al^{3+} likely substitutes for Mn^{3+} just like Fe^{3+} does, although the overall degree of such substitution appears to be rather low.

Drillcores from the N'chwaning and Gloria mine areas show equal variability in braunite compositions. Drillcore N92I has two types of braunite: the upper ore layer is predominantly made up of braunite II, with Fe_2O_3 content reaching as high as 16 wt. % at an average of circa 12 wt.% (Table 4). By contrast, the braunite analysed in the lower ore layer is chemically more intermediate in composition, by recording relatively lower CaO and SiO_2 abundances at a ratio of approximately 1:1. This braunite may therefore be an intermediate species like braunite "new", and thus not true braunite II. Nevertheless, in terms of Fe-content it is broadly similar to braunite II of the upper ore layer, with some values reaching as high as 18 wt.%. Similarly, the average Fe-oxide content of this braunite is also a bit higher, at approximately 14 wt.%.

Drillcore N95A also contains two compositional types of braunite that can be identified and grouped based on both iron- and calcium-content: the upper ore layer contains braunite with relatively higher Fe_2O_3 and CaO content than the lower ore layer. Consequently, the Mn_2O_3 content of braunite in the lower ore layer is higher by a few wt.% than that of the upper ore layer. In terms of overall Fe-oxide content, the range of values is relatively lower than in other ore intersections analysed in this study, and the same applies to the average and maximum values as well (Table 3.14). Average Fe-contents in braunite from this drillcore are respectively 6.03 wt.% for the upper ore layer and 1.83 wt.% for the lower ore layer. The braunite compositions for both ore layers seem to suggest the presence of standard Ca-poor braunite, as the silica contents average very closely around the value of 10 wt.%. This suggests that the high Ca-contents (5.8 wt.% and 3.2 wt.%) are probably the result of substitutions for Mn^{2+} and are not associated with

the Si-Ca compositional relationship seen in standard Ca-rich varieties of braunite (mainly braunite II).

As indicated in the petrography chapter previously, braunite is only a minor to trace component in the lower ore layer of drillcore N95E. The upper ore layer hosts a type of braunite that is similar in composition to that of N95A, in that it appears to be an intermediate member between standard braunite of about 10wt.% SiO_2, and calcic braunite. The average SiO_2- and CaO-content of that braunite is 10.9 and 5.8 wt.%. respectively, which is not typical of braunite II and possibly more closely resembles that of braunite "new". However, the fact that the Si-content of this braunite is typical of Ca-poor braunite, possibly suggests that in this instance at least there is substantial substitution of Ca^{2+} for Mn^{2+} in the structure of braunite. This is interpreted as possibly a localised environment of high Ca availability which agrees with the fact that the same assemblage contains the calcic manganese oxide marokite.

In drillcore GL57 from the Gloria mine area, braunite in the lower ore layer is typical of that which characterizes classic Mamatwan-type low-grade precursor ore. For this reason and due to its very fine-grained texture, it was not targeted for EPMA analyses. In the upper ore layer, which is characterized by more recrystallized textures, the contained braunite has slightly lower Si-content than typical primary/diagenetic braunite at 7.2 wt.%, and Ca-content at 1.2 wt.%. Such composition is thought to be indicative of the so-called braunite "new". The average Fe-content in this braunite (2.3 wt.%) is amongst the lowest seen in the braunite assemblages targeted for EPMA analyses in this study.

3.4. Drillcore-specific analyses of hausmannite

Contrary to the composition of braunite, and specifically the interplay between Ca, Si and Fe in the mineral structure, hausmannite is a chemically much simpler manganese oxide mineral. Therefore, the main emphasis placed on hausmannite will be on the iron partitioning in its structure, and the variability of iron concentration within each ore layer and each drillcore where possible. Note that in the case of hausmannite, manganese concentrations are plotted as Mn_3O_4.

In drillcore W162, hausmannite is an abundant ore-forming component. The hausmannite composition in this drillcore can be grouped based on iron content: the lower ore layer contains almost Fe-free hausmannite with average iron abundance well below 0.5 wt.%. Such compositions are amongst the lowest seen in the sample set examined in this thesis. Conversely, hausmannite in the upper ore layer has iron content ranging between 1-5 wt.%. Drillcore W136 also has two compositional types of hausmannite similarly to drillcore W162, with the main difference being the range of iron abundances in each ore layer. Specifically, the hausmannite grains analysed from the upper ore layer show a spread of Fe_2O_3 values from as low as less than 1wt.% to as high as over 15 wt.%. The hausmannite grains from the lower ore layer are similarly high-ranging in terms of Fe_2O_3 content, however, maximum values barely exceed the value of 8 wt.%.

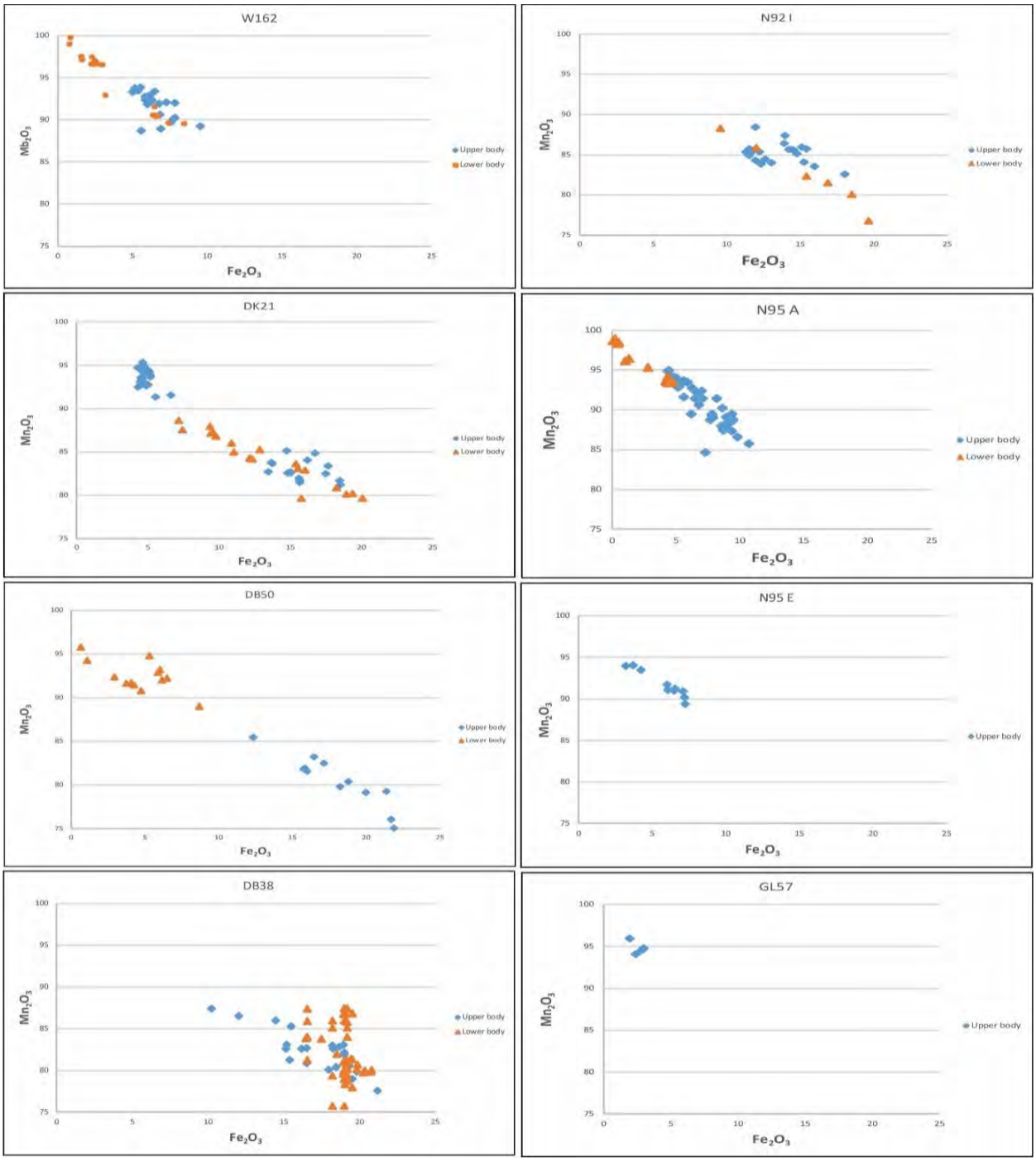

Figure 3.2: Binary plots illustrating the relationship between Mn_2O_3 *vs* Fe_2O_3 contents for braunite group minerals of this study. Data for the upper ore layers are shown in blue, for the lower ore layers in orange.

In drillcore DB7, the iron content of hausmannite in the lower ore layer has a wide range of values, from less than 1 wt.% to over 8 wt.%. By contrast, the hausmannite in the upper ore layer displays a relatively lower range of values, between 5-10 wt. %, at an average which is

consequently higher. Drillcore DK21 shows a comparable situation in hausmannite composition between the upper and lower ore layers to that of drillcore DB7, except that maximum Fe content in the lower ore layer does not exceed 5 wt.%, whereas the upper ore layer has a relatively wider range between 2 and 12 wt.% at an average of just over 5 wt.%.

The situation does not change much with drillcore W125, which shows a larger range of hausmannite Fe_2O_3 from the lower ore layer (1-8 wt.%), at an average of just below 4 wt.%. The upper ore layer has relatively higher average Fe content at 5.4 wt.% across an arguably narrow range of individual spot analyses. In summarising, all afore-mentioned three drillcores show consistently higher content of Fe in the upper ore layer and individual analyses that may show either relatively large compositional ranges or relatively narrow ones from one ore layer to the other.

With regard to drillcores N95A and DB50, hausmannite is a dominant phase only in the upper and lower ore layer respectively. The hausmannite grains analysed from drillcore N95A have a much larger spread in their Fe content from 1.5 to 8.4 wt.% at an average of just below 4 wt.%. By contrast, five analyses of hausmannite grains from drillcore DB50 show a comparatively higher Fe content at an average of just below 9 wt.%.

Drillcore N94J is different to every other of the above-mentioned drillcores with respect to hausmannite composition. The most evident difference is the very low abundances of Fe in both ore layers. Specifically, both the upper and lower ore layers have abundant hausmannite grains, with Fe contents below 1 wt.% in almost all instances. The expectation, therefore, is that the ore grade in this drillcore with respect to bulk Mn content would be among the highest. This is confirmed by results in one of the parallel MSc studies (Mr S. Dorbor, personal communication).

Drillcore GL57 from the Gloria mine area contains hausmannite in the upper ore layer assemblage, along with braunite. Hausmannite grains in that ore layer are generally low in iron at levels not exceeding 3 wt.%. These are comparable to the ones registered only in another drillcore, specifically N94J above.

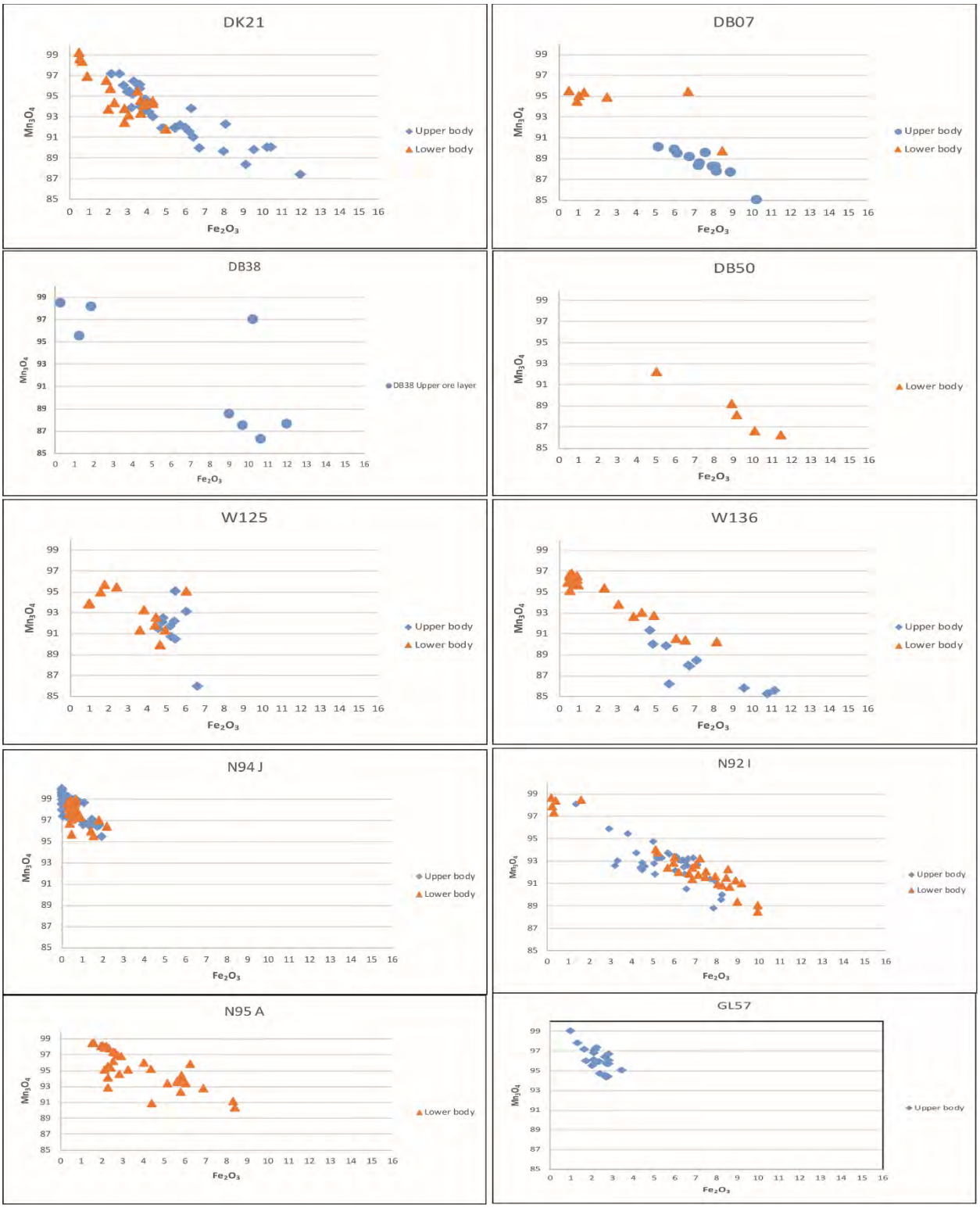

Figure 3.3: Binary plots illustrating the relationship between Mn_3O_4 *vs* Fe_2O_3 contents for hausmannite from this study. Data for the upper ore layers are shown in blue, for the lower ore layers in orange.

Finally, drillcore N92I is located very proximal to the major graben fault present in the N'chwaning and Wessels mining areas. This drillcore also shows some apparent compositional differences compared with other drillcores with respect to hausmannite. Both the lower and upper ore layers show wide-ranging hausmannite compositions, with average Fe contents that are similarly high (averages respectively at 6.3 and 7.5 wt.%). There is a possibility that the specific locality of that drillcore may be connected to the high Fe content in both ore layers due to the proximity to the graben faults. This possible connection will be discussed further in the final chapter that follows.

3.5. Mineral-specific trace element analysis *via* LA-ICP-MS

Trace element analysis was carried out on selected samples from the 12 drillcores using LA-ICP-MS. This is a mineral-specific analytical technique that has probably not been applied to the high-grade KMF manganese ores of the Wessels type before. Laser ablation inductively coupled plasma mass spectrometry (LA-ICP-MS) is becoming one of the highly and widely used methodologies for the determination of major, minor and trace elements in solids, as well as isotope-ratio measurements. During this process, samples are placed in a sample holder and enclosed in an airtight, closed ablation chamber, which is flushed with an inert gas such as argon or helium acting as carrier gas, and the laser beam is focused or imaged onto the sample surface through a cell window (Fig. 3.4). Provided the intensity of the beam is high enough and irradiance is also sufficiently high, the material will be ablated generating vapor, particles, and agglomerates that is transported to the plasma of the ICP-MS for reading (Gunther and Hattendorf, 2005).

3.5.1. Advantages of LA-ICP-MS in the analysis of geological samples

As mentioned above, LA-ICP-MS is being recognized as a viable tool for quality microanalysis, especially in the geological sciences because with this technique very small areas can be analysed and the level of instrument sensitivity involved allows for trace-element determinations at the micro-meter scale. Trace and ultra-trace analyses in a wide variety of minerals (Gunther and Hattendorf, 2005) and a full range of petro-genetically important trace elements can be determined at a rate of approximately 10 samples per hour (Perkins et al, 1993). The main advantages of the LA-ICP-MS in geological sciences is its ability to perform spatially resolved

analyses at the µm scale, and also perform bulk analyses depending on ablation spot size. Even though sensitivity is still a major area of further research, the technique already provides superior LODs by comparison with other solid-sampling techniques such as XRF (Gunther and Hattendorf, 2005). Furthermore, short analysis times and minimal sample preparation make it especially attractive to researchers.

3.5.2. Factors affecting accurate elemental analysis with LA-ICP-MS

Although the LA-ICP-MS is a reliable form of analysis, the accuracy and precision of elemental analyses can be limited by many factors including:

- laser ablation conditions;
- ICP-MS analytical conditions;
- instrumental sensitivity drift;
- matrix effects between the sample and standards;
- fractionation effects;
- the accuracy of the recommended values for reference materials used for calibration; and,
- the internal standard/s used for normalization.

These limitations can however be addressed; reference materials are used in LA-ICP-MS as samples for qualitative calibration, quality control and assurance, and the development of methods and for inter-laboratory comparisons of analyses data (Yongsheng *et al*, 2013; Perkins *et al*, 1993. Two types of reference materials were used in this study (Figure 19); a synthetic reference glass, from the National Institute of Standards and Technology (NIST), and a geological reference glass with natural compositions from the USGs, BHVO-2G, which is acquired by direct melting of natural rocks and soil powders.

Other factors, as mentioned earlier, that must be taken into consideration when one is performing this type of analyses on these types of rocks, were issues such as sensitivity drift and the use of internal standards. Sensitivity drift in LA-ICP-MS analysis is one of the most important factors that influences the uncertainty of an analysis; the drift can occur during laser ablation and ICP-MS analysis processes. Internal normalization is a classic method for correcting the ICP-MS sensitivity drift.

Calibration is often done using the aforementioned glass standards made from silicates materals. These can also be used to analyse for metal oxides such as ones being investigated in this study. Over the years, the technique of analysing element concentrations with LA-ICP-MS has been widely and maturely applied to numerous geological samples (e.g. Yongsheng *et al*, 2013; Perkins *et al*, 1993). Given the research status and problems mentioned associated with elemental analysis using LA-ICP-MS, Yongsheng *et al* (2013) suggest the following work to be conducted in the future: (1) development of matrix-matched reference materials for different minerals (especially for metal oxides and sulphides as silicate glass standards that are used in the case of metal oxides); (2) the establishment of accurate analysis methods with a high spatial resolution for natural minerals; (3) the development of a common protocol for data reduction and

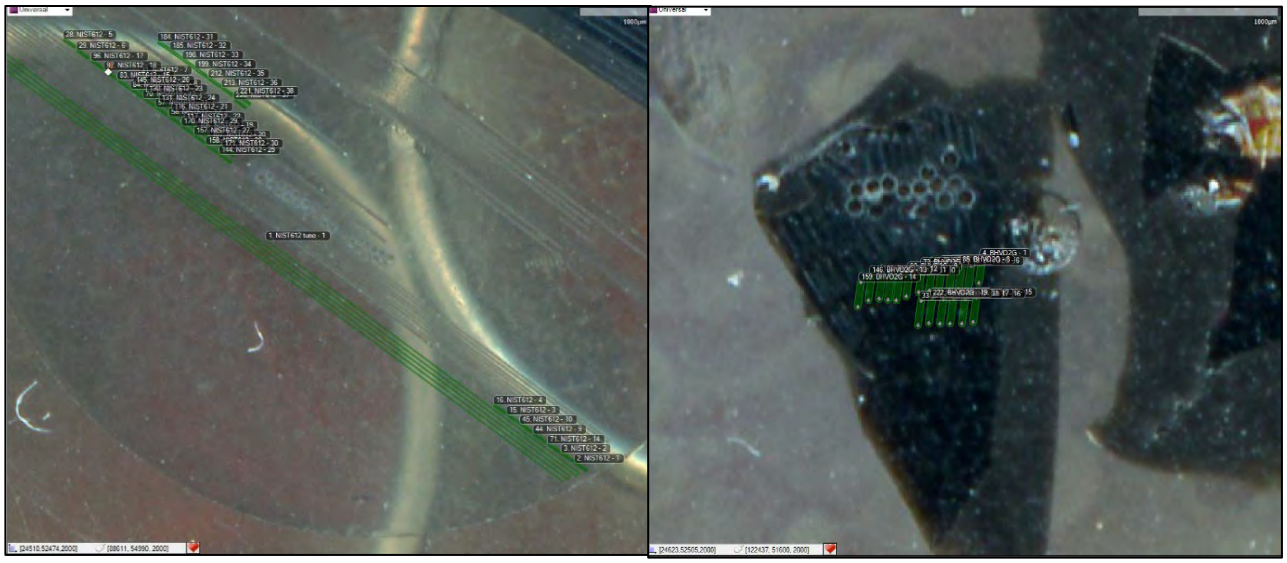

reporting for scientists to be able to compare and interpret these data accurately; and (4) the expansion of the application areas of element analysis using LA-ICP-MS. All factors were taken into consideration during analysis and data treatment of this study.

Figure 3.4: Microscope image illustrating the reference material glasses used in this study namely NIST612 and BHVO2G (green lines represent areas of ablation)

3.6. LA-ICP-MS analyses of Wessels-type Mn ore minerals

A small number of samples (7) were selected from different cores from the northern KMF for trace element spot analysis using LA-ICP-MS instrumentation. Samples were selected after the EPMA analyses was carried out on them, to determine their overall mineral chemistries and relative variations. As illustrated in the previous sections, mineralogically the ores contain variable modal abundances of two ore-forming minerals, namely braunite (I, II, "new") and hausmannite (Hewett, 1972; Jarosch, 1978; De Villiers, 1980; Moore and Araki, 1987; Gutzmer and Beukes, 1995, 1996), and less so those of bixbyite, marokite and manganite. In terms of accessory mineral species, the minerals andradite, barite and carbonates (calcite and/or dolomite) appear to dominate. Microprobe analyses of braunite grains reveal a wide range of Fe_2O_3 contents from as low as <1wt% to as high as >22 wt% (see section 3.3, this chapter). Both the bottom and the top ore layers record a comparable range in braunite compositions. Similarly, microanalyses for hausmannite grains record Fe_2O_3 contents that reach a maximum value for both the top and bottom ore layers at 15 wt.% (section 3.4 earlier). Analytical results from individual drillcores generally display tight clustering of braunite and hausmannite concentrations for both Mn vs Fe in x-y space, though exceptions to this do exist for certain drillcores (e.g. drillcore W136).

3.7. Trace element compositions of braunite and hausmannite

It was shown in the previous sections that both braunite-group minerals and hausmannite are capable of hosting substantial iron. The iron content can vary according to drillcore and from one Mn ore layer to another. Braunite grains with varying iron content were thus selected for LA-ICP MS, and a similar principle was applied in the case of hausmannite grains. The analyses obtained were normalised against low-grade Mamatwan type ore for comparison purposes (bulk-rock analytical data for low-grade ore are included in the APPENDIX, courtesy of Dr X. Mhlanga (Mhlanga, 2020).

Trace element concentrations obtained (Figures 3.5 and 3.6) show substantial variability across the two ore layers and across individual drillcores. For both braunite and hausmannite, trace alkali and alkali earths (such as Ba, Li and Sc) have normalized concentration ranges against bulk low- grade Mn ore that fluctuate generally between 0.1 and 10, and occasionally as high as

>100 (particularly for Sc). Selected trace metals, especially from the transition group (Co, Zn, Cu) as well as lanthanides (La, Ce) show relatively higher concentrations by comparison, that may reach values on the order of 100s ppm relative to those of bulk low-grade precursor Mn ore. Lead, in particular, registers concentration ratios against bulk low grade Mn ore in excess of 1000 in some ore samples.

One particular drillcore (N92I) located proximally to a major graben fault relative the other selected cores, displays trace element concentrations that are approximately an order of magnitude higher than those for the other drillcores. Iron abundances in hausmannite and braunite from the same ore samples are also consistently high. There is, however, no obvious systematic relationship that can be obtained between major element variation (essentially variation in Fe) in individual braunite and hausmannite grains, and corresponding trace element variations. For example, drillcore DB38 contains braunite with even higher Fe content than braunite from drillcore N92I, yet the corresponding trace element analyses reveal relatively low concentrations, comparable to those from other low Fe counterparts.

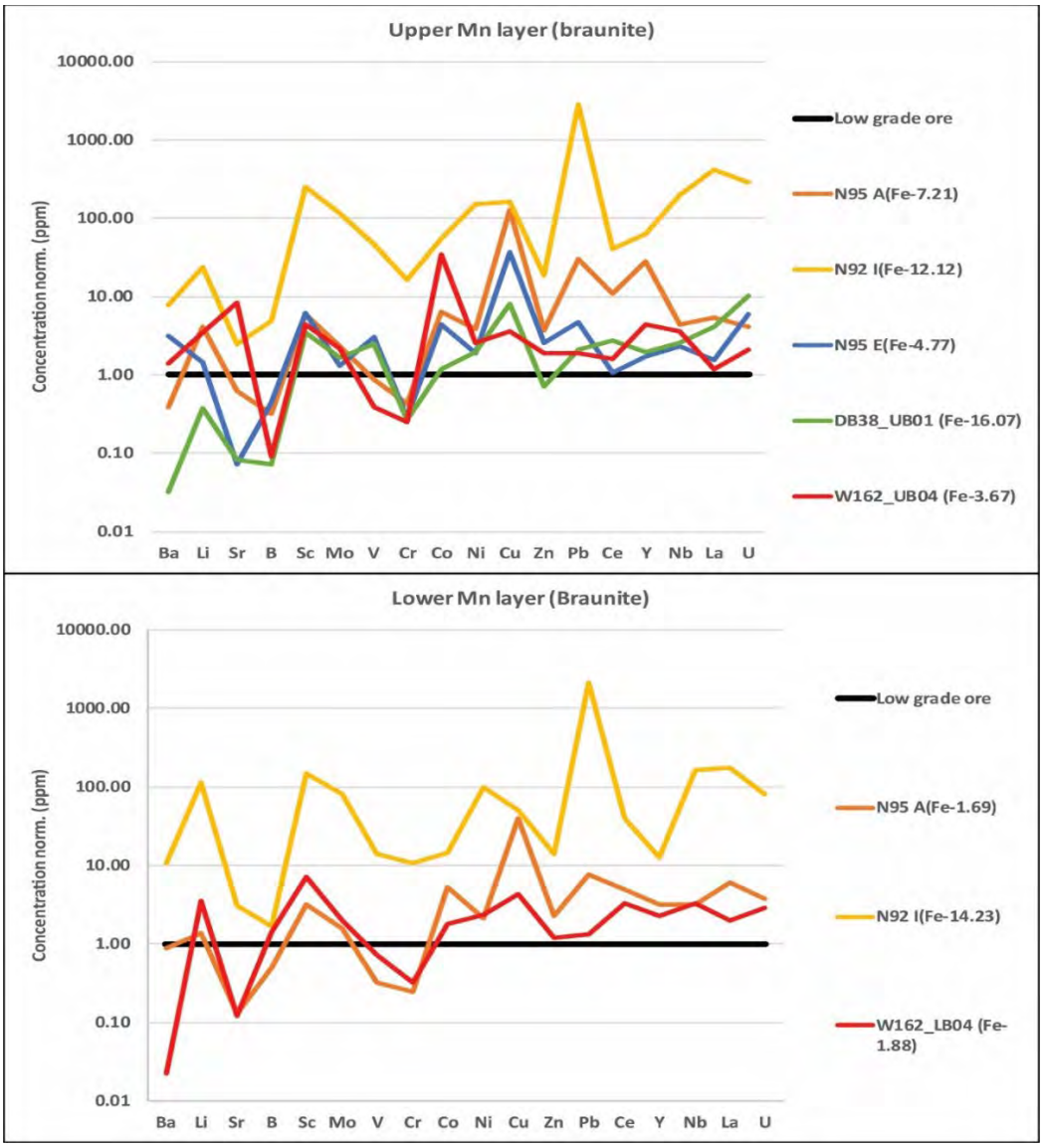

Figure 3.5: Spidergrams of LA-ICP-MS trace element data for braunite from high grade Mn ore of the northern KMF, normalised against respective average data of bulk low-grade Mn ore from Gloria Mn mine. Iron content (determined as Fe_2O_3 through EPMA) of the braunite grains is highlighted in the legend.

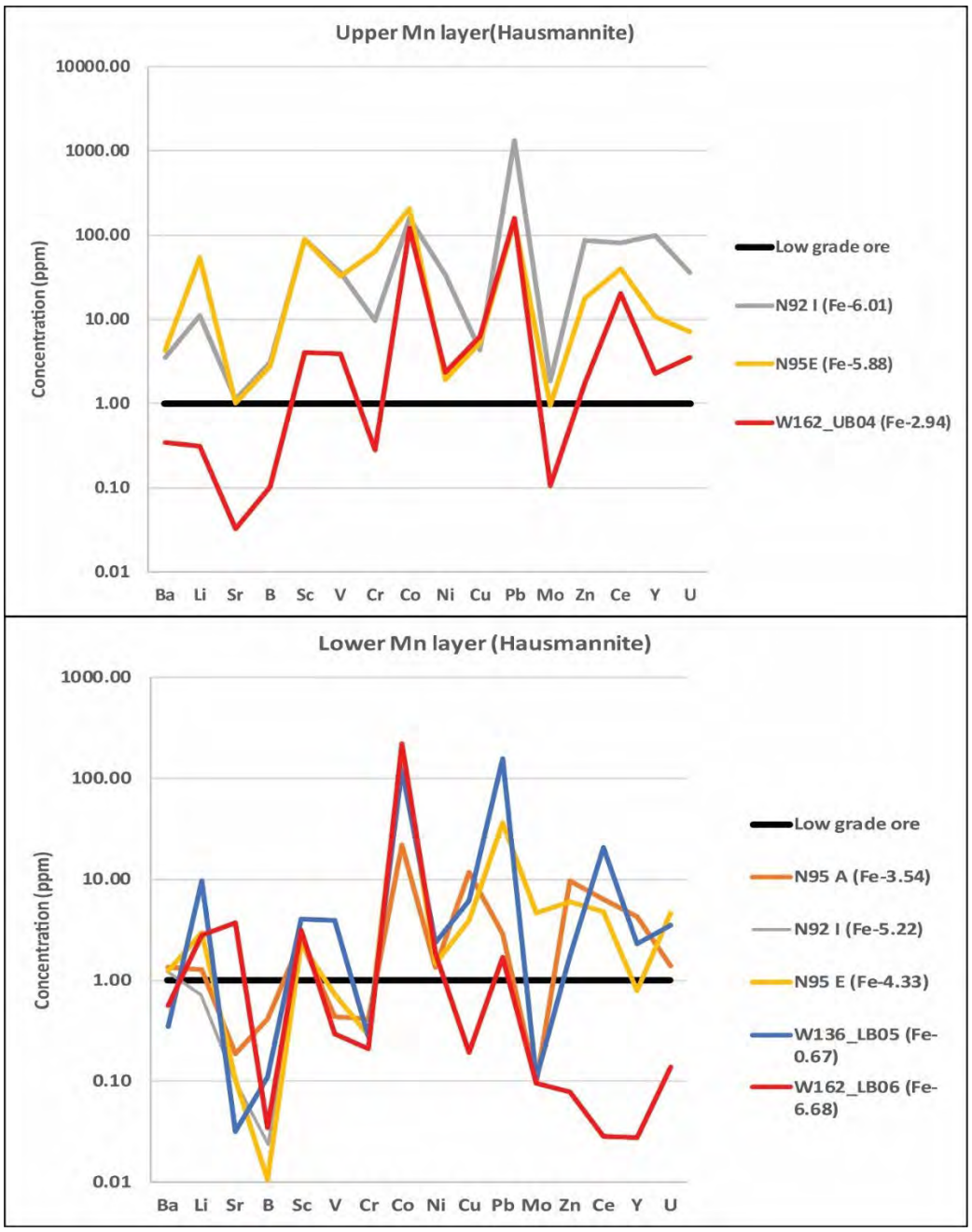

Figure 3.6: Spidergrams of LA-ICP-MS trace element data for hausmannite from high grade Mn ore of the northern KMF, normalised against respective average data of bulk low-grade Mn ore from Gloria Mn mine. Iron content (determined as Fe_2O_3 through EPMA) for the same grains is shown in the legend.

4. DISCUSSION AND CONCLUSIONS

As indicated in the introductory sections of this thesis, the present study attempts, probably for the first time, to elucidate the origins of compositional variability in the Wessels type ores, by exploring the mineralogy and mineral chemistry of not only the lower manganese layer but also the upper one. It is perhaps important here to reiterate the overarching motivation of this study, which is centred around the following two-fold hypothesis: firstly, if the prevailing fault-controlled model for Wessels-type ore formation is correct (Gutzmer and Beukes, 1995), then one would reasonably expect that each ore layer will record comparable mineralogical associations in space, given that the original protolith controls are almost indistinguishable – both mineralogically and geochemically (Mhlanga, 2020) – and the postulated faults-conduits for fluid flow are essentially vertical and dissect the entire Hotazel Formation. Secondly, the attractive global market for Mn ore and overall demand for steel manufacture, results in the increasing interest in the upper ore layer as an important additional resource of manganese. It is therefore crucial for mine geologists involved in the exploitation of Wessels-type ore, to be able to know if the same model of mineralogical and geochemical variability – and thus grade distribution – can be applied to both ore layers. If it cannot, then it becomes clear that the long-standing fault-controlled model of Gutzmer and Beukes (1995) may warrant revision, and/or other controls of mineralogical and geochemical variability may need to be additionally considered.

4.1. Bulk mineralogy and textural variations across 3D space

Table 4.1 provides a summary of the mineralogy of Wessels-type ore as determined through the mineralogical work on the 12 drillcores selected for this study. In terms of micro-textures of high-grade Mn ore, these vary significantly across drillcores and within each drillcore (Figure 4.1, 4.2, 4.3). For convenience, a textural subdivision of the ores is thus made here on the simple basis of whether primary lamination and ovoids that typify the postulated low-grade Mn precursor ore, appear to be pseudomorphically preserved or not. It should be noted, however, that textural observations here are confined to a hand-specimen (i.e. “thumbnail” quartered-core samples) and thus small scales; it is therefore possible that even ore intersections that do not

display characteristic lamination from the precursor "protore", they may in fact still do so on a larger (i.e. mine stope or outcrop) scale.

Table 4.1. Summary of mineralogical composition of high-grade Wessels-type ore as determined on the 12 selected drillcores used in this thesis. Key: XXX = abundant; XX = common; X = minor

Upper Mn ore layer	W162	W136	W125	DB38	DB7	DB50	DK21	N92 I	N94 J	N95 A	N95 E	GL57
Andradite	XXX	-	XX	-	XX	-	-	X	-	X	-	-
Apatite	-	X	-	-	-	-	X	-	-	-	-	-
Barite	X	-	-	X	-	XX	X	X	XX	-	X	-
Bixbyite	-	-	-	-	-	-	-	-	-	-	-	-
Braunite	XX	-	-	-	X	-	X	-	XX	XX	X	-
Braunite "new"	XXX	-		-	-	-	XX	-	-	XXX	XX	XX
Braunite II	-	-	-	XX	-	XXX	XXX	XX	-	-	-	-
Calcite	XX	X	XX	XX	-	XXX	X	XX	X	-	XX	XX
Dolomite	XX	-	-	XX	-	-	-	-	-	XX	-	X
Hausmannite	X	XXX	XXX	XXX	XXX	X	XX	XXX	XXX	X	XXX	XX
Hematite	X	-	-	X	-	-	-	X	X	-	X	X
Manganite	-		-	-	-	-	-	-	-	-	-	-
Marokite	-	XXX	-	-	-	-	-	X	X	-	XX	-
Strontianite	-	-	-	-	-	-	XXX	-	-	-	-	-
Lower Mn ore layer												
Andradite	X	XX	XX	XX	-	-	X	XX	-	-	XX	-
Apatite	-	-	-	-	-	-	-	-	-	-	-	-
Barite	X	-	XX	X	-	X	X	-	X	-	X	-
Bixbyite	-	-	-	-	-	-	-	-	X	-	-	-
Braunite	-	-	XX	-	-	XXX	-	-	-	X	-	XXX
Braunite "new"	X	-		-	-	-	XX	X		XX	-	-
Braunite II	X	-	-	XXX	X	-	XX	-	-	-	-	-
Calcite	XX	XX	XX	XX	XX	XX	X	XX	XX	X	-	X
Dolomite	-	-	-	-	-	-	-	-	-	-	-	-
Hausmannite	XXX	XXX	XXX	X	XXX	X	XXX	XXX	XXX	XXX	XXX	X
Hematite	-		-	X	X	-	-	X	-	X	-	-
Manganite	-		-	-	-	-	-	-	-	-	X	-
Marokite	-		-	-	-	-	X	-	-	-	X	-
Strontianite	-		-	-	-	-	-	-	-	-	-	-

Where preservation of laminae and ovoids of possible primary origin appear to be absent and thus completely destroyed, textures are usually defined by massive, micro-crystalline Wessels-type ore often containing crosscutting veins and vugs/fissures filled out by secondary mineralogy. Where replacement – and thus preservation of primary carbonate laminae and ovoids – is inferred, the secondary manganese mineralogy (mainly hausmannite and less so braunite II) is thought to have replaced the primary carbonate-rich assemblages through basic reactions such as the one below:

$$3CaMnCO_3 + 2O_2 = Mn_3O_4 + 3CaCO_3$$

The above is a hausmannite-forming reaction whereby ideal kutnohorite is oxidized to form hausmannite and secondary calcite; andradite would also possibly form as a product implicating

decarbonation and incorporation of Fe and Si through a similar reaction. Texturally, hausmannite is observed to assume the shape and orientation of the carbonate that has been replaced. Such assemblages and textures are documented from drillcore DB7 in the upper ore layer, and drillcores W136, W162, N92I, N94J and N95E in the lower ore layers.

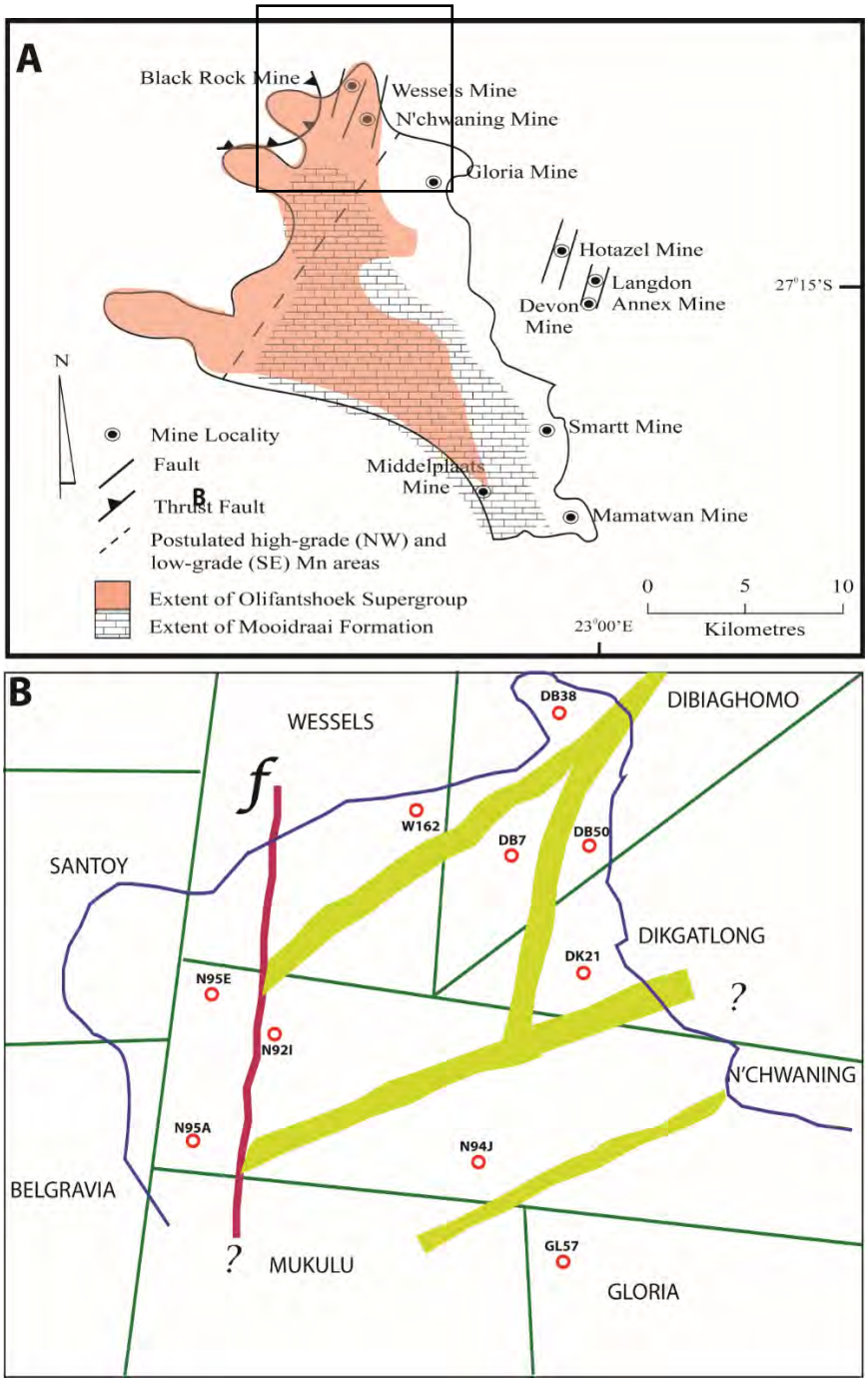

Figure 4.1. A. Map, of the KMF illustrating major geological features, mine localities and the high Mn-grade area containing Wessels-type ore (inset). B. Enlargement of the northernmost KMF illustrating farm boundaries, major structures and borehole locations used in this study.

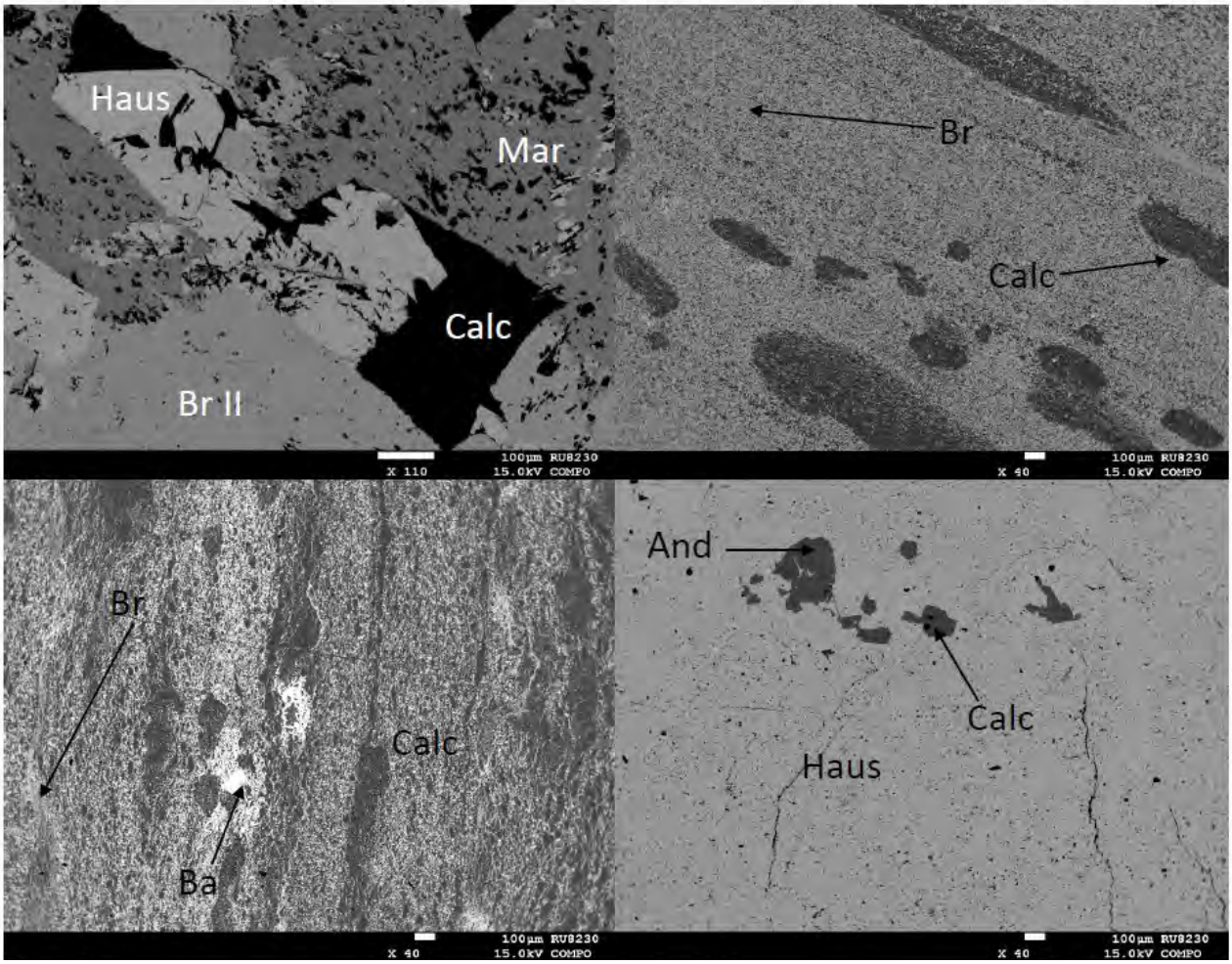

Figure 4.2: Representative textures of high-grade Mn ore in the northernmost KMF. Top left: upper ore body, N94J. Top right: lower ore body, W162. Bottom left: upper ore body, GL57. Bottom right: lower ore body, N95E.

As mentioned earlier, barite and andradite in the KMF are considered to be hydrothermal forming minerals and thus one would expect them to be more abundant in highly altered ores where primary structures are not preserved. Indeed, where primary laminations are preserved, minerals such as barite, andradite and less commonly marokite, are essentially low in abundance or absent. Based on these observations, a tentative conclusion can be drawn that the andradite in the Wessels-type ore is of a clear secondary origin in ores affected more profoundly by

hydrothermal activity, and the same would apply with respect to barite. Both the garnet and the barite are present usually as anhedral to subhedral grains, commonly found in massive micro-clusters but also in micro-vugs and cracks. Barite formation requires addition of both barium and sulphate from the hydrothermal fluid involved, as the primary protore does not contain sufficient abundances of either of these chemical species (Tsikos et al., 2003; Mhlanga, 2020). By contrast, formation of andradite may have only involved re-distribution of Si, Fe and Ca, which can all be sourced from the breakdown of hematite, braunite and calcite in the Mn protore.

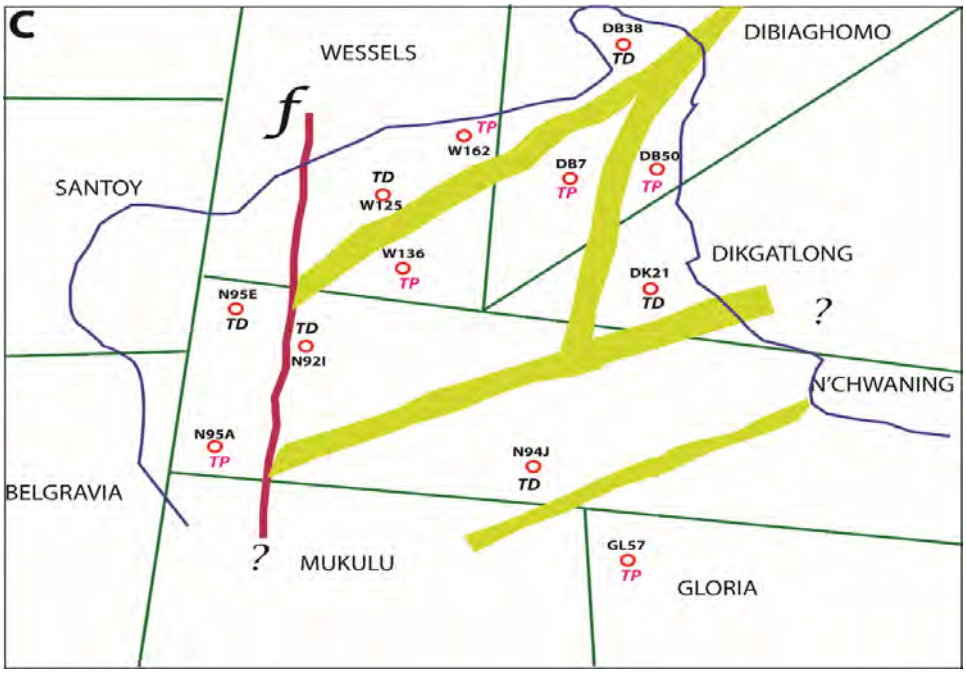

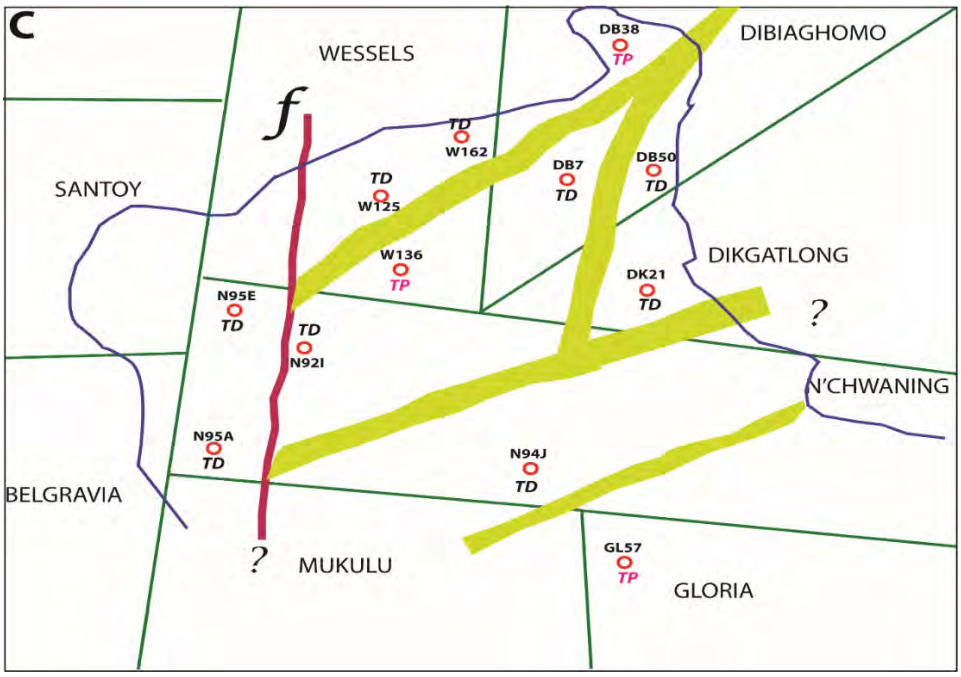

Figure 4.3: Textural variations in high-grade ores across space and within a given drillcore, northernmost KMF. TP stands for "texture preservation", while TD stands for "texture destruction". See text for details.

It should be noted that, from a chemical point of view, the andradite in the KMF ores is not manganese rich, as it only contains approximately 1 wt.% in the structure. The reasons for the exclusion of substantial Mn^{3+} from the andradite structure are not known to the author, but it may have to do with the physico-chemical conditions of formation and possibly the requirement for high pressures for trivalent manganese incorporation into the andradite lattice (Nishizawa and Koizumi, 1975).

With respect to texture preservation across space (Fig. 4.3), drillcores DB50, DB38, DB7, W136, W162, N95A and GL57 exhibit primary texture preservation even through the effect of proposed alteration events manifests in significant changes in mineralogy. The majority of the drillcores that show preserved primary textures are therefore mainly from the Wessels area, with the exception of drillcore N95A which is from N'chwaning area, and GL57 from the Gloria area. It is worth noting that lamination is mainly preserved in the upper ore layer while the lower ore layer has a more common microcrystalline texture devoid of obvious primary preservation. This indicates possibly that the lower ore layer may have experienced a more intense degree of re-crystallisation through fluid-rock interaction, or it may record a different/additional hydrothermal signature to the one that affected the top ore layer in the same localities.

4.2. Braunite compositional variability in 3D space

One of the points that becomes readily apparent from the data presented in the previous sections, is that high-grade Mn ore from the northernmost KMF shows large modal mineralogical and geochemical variability in three-dimensional space. Intuitively, such variability would require open-system chemical exchange with respect to every major element implicated in the ore chemistry. This would apply so long as the precursor low-grade Mn ore had little inherent lateral variability in its mineralogical and chemical composition for both the bottom and top ore layers. The foregoing is summarily encapsulated in the generalized reaction below, which describes in a simplistic way the overall transformation of low grade to high grade Mn ore in the northern KMF:

braunite + Mn carbonate + hematite + fluid →

braunite II + hausmannite + andradite + carbonate + barite

Both braunite II and braunite "new", are reported to be present only in the Wessels-type ore (Kleyenstuber, 1984; Gutzmer and Beukes 1995, 1996). Together with bixbyite, they are thought to be reaction products of oxidizing hydrothermal fluids that would have reacted with primary braunite and carbonate minerals from Mamatwan-type ore, leading to silica and calcium mobilisation following mineral breakdown. The circulation of such fluids is supported by the Wessels-type mineral assemblages where secondary hausmannite and braunite II, along with barite and andradite, would have formed largely through silica dissolution and mobility from the primary protore. Minerals such as bixbyite would instead form from similar secondary fluids whereby the abundances of Ca and Si may have been progressively depleted by means of earlier braunite II- and andradite-forming reactions. By contrast, formation of Mn minerals such as marokite would suggest excess Ca in a chemically more evolved hydrothermal fluid, following Si incorporation during braunite II and andradite formation.

Based on the mineral-chemical results presented earlier in this thesis (see summary Fig. 4.4 below), the generalised Wessels-type ore-forming reaction above suggests that Fe-rich varieties of the major ore forming minerals hausmannite and braunite could conceivably take up as much

Fe as to have prevented much free hematite formation during the development of high-grade ore. This is further supported by the scarcity of free hematite grains observed in high grade ore in this study, and by the common occurrence of andradite as an additional key Fe^{3+}-hosting mineral.

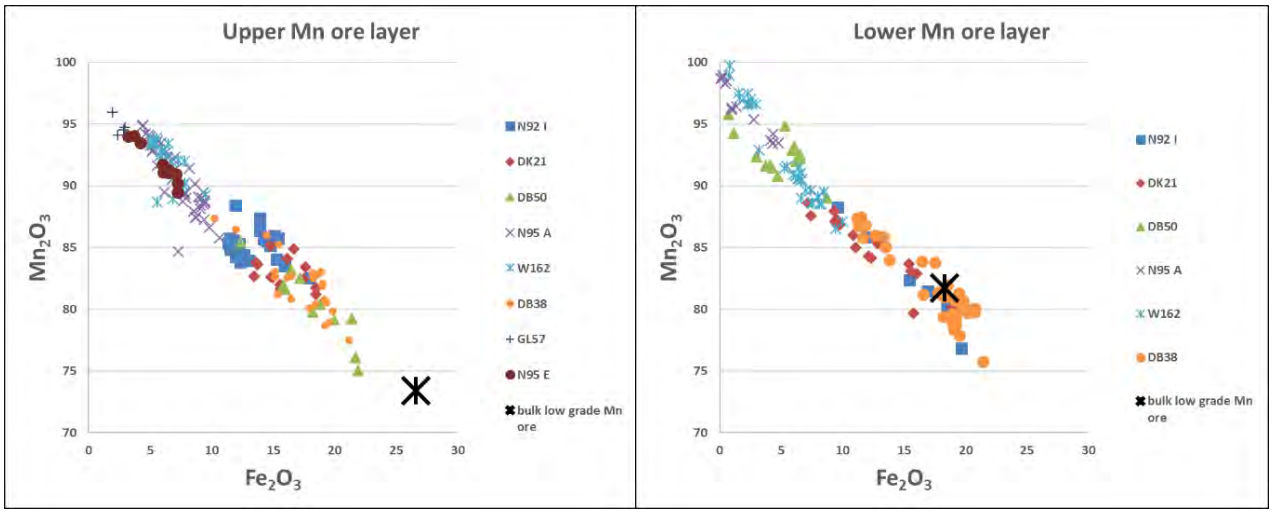

Figure 4.4: Summary of Fe_2O_3 against Mn_2O_3 data for braunite from the upper and lower Mn ore bodies. Also plotted is the data for bulk average, low-grade Mn ore precursor as obtained for both ore layers from the Gloria Mn mine in the northern KMF (Mhlanga, 2020).

Figure 4.4 presents a summary of all microprobe analyses of braunite grains from this study, which reveals the overall wide range of Fe_2O_3 contents from as low as <1wt% to as high as >22 wt. %. Analytical results from individual drillcores display a relatively tight clustering of braunite compositions, as illustrated also in previous chapters. Individual drillcores may also contain different compositional types of braunite in each of the two ore layers (upper and lower), as also shown in the summary mineralogy table shown earlier in this chapter (Table 4.1).

It is notable that both the bottom and the top ore layers record a comparable range in braunite compositions. Given that the postulated primary Fe_2O_3 content of precursor low-grade ore falls within the range of iron contents in braunite, means that Fe in the lower Mn ore-layer can be hosted almost entirely in newly-formed braunite II (or "new"), without any need for free hematite to account for any excess iron present. The situation is slightly different for the upper ore-layer which in its primary low-grade state may have contained more iron that the contents that hydrothermal Ca-braunite can account for. Nevertheless, these findings lend credence to the generally low abundance of hematite in the Wessels-type ores.

The distribution maps of Figure 4.5 provide some additional insights with regards to the compositions of braunite in three-dimensional space. In general, relatively low-Ca braunite varieties appear to dominate in the Wessels area and in proximity to the sub-outcrop of the Hotazel Formation, whereas the more calcic braunite (essentially typical braunite II) seems to dominate in the N'chwaning area in proximity to the graben fault. This indicates a rather crudely defined first-order transition in the Wessels-type ores, from Ca-poor braunite dominating to the NE in the Wessels area, giving way to more calcic braunite in a SW direction. The relative dominance of andradite along with braunite-II rich ores therefore suggests an overall trend of increasing Ca in Wessels-type ore in a SW direction from the Wessels to the N'chwaning mine, which from a structural viewpoint is analogous with the general direction from the Hotazel Formation sub-outcrop (i.e. the limit of the lateral extent of the Hotazel Formation underneath the overlying Kalahari sand cover) towards the major graben structure.

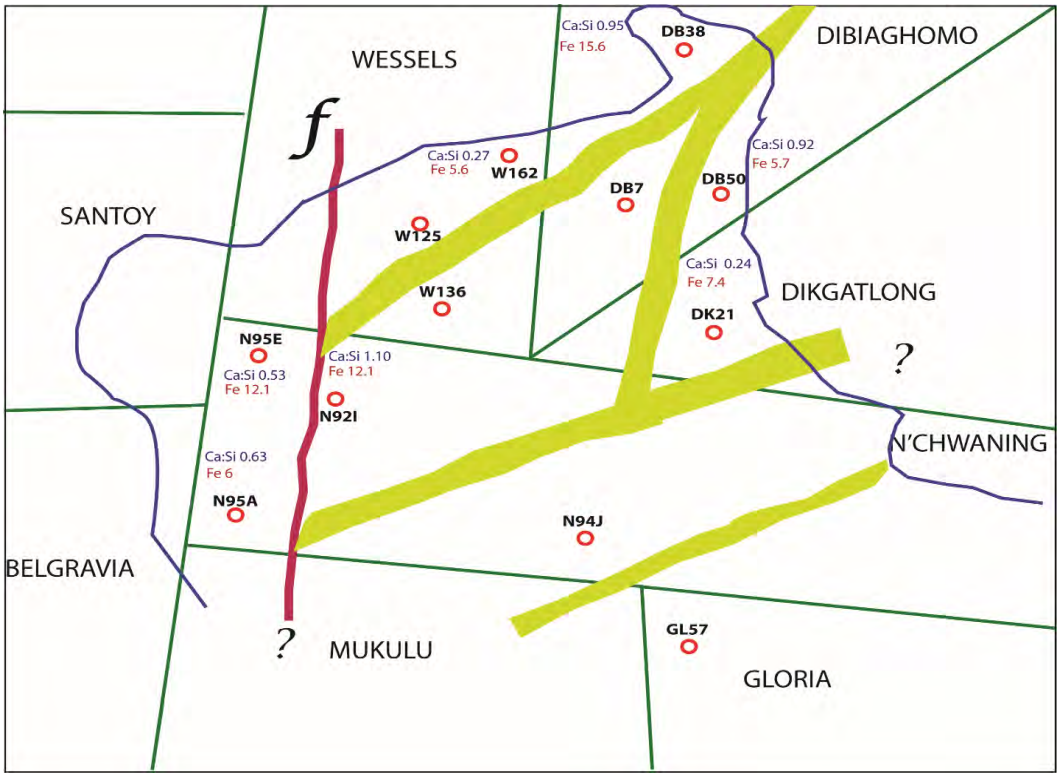

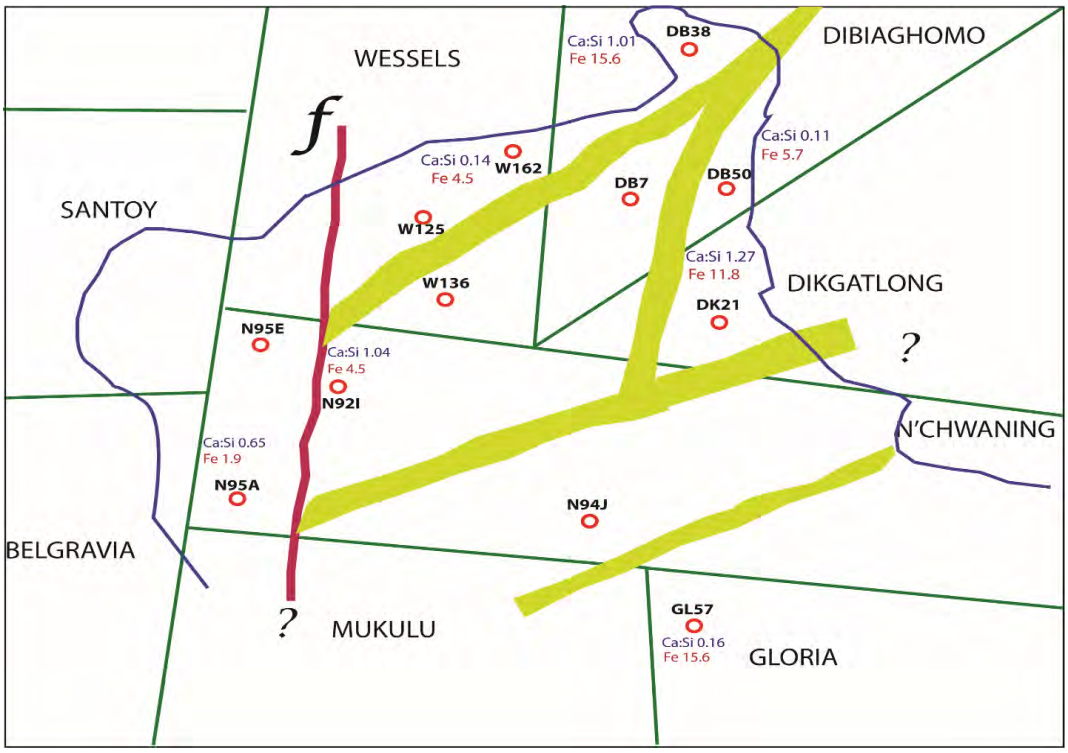

Figure 4.5. Map showing the compositional distribution of braunite group minerals in the northernmost KMF. Shown is the Ca:Si ratio indicating different braunite compositions and their corresponding Fe_2O_3 content. Note the location of NE-SW dykes (green bands) and the major N-S graben fault (red line).

4.3. Compositional variability of hausmannite in 3D space

In a similar manner to braunite, hausmannite in Wessels-type ores is also shown to be not only an abundant ore-forming mineral, but also equally capable to host much iron in its structure. Based on all data obtained from hausmannite microanalyses as displayed in Figure 4.6, the hausmannite in the upper ore layer has relatively higher Fe content than the lower ore layer, which obviously translates into correspondingly lower Mn content, as trivalent iron displaces Mn^{3+} in the mineral structure. It is interesting to stress, however, that hausmannite definitely does not outshine braunite as an Fe host: in the previous section, it was noted that braunite can have Fe contents as high as 22wt%, whereas in the case of hausmannite, a maximum concentration of 15wt% in the hausmannite structure is recorded, specifically in the upper ore layer (Figure 27). This would mean that Wessels-type ores rich in hausmannite but poor in braunite, are more likely to contain at least some free hematite as an additional iron host, something which appears to be corroborated by the bulk mineralogical results of Table 7, especially with reference to the upper Mn ore-layer.

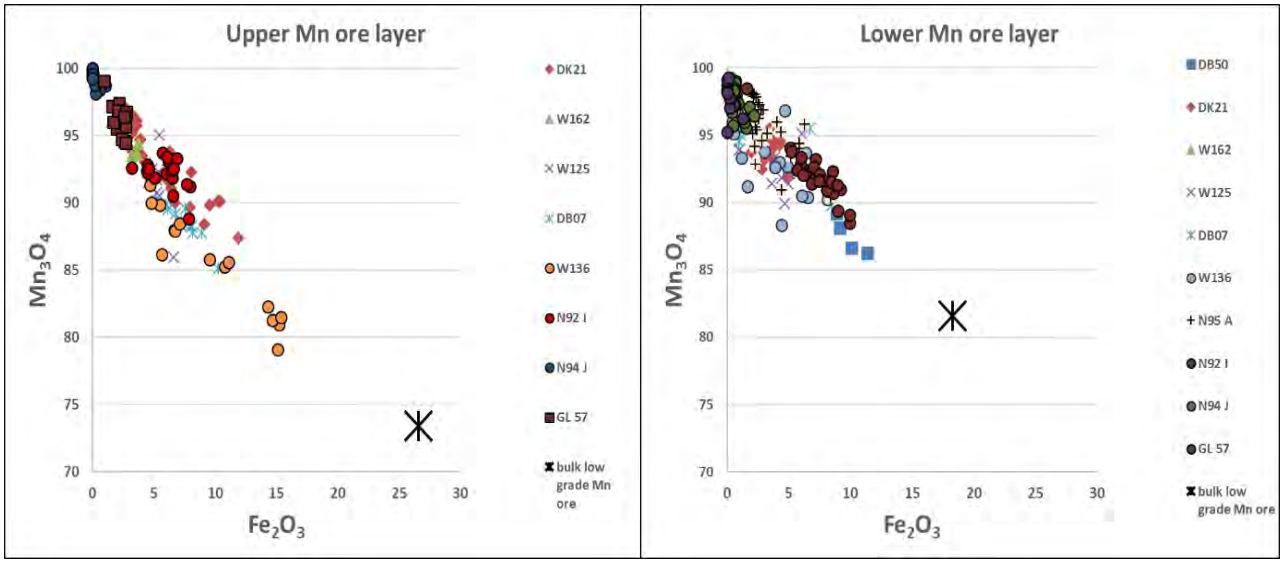

Figure 4.6: Summary of Fe_2O_3 against Mn_3O_4 values for hausmannite from the upper and lower Mn ore bodies, Also plotted is the datum for bulk average low grade Mn ore precursor for each ore-layer, as obtained from the Gloria Mn mine in the northernmost KMF.

The simple hausmannite mineral chemistry which involves essentially only Fe and Mn partitioning in the mineral structure, provides some further insights into the spatial distribution of hausmannite compositions in three-dimensional space. As illustrated in the maps of Figure 4.7,

the abundance of iron in hausmannite appears to be reaching maximum values for the upper Mn ore layer in the northern part of Wessels mine, including two drillcores from the NW corner of the N'chwaning Farm area. By contrast, hausmannite with substantially lower Fe contents appear further south in the main N'chwaning area and also Gloria. The dominance of high Fe content in hausmannite for the majority of drillcores studied, could be a function of the higher Fe content of the primary protore for the upper Mn layer. However, the fact that values iron contents in hausmannite can drop below 1wt% (see drillcore N94J), means that high bulk Fe in the upper ore layer does not always mean high iron abundance in hydrothermal hausmannite. It follows that the behavior of Fe during Wessels-type ore formation may have been open, which means that iron was transported in hydrothermal solutions during high-grade ore formation, at least to some extent.

The situation with the lower ore-body when it comes to the iron content in hausmannite, is somewhat different. Over most part of the Wessels and N'çhwaning mine areas, the abundance of Fe in hausmannite is relatively low, except for drillcores near the graben fault where maximum iron contents are seen. This is probably a function of local iron addition in these areas as a result of hydrothermal fluid circulation related to the major graben fault. Otherwise, the overall lower Fe content in the lower Mn ore layer must be related to the lower Fe contents in the primary protore as seen in the Gloria mine area (Mhlanga 2020).

4.4. Trace element data and geometallurgical implications

The few analyses of the trace element composition of braunite and hausmannite grains presented in the last chapter, allow for some conclusions to be made that have both fundamental and potential practical implications. For that reason, selected data as obtained with the LA-ICP-MS technique for both braunite and hausmannite from specific samples, are plotted again here along with corresponding bulk-ore data for N'çhwaning high-grade ore (data from Gutzmer and Beukes, 1995). All data, namely bulk and mineral specific analyses, have been normalized against the bulk composition of primary low-grade ore from Gloria Mn mine (Mhlanga 2020), which is taken throughout this thesis as the closest precursor protore composition for both ore layers. The resultant spidergrams therefore show mineral-specific results along with

corresponding bulk ore ones from the literature, and the “1” line corresponds to the base line for precursor low-grade Mn ore in each case.

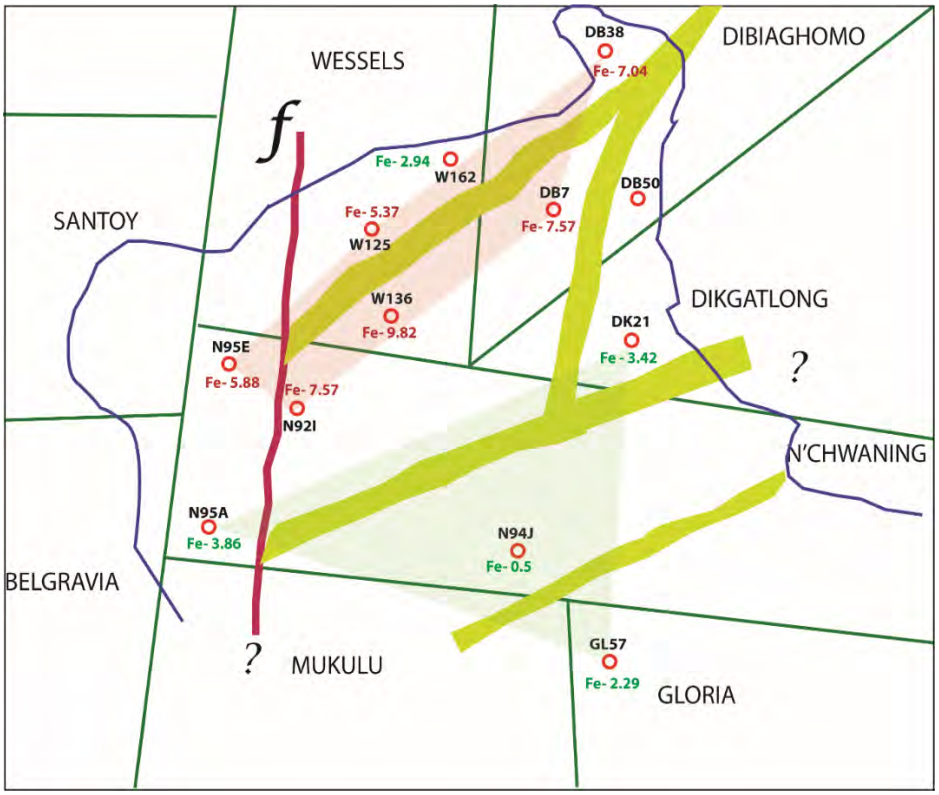

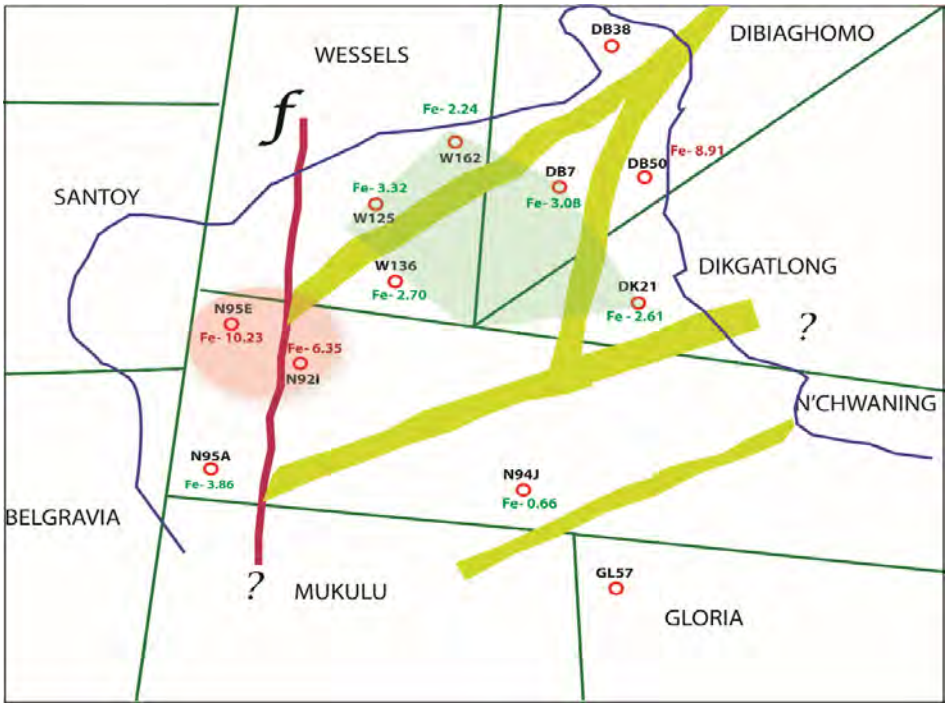

Figure 4.7: Iron content (as Fe_2O_3) of hausmannite grains from the upper ore layer (top) and the lower ore layer (bottom) shown across the northernmost KMF. Green highlighted zones represent values below 5wt.% Fe and red highlighted ones show those above 5wt.% Fe.

The spidergrams shown for both braunite and hausmannite trace element compositions (Figures 4.8, 4.9) suggest that both minerals can serve as excellent trace element hosts during high-grade Mn ore formation, and can therefore account for the bulk ore trace element geochemistry in their own right. The large relative enrichment in trace element concentrations of high-grade ore also probably requires a significant open system contribution from circulating hydrothermal fluids, rather than simple redistribution of these elements from precursor ore as suggested previously (Chetty and Gutzmer, 2012). The widespread presence of barite (i.e. addition of hydrothermally sourced Ba and S) and the documented common occurrence of aegirine-rich assemblages at BIF-Mn ore contacts (metasomatic addition of Na; Tsikos and Moore, 2005) lend additional support to this suggestion.

Figure 4.8: Spidergrams of LA-ICP-MS trace element data for braunite from high grade Mn ore of the northern KMF (N'chwaning Mn mine), normalised against respective average data of bulk low-grade Mn ore from Gloria Mn mine. Braunite-hosted iron (Fe_2O_3) contents are highlighted in the legend. Corresponding bulk ore data are plotted for comparison

Compositional evidence from a single drillcore (N92I) close to a major fault structure, has raised the possibility that extreme hydrothermal input of trace elements may be related to localized, structurally enhanced fluid-flow. Future supporting evidence will be needed to firmly establish such a relationship. From a geo-metallurgical viewpoint, a key implication of the current study is that there is probably no single control for the distribution of trace elements in the high-grade Mn ores of the KMF. Our results do demonstrate, however, that sound and thorough understanding of the trace element composition of standard ore-forming Mn minerals can provide key clues into the trace element variability of Mn ore without the need to consider exotic accessory mineralogy. Application of trace element analyses on ore-forming Mn minerals using LA-ICP-MS techniques has therefore clear potential to add crucial value to the metallurgical process for Mn ore.

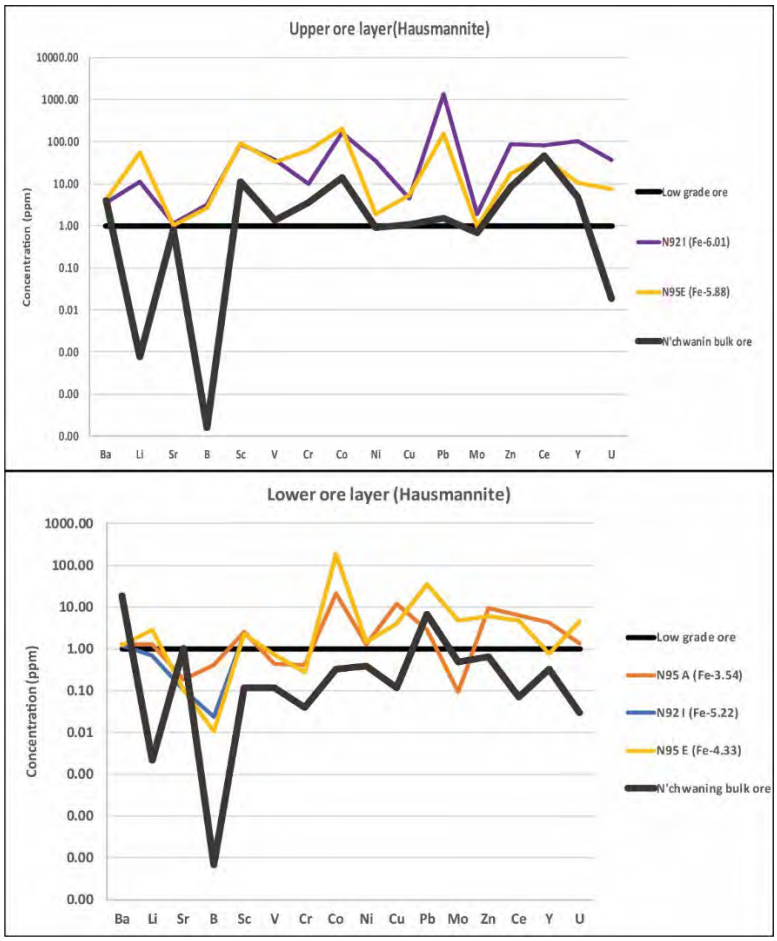

Figure 4.9: Spidergrams of LA-ICP-MS trace element data for hausmannite from high grade Mn ore of the northernmost KMF, normalised against respective average data of bulk low-grade Mn ore from Gloria Mn mine. Iron (Fe_2O_3) content within the braunite is highlighted in the legend. N'chwaning bulk ore data plotted for comparison.

4.5. Genetic implications and conclusions

This study dealt with the three-dimensional mineralogical and mineral-chemical variability in high-grade Mn ore from the northernmost KMF (Wessels, N'chwaning and Gloria mines), with main aim to understand the controls of that variability in light of existing genetic models. The results demonstrate that there is a significant variation in the mineralogical and geochemical characteristics of these Mn ores both vertically and laterally. Mineralogically, the ores contain variable modal abundances of the ore-forming minerals braunite (I, II, "new") and hausmannite, and much less so of bixbyite, marokite and manganite. In terms of accessory mineral species, the minerals andradite, barite and carbonates (calcite and/or dolomite) dominate. Variations in

qualitative mineralogy and relative modal mineral abundance are significant laterally across the different drillcores for each of the two layers examined, and is even also observed between the upper and lower Mn ore layers within a single drillcore. An extreme example of the latter situation is the case of drillcore GL57 from the Gloria Mine area, where the upper ore-layer is made up of high-grade Mn ore, whereas the lower ore layer contains classic low-grade, Mamatwan-type Mn ore.

Consideration of the three-dimensional distribution of textural types of high-grade Mn ore on the basis of whether primary ore textures are preserved or not, revealed that primary texture preservation is more prominent in the Wessels mine and particularly the northern part of the area in proximity to the so-called Hotazel Formation "suboutcrop". In that area, the main ore-forming mineral appears to be hausmannite and less so Ca-poor braunite, suggesting that higher Mn ore grades would be expected here. Texture destruction, by contrast, seems to be affecting the ores that are dominated by braunite II (along with much andradite, barite and secondary calcite), and therefore naturally contain increased Ca and Si. The mineral chemical signatures of braunite across space seem to corroborate these findings: braunite II becomes more dominant as one moves in a broadly southwesterly direction towards the major graben fault structure, and this can be taken as also signifying an overall decline in the Mn ore grade in the same direction. With regards to hausmannite chemistry in space, the increased Fe content near the graben fault probably indicates introduction of Fe from fluids circulating along that fault (and this applies to braunite from the same area), and it also shows a higher Fe content in the upper ore layer which is probably a result of inheritance of higher primary Fe in the low-grade protore.

There are multiple post-depositional alteration events that seem to have affected the KMF ores (Wessels, Smartt, Mamatwan) with the Wessels event of Gutzmer and Beukes (1995) being the main one that results in the spectacularly diverse and intricate mineralogy observed in the northernmost KMF. The prevailing model by Gutzmer and Beukes (1995, 1996) for the Wessels event, proposes that hydrothermal circuation along major N-S-striking and minor E-W-striking faults may have affected Mamatwan type ore by transforming it into oxide-rich, carbonate-poor high-grade Wessels-type manganese ore (Gutzmer and Beukes, 1995; Beukes et al., 1995). This reported overall transformation of Mamatwan type ore would have primarily involved the breakdown of earlier sedimentary carbonate minerals. It was further noted by the same authors,

that the degree of alteration and Mn enrichment would be at its highest immediately adjacent to the fault structures, which are reported as the key feeder channels (see Figure 4.10). Predictable mineral assemblages would therefore develop away from the faults in both ore layers exposed to the process, over distances of a few 10s of meters to perhaps just over 100m distance from the fault zones (Gutzmer and Beukes, 1995). With time, these zones of alteration adjacent to the feeder channel would have widened as hydrothermal overprinting continued (Figure 4.10).

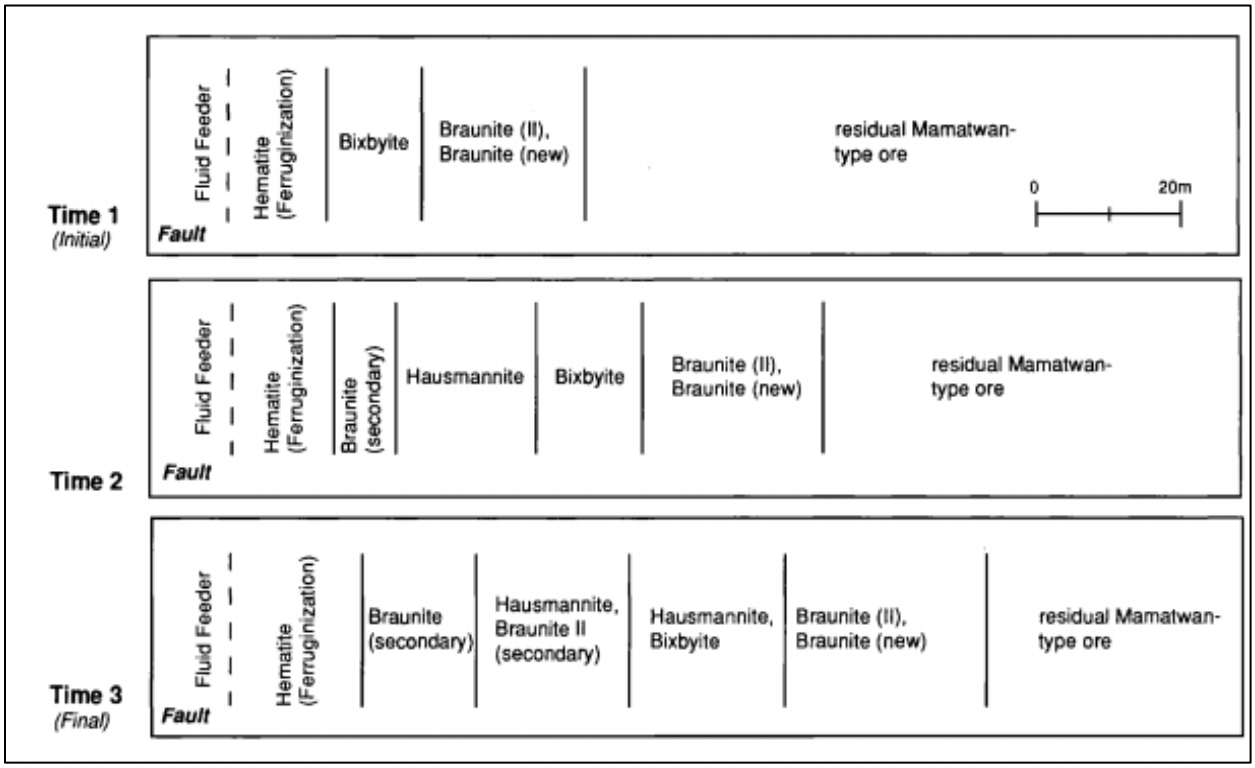

Figure 4.10: Paragenetic model for the temporal and spatial development of zones of different manganese ore types relative to feeder channels (from Gutzmer and Beukes, 1995).

The present study adds a new dimension to the existing model of Gutzmer and Beukes (1995): it considers both ore layers (upper and lower) in the Hotazel Formation, and assumes a protolith for both that must have been of very similar composition, as shown from previous studies at the Gloria Mine area where precursor Mamatwan-type ore is being exploited at present (Mhlanga, 2020). The present study was also conducted over a much larger geographical area than the one which is considered in the fault-controlled model of Gutzmer and Beukes (1995), but the lack of outcrop and necessity to study drillcore material makes difficult to extract results that show continuity in space. Despite these problems, the results presented here provide some important

new information which seems to be at variance with the prevailing faut-controlled model: firstly, it appears as though the richest Mn ore that contain hausmannite and not so much braunite, are concentrated further away from the major graben fault which would arguably have acted as one of the main hydrothermal fluid pathways. Secondly, there is significant heterogeneity in mineralogy and geochemistry between the two ore layers, whether one looks at these two ore-layers across different drillcores, but also within a given drillcore. Thirdly, the situation with drillcore GL57 is especially telling, because here the upper ore layer only is high grade while the lower ore-layer shows no evidence of hydrothermal alteration and metal upgrading.

The above observations collectively come into conflict with a hydrothermal alteration model involving vertical fault conduits (Gutzmer and Beukes, 1995; Beukes *et al*, 1995) in a very gently-dipping (near-horizontal) sedimentary sequence (the Hotazel strata in the northernmost KMF have a true SW dip that barely exceeds 15 degrees). Simply speaking, it is hard to envisage such diverse hydrothermal effects on all scales through a single hydrothermal alteration model operating along vertical faults, on two ore layers that would have had very similar primary mineralogical and geochemical composition and are stratigraphically separated by only a few meters of BIF. It is therefore considered both possible and plausible, that hydrothermal activity was not confined to a single fault-controlled fluid event in space and time, but rather consisted of several discrete temporal events which may have utilised a variety of structural conduits. Among such conduits is possibly the unconformity between the Hotazel strata and the overlying Olifantshoek sedimentary sequence (Land et al., 2017), in accordance with previous suggestions for unconformity-controlled alteration effects in the Hotazel Formation (Tsikos *et al*, 2003), and resultant variability in the degree and style of alteration effects in a top-down sense. Whatever the case, the origin of the Wessels type Mn ores in the KMF remains a highly fertile area for future and rigorous research.

5. BIBLIOGRAPHY

Armstrong, F.A. (2008). Why did Nature choose manganese to make oxygen? *Phil. Trans. Biol. Sci.,* **363**, 1263-1270.

Baron, V., Gutzmer, J., Rubdlo, H. and Tellgref, R. (1998). The influence of iron substitution on the magnetic properties of hausmannite, $Mn^{2+}(Fe,Mn)O_4$. *American Mineralogist,* **83**, 786-793.

Bau, M., Romer, R.L., Lüders, V., Beukes, N.J. (1999). Pb, O, and C isotopes in silicified Mooidraai dolomite (Transvaal Supergroup, South Africa): Implications for the composition of Paleoproterozoic seawater and 'dating' the increase of oxygen in the Precambrian atmosphere. *Earth and Planetary Science Letters*, **174**, 43-57.

Beukes, N.J. (1983). Palaeoenvironmental setting of iron-formations in the depositional basin of the Transvaal Supergroup, South Africa, in Trendall, A.F. and Morris, R.C. (Eds.), *Iron-Formation: Facts and Problems*. Elsevier Science, Amsterdam, pp. 131–209.

Beukes, N.J. and Klein, C. (1990). Geochemistry and sedimentology of a facies transition - from microbanded to granular iron-formation - in the early Proterozoic Transvaal Supergroup, South Africa. *Precambrian Research*, **47**, 99-139.

Beukes, N.J., Klein, C., Kaufman, A.J., and Hayes, J.M. (1990), Carbonate petrography, kerogen distribution, and carbon and oxygen isotope variations in an early Proterozoic transition from limestone to iron-formation deposition, Transvaal Supergroup, South Africa. *Economic Geology*, **85**, 663-690.

Beukes, N.J., Burger, A.M. and Gutzmer, J. (1995). Fault-controlled hydrothermal alteration of Palaeoproterozoic manganese ore in Wessels Mine, Kalahari manganese field, *Sourth African Journal of Geology*, **98**, 430–451.

Blignaut, L.C. (2017). *A Petrographical and Geochemical Analysis of the Upper and Lower Manganese Ore Bodies from the Kalahari Manganese Deposit, Northern Cape, South Africa – Controls on Hydrothermal Metasomatism and Metal Upgrading*". Ph.D thesis (unpbl.) University of Johannesburg, 248 pp.

Boardman, L.G. (1941). The Black Rock Manganese Deposit in the South-Eastern Kalahari", *Transactions of the Geological Society of South Africa*, **44**, 51–60.

Cairncross, B. and Beukes, N.J. (2013). *The Kalahari Manganese Field, The Adventure Continues*. Struik Nature, Random House Struik (Pty) Ltd.

Cairncross, B., Tsikos, H. and Harris, C. (2000). Prehnite from the Kalahari manganese field, South Africa, and its possible implications, *South African Journal of Geology*, 103, 231–236.

Chetty, D. (2008). *A geometallurgical evaluation of the ores of the northern Kalahari Manganese Deposit , South Africa*", Ph.D. thesis (unpbl.), University of Johannesburg, 271 pp.

Chetty, D. and Gutzmer, J. (2012). REE redistribution during hydrothermal alteration of ores of the Kalahari Manganese Deposit. *Ore Geology Reviews*, **47**, 126–135.

Cornell, D.H., Schütte, S.S., and Eglington, B.L. (1996). The Ongeluk basaltic andesite formation in Griqualand West, South Africa: Submarine alteration in a 2222 Ma Proterozoic sea. *Precambrian Research*, **79**, 101-123.

de Villiers, J.E. (1983). The Manganese Deposits of Griqualand West, South Africa: Some Mineralogical Aspects, *Econ. Geol.,* **78**, 1108–1118.

de Villiers, J.P.R. (1970). The geology and mineralogy of the Kalahari Manganese Field north of Sishen, Cape Province. *Geological Survey of Southern Africa*, Memoir 59, Pretoria, 84pp.

de Villiers, J.P., and Buseck, P.R. (1989). Stacking variations and nonstoichiometry in the bixbyite-braunite polysomatic mineral group. *American Mineralogist*, **74**, 1325-1336.

de Villiers, P.R., and Herbstein, F.H. (1968) Second occurrence of marokite. *American Mineralogist*, **53**, 495-496.

Dixon, R.D. (1989). Sugilite and associated metamorphic silicate minerals from Wessels Mine Kalahari manganese field. *Bulletin - Geological Survey South Africa*, **93**, 47 p.

Du Plooy, A.P. (2002), *Geochemistry and Mineralogy of Supergene Altered Manganese Ore below the Kalahari Unconformity in the Kalahari Manganese Field, Northern Cape, Province, South Africa*. MSc thesis (unpbl.), Rand Afrikaans University, 125p.

Fairey, B., Tsikos, H., Corfu, F., and Polteau, S. (2013). U-Pb systematics in carbonates of the Postmasburg Group, Transvaal Supergroup, South Africa: Primary versus metasomatic controls. *Precambrian Research*, **231**, 194-205.

Frankel, J.J. (1958). Manganese ores from the Kuruman District, Cape Province, South Africa, *Economic Geology*, **53**, 577–597.

Gumsley, A.P., Chamberlain, K.R., Bleeker, W., Söderlund, U., de Kock, M.O., Larsson, E.R. and Bekker, A. (2017). Timing and tempo of the Great Oxidation Event. *Proc. Nat. Ac. Sci.*, **114**, 1811–1816.

Günther, D., and Hattendorf, B. (2005) Solid sample analysis using laser ablation inductively coupled plasma mass spectrometry. *Trends in Analytical Chemistry*, **24**, 255-265.

Gnos, E., Armbruster, T. and Villa, I.M. (2003). Norrishite, $K(Mn_2^{3+}Li)Si_4O_{10}(O)_{(2)}$, an oxymica associated with sugilite from the Wessels Mine, South Africa: Crystal chemistry and Ar^{40}-Ar^{39} dating. *American Mineralogist*, **88**, 189–194.

Gutzmer, J. (1996). *Genesis and alteration of the Kalahari and Postmasburg manganese deposits, Griqualand West, South Africa.* PhD dissertation (unpbl), Rand Afrikaans University, 266 p.

Gutzmer, J. and Beukes, N.J. (1995). Fault-Controlled metasomatic alteration of Early Proterozoic sedimentary manganese ores in the Kalahari Manganese Field, South Africa, *Economic Geology*, **90**, 823–844.

Gutzmer, J. and Beukes, N.J. (1996). Mineral paragenesis of the Kalahari managanese field, South Africa. *Ore Geology Reviews*, **11**, 405–428.

Gutzmer, J. and Beukes, N.J. (1997). Effects of mass transfer, compaction and secondary porosity on hydrothermal upgrading of Paleoproterozoic sedimentary manganese ore in the Kalahari manganese field, South Africa", *Mineralium Deposita*, **32**, 250–256.

Gutzmer, J., Beukes, N.J., Kleyenstüber, A.S.E., Burger, A.M. (1995). Magnetic hausmannite from hydrothermally altered manganese ore in the Paleoproterozoic Kalahari manganese deposit, Transvaal Supergroup, South Africa. *Mineral. Mag*., **59**, 703–716.

Gutzmer, J., Du Plooy, A.P. and Beukes, N.J. (2012). Timing of supergene enrichment of low-grade sedimentary manganese ores in the Kalahari Manganese Field, South Africa. *Ore Geology Reviews*, **47**, 136–153.

Golden, D.C., Chen, C.C., Dixon, J.B. (1987) Transformation of birnessite to buserite, todorokite, and manganite under mild hydrothermal treatment. *Clays and Clay Minerals*, **35**, 271-280.

Hewett, D.F. (1972) Manganite, Hausmannite, Braunite: Features, Modes of Origin. *Economic Geology*, **67**, 83-102.

Jarosch, D. (1987). Crystal structure refinement and reflectance measurements of hausmannite, Mn_3O_4. *Mineralogy and Petrology*, **37**, 15-23.

Johnson, J.E., Webb, S.M., Ma, C., Fischer, W.W. (2016) Manganese mineralogy and diagenesis in the sedimentary rock record. *Geochimica et Cosmochimica Acta*, **173**, 210-231.

Kleyenstüber, A.S.E. (1984). The mineralogy of the manganese-bearing Hotazel Formation of the Proterozoic Transvaal sequence in Griqualand West, South Africa", *Geological Society of South Africa Transactions*, **87**, 257–272.

Kleyenstüber, A.S.E. (1993)Si. gnificant characteristics of the manganese ores and some of the minerals occurring in the Proterozoic Kalahari Manganese Field, South Africa. *Resource Geology*, **17**, 2–11.

Kuleshov, V. (2016) Isotope Geochemistry: The Origin and Formation of Manganese Rocks and Ores. Elsevier Science, 440 p.

Maynard, J.B. (2010) The chemistry of manganese ores through time: A signal of increasing diversity of earth-surface environments. *Economic Geology*, **105**, 535-552.

Mhlanga, X.R. (2020). *A reappraisal of the origin of the Hotazel Fe-Mn Formation in an evolving early Earth system through the application of mineral-specific geochemistry, speciation techniques and stable isotope systematics*. PhD thesis (unpbl.), Rhodes University, 161 p.

Moore, P.B. and Araki, T. (1976) Braunite: its structure and relationship to bixbyite, and some insights on the genealogy of fluorite derivative structures. *American Mineralogist*, **61**, 1226-1240

Moore, J.M., Tsikos, H. and Polteau, S. (2001). Deconstructing the Transvaal Supergroup, South Africa: implications for Palaeoproterozoic palaeoclimate models. *Journal of African Earth Sciences*, **33**, 437–444.

Nishizawa H, Koizumi M (1975). Synthesis and infrared spectra of $Ca_3Mn_2Si_3O_{12}$ and $Cd_3B_2Si_3O_{12}$ (B: Al, Ga, Cr, V, Fe, Mn) garnets. *American Mineralogist*, **60**, 84–87.

Okita, P.M., Shanks III, W.C. (1992). Origin of stratiform sediment-hosted manganese carbonate ore deposits: Examples from Molango, Mexico, and TaoJiang, China. *Chemical Geology*, **99**, 139-163.

Olsen S, Tangstad M, and Lindstad T (2007). *Production of manganese ferroalloys*. Tapir Academic Press, Norway.

Ostwald, J. (1992). Mineralogy, paragenesis and genesis of the braunite deposits of the Mary Valley Manganese Belt, Queensland, Australia. *Mineralium Deposita*, **27**, 326–335.

Park, C.F. Jr, (1956) On the origin of manganese. In: *Symposium sobre yacimientos de manganeso*: Proceedings 20th International Geological Congress, Mexico, v. 1, p. 75-98.

Perkins, W.T., Pearce, N.J.G., and Jeffries, T.E. (1993) Laser ablation inductively coupled plasma mass spectrometry: A new technique for the determination of trace and ultra-trace elements in silicates. *Geochimica et Cosmochimica Acta*, **52**, 475-482.

Robie, R.A., Huebner, J.S., and Hemingway, B.S. (1995). Heat capacities and thermo-dynamic properties of braunite (Mn_7SiO_{12}) and rhodonite ($MnSiO_3$). *American Mineralogist*, **80**, 560-575.

Schier, K., Bau, M., Smith, A.J.B., Beukes, N.J., Coetzee, L.L. and Viehmann, S. (2020). Chemical evolution of seawater in the Transvaal Ocean between 2426 Ma (Ongeluk Large Igneous Province) and 2413 Ma ago (Kalahari Manganese Field). *Gondwana Research*, **88**, 373-388.

Schneiderhan, E.A., Gutzmer, J., Strauss, H., Mezger, K. and Beukes, N.J. (2006). The chemostratigraphy of a Paleoproterozoic MnF-BIF succession - The Voëlwater Subgroup of the Transvaal Supergroup in Griqualand West, South Africa. *South African Journal of Geology*, **109**, 63–80.

Siahi, M., Tsikos, H., Rafuza, S., Oonk, P.B.H., Mhlanga, X.R., van Niekerk, D., Mason, P.R.D., and Harris, C. (2020) Insights into the processes and controls on the absolute abundance and distribution of manganese in Precambrian iron formations. *Precambrian Research*, **350**, doi:105878.

Tsikos, H. (1999). *Petrographic and Geochemical Constraints on the Origin and Post-Depositional History of the Hotazel Iron-Manganese Deposits, Kalahari Manganese Field. South Africa***.** PhD thesis (unpbl), *Rhodes University, 230p*

Tsikos, H. and Moore, J.M. (1997). Petrography and geochemistry of the Paleoproterozoic Hotazel iron-formation, Kalahari Manganese Field, South Africa: Implications for Precambrian manganese metallogenesis. *Economic Geology*, **92**, 87–97.

Tsikos, H., Moore, J.M., Harris, C. (2001) Geochemistry of the Palæoproterozoic Mooidraai Formation: Fe-rich limestone as end member of iron formation deposition, Kalahari Manganese Field, Transvaal Supergroup, South Africa. *Journal of African Earth Sciences*, **32**, 19-27.

Tsikos, H. and Moore, J.M. (2005). Sodic metasomatism in the Palaeoproterozoic Hotazel iron-formation, Transvaal Supergroup, South Africa: Implications for fluid-rock interaction in the Kalahari manganese field. *Geofluids*, **5**, 264–271.

Tsikos, H., Beukes, N.J., Moore, J.M. and Harris, C. (2003). Deposition, diagenesis, and secondary enrichment of metals in the Paleoproterozoic Hotazel Iron Formation, Kalahari Manganese Field, South Africa", *Economic Geology*, **98**, 1449–1462.

Liu, Y.S., Hu, Z.C., Li, M., and Gao, S. (2013). Applications of LA-ICP-MS in the elemental analyses of geological samples. *Chinese Science Bulletin*, **58**, 3863-3878.

Von Damm, K.L. (1990) Seafloor hydrothermal activity: black smoker chemistry and chimneys. *Annual Review of Earth Planetary Sciences*, **18**, 173-204

APPENDIX

1. Elemental ratio maps used for core selection at N'chwaning mine

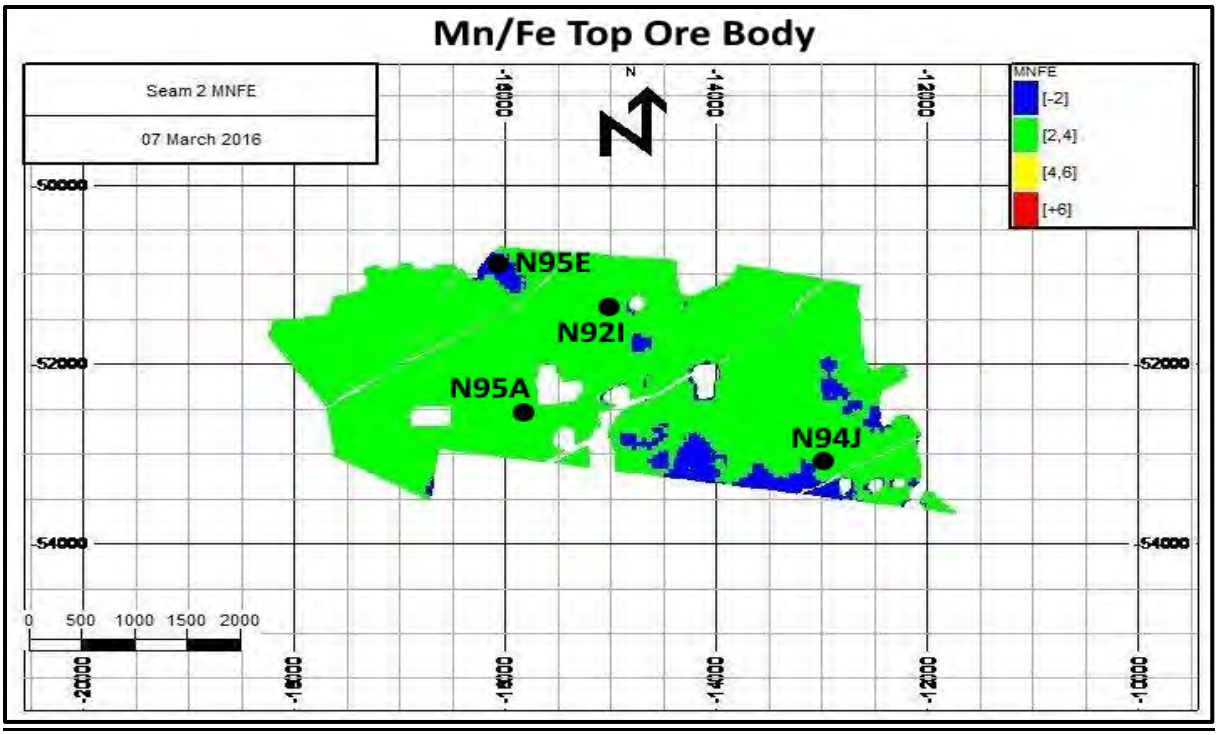
Mn/Fe Top Ore Body
Seam 2 MNFE
07 March 2016
MNFE
[-2]
[2,4]
[4,6]
[+6]
N95E
N92I
N95A
N94J
0 500 1000 1500 2000

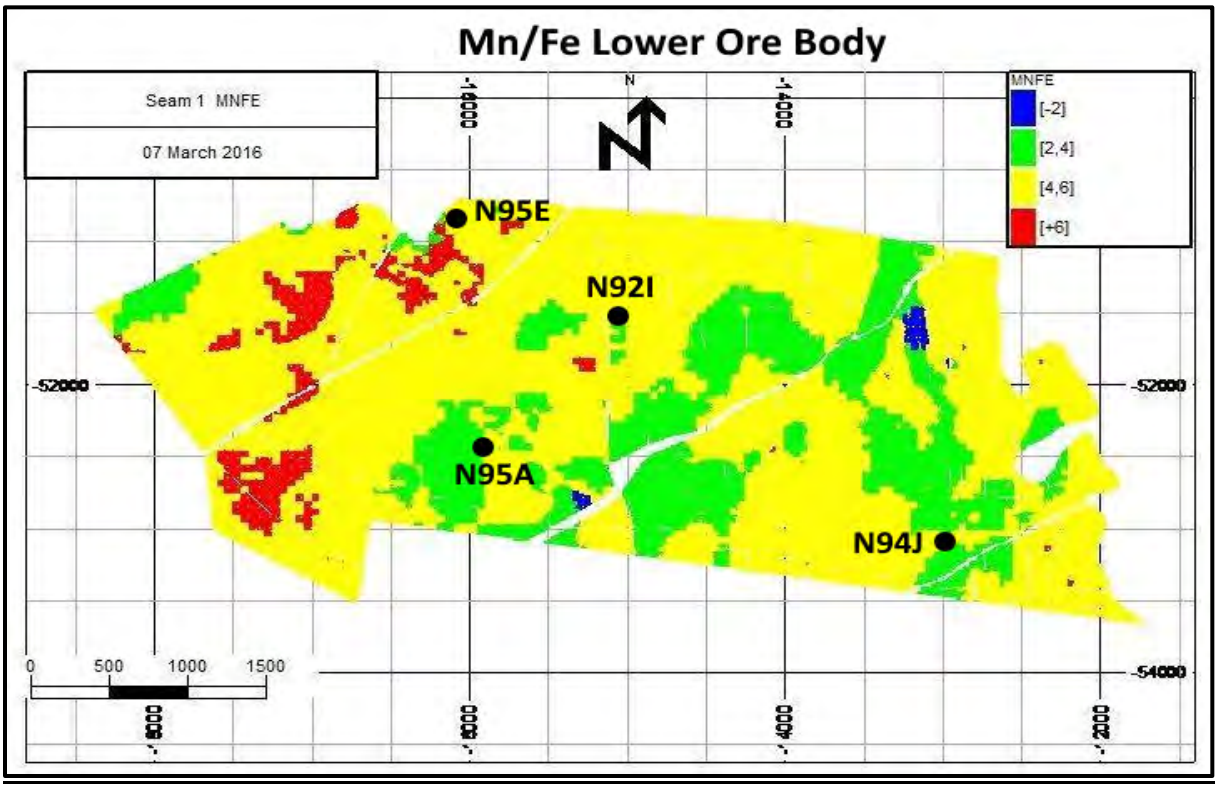
Mn/Fe Lower Ore Body
Seam 1 MNFE
07 March 2016
MNFE
[-2]
[2,4]
[4,6]
[+6]
N95E
N92I
N95A
N94J
0 500 1000 1500

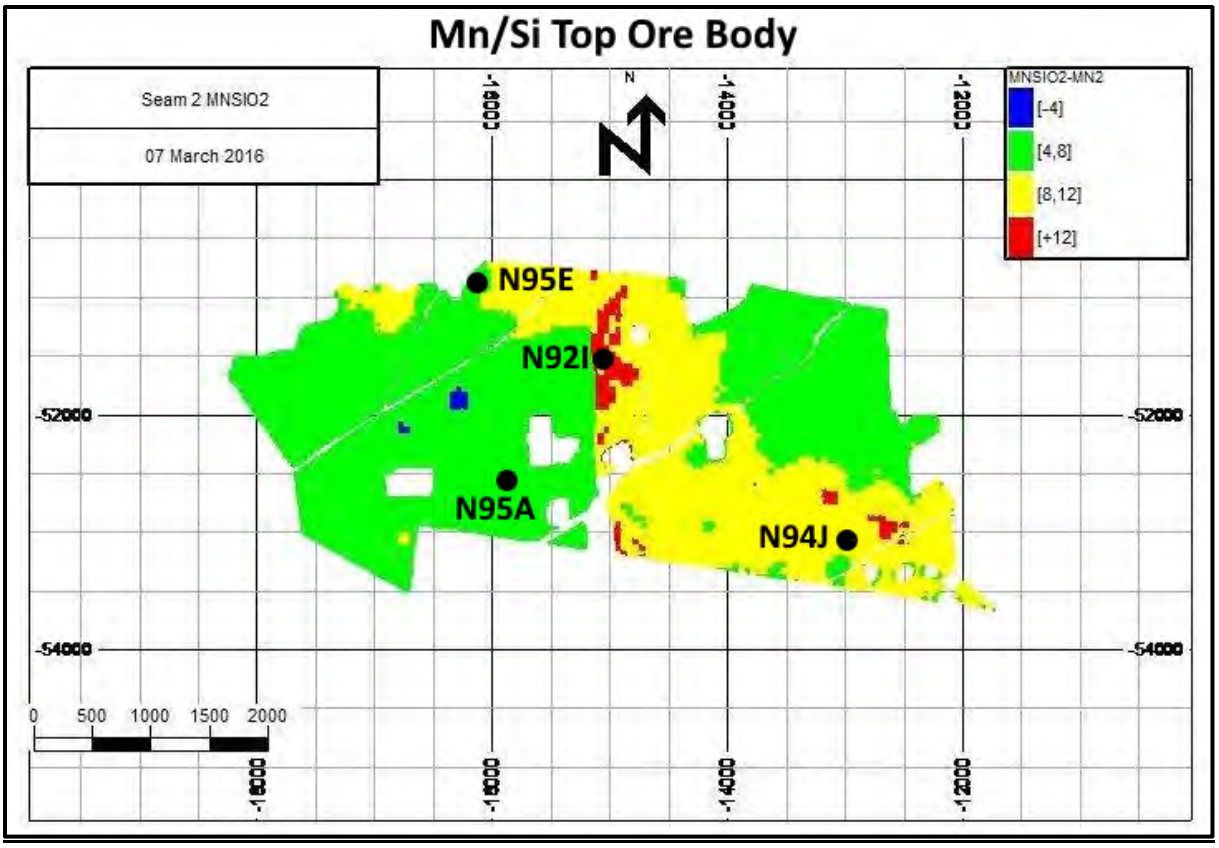
Mn/Si Top Ore Body
Seam 2 MNSIO2
07 March 2016
MNSIO2-MN2
[-4]
[4,8]
[8,12]
[+12]
N
N95E
N92I
N95A
N94J
-52000
-54000
0 500 1000 1500 2000

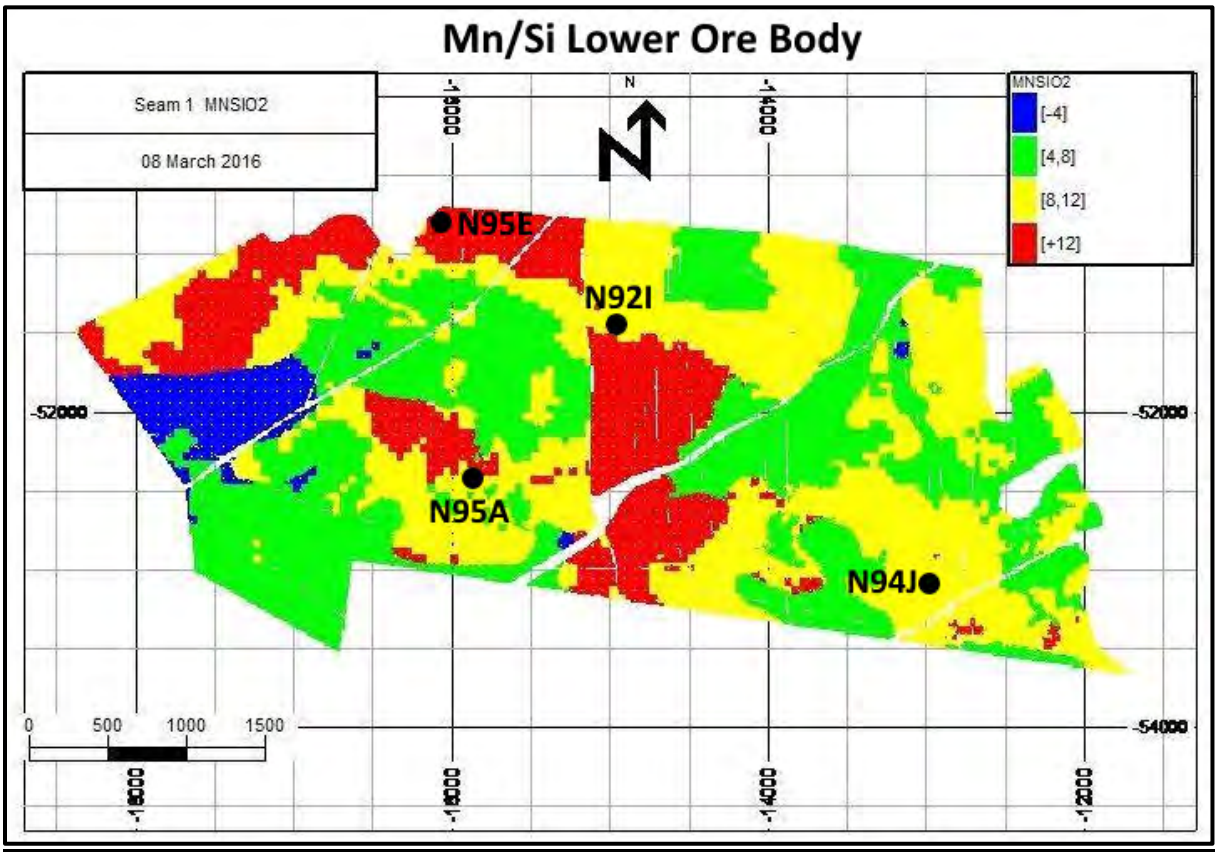
Mn/Si Lower Ore Body
Seam 1 MNSIO2
08 March 2016
MNSIO2
[-4]
[4,8]
[8,12]
[+12]
N
N95E
N92I
N95A
N94J
-52000
-54000
0 500 1000 1500

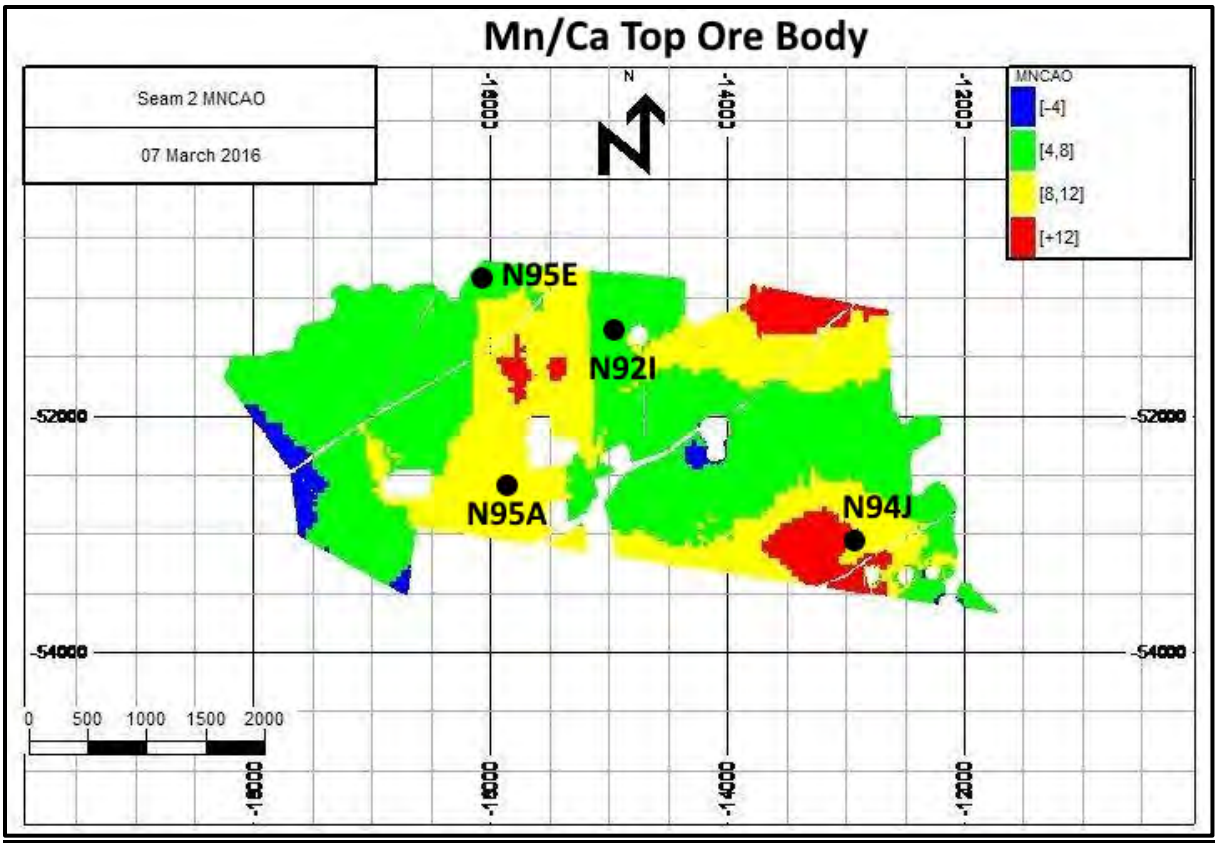
Mn/Ca Top Ore Body
Seam 2 MNCAO
07 March 2016
N
MNCAO
[-4]
[4,8]
[8,12]
[+12]
N95E
N92I
N95A
N94J
-52000
-54000
0 500 1000 1500 2000
-16000
-14000
-12000

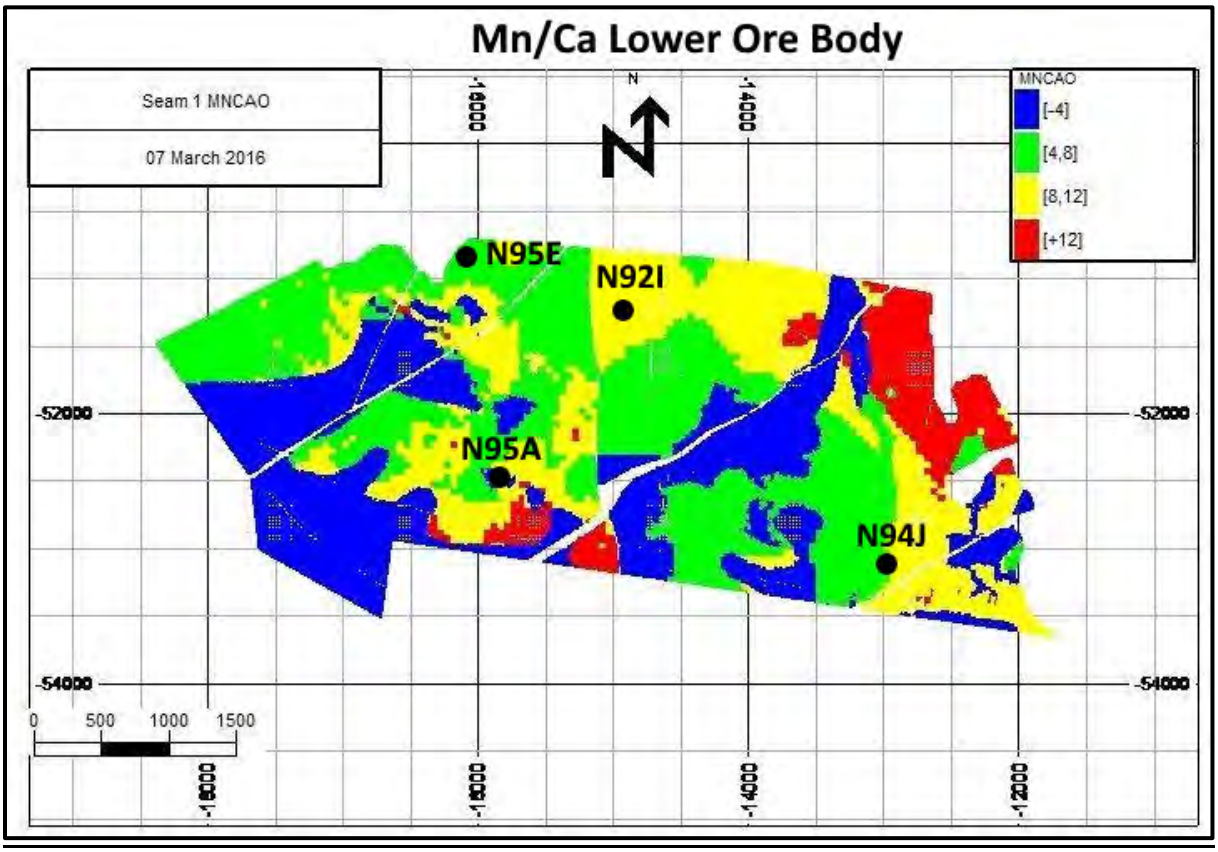
Mn/Ca Lower Ore Body
Seam 1 MNCAO
07 March 2016
N
MNCAO
[-4]
[4,8]
[8,12]
[+12]
N95E
N92I
N95A
N94J
-52000
-54000
0 500 1000 1500
-16000
-14000
-12000

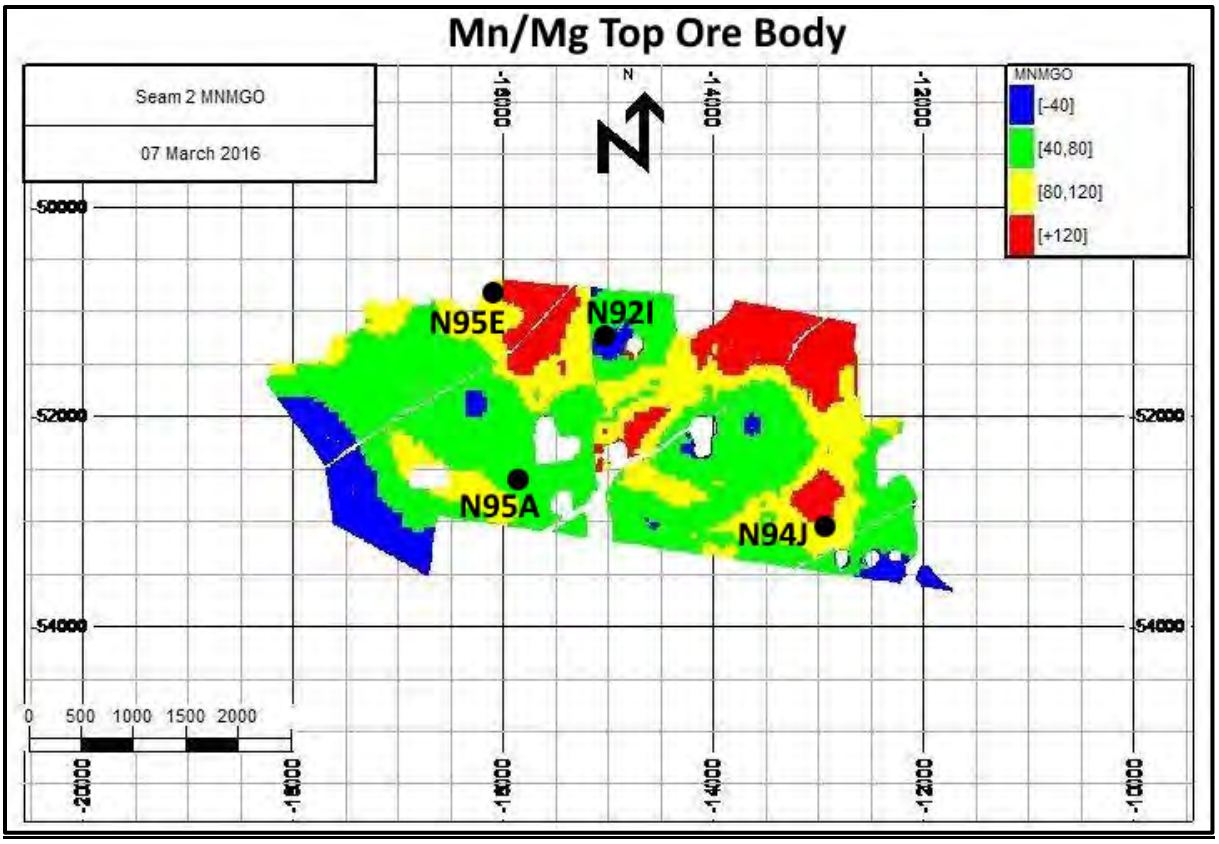
Mn/Mg Top Ore Body
Seam 2 MNMGO
07 March 2016
N
MNMGO
[-40]
[40,80]
[80,120]
[+120]
N95E
N92I
N95A
N94J
-50000
-52000
-54000
-18000
-16000
-14000
-12000
0 500 1000 1500 2000

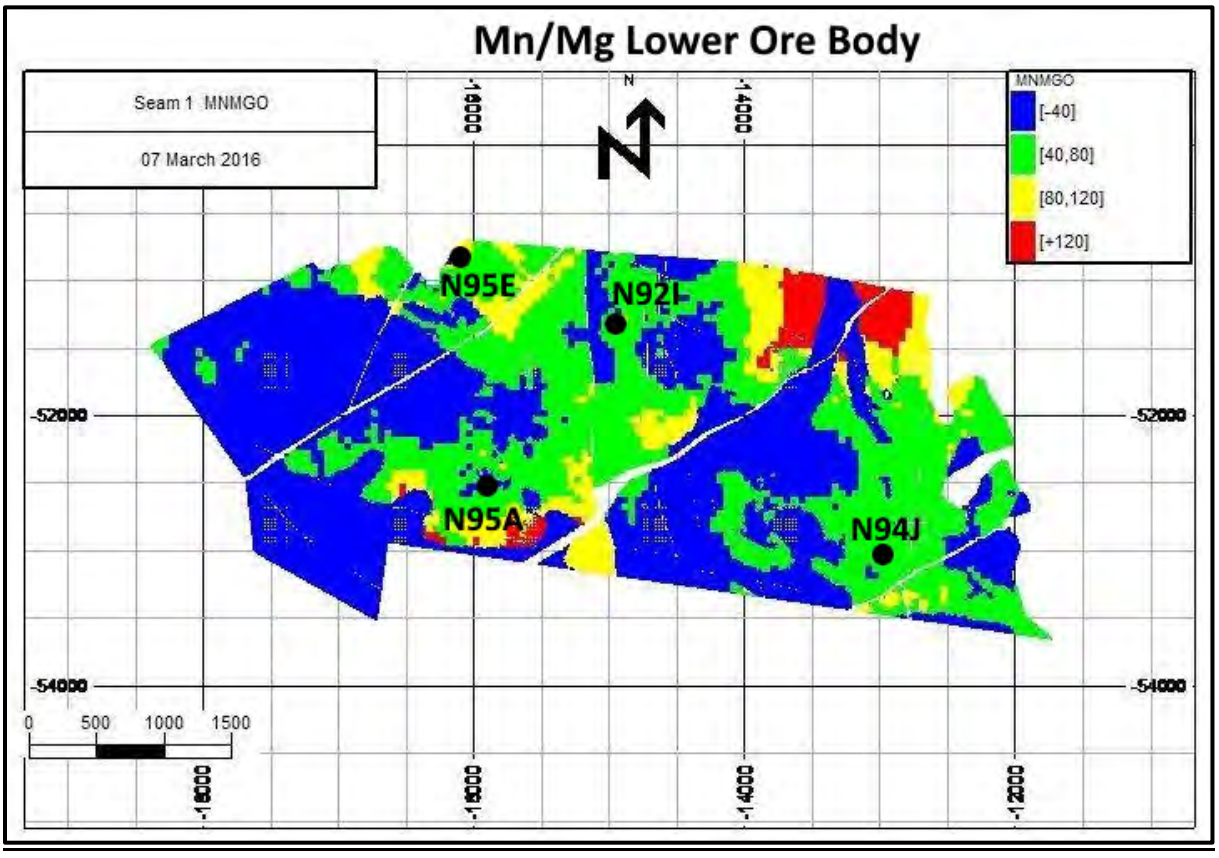
Mn/Mg Lower Ore Body
Seam 1 MNMGO
07 March 2016
N
MNMGO
[-40]
[40,80]
[80,120]
[+120]
N95E
N92I
N95A
N94J
-52000
-54000
-18000
-16000
-14000
-12000
0 500 1000 1500

2. Mineral-specific geochemical analysis: LA-ICP-MS

Table A1: ***Trace element data for hausmannite mineral grains***

	MTOt	MTOb	T14	GH2	GH8	S1	S7	W136	W162	W162
Li	**13.00**	**4.67**	**5.96**	**142.97**	**3.32**	**699.27**	**13.77**	**44.41**	**3.97**	**12.91**
Sn	**0.00**	**0.00**	**0.83**	**75.50**	**0.91**	**43.53**	**0.75**	**1.73**	**0.79**	**0.85**
W	**0.00**	**0.00**	**1.78**	**192.88**	**3.72**	**75.55**	**0.60**	**2.38**	**2.92**	**0.07**
B	**622.00**	**1457.00**	**600.51**	**1921.77**	**34.55**	**1696.75**	**15.39**	**158.65**	**62.71**	**50.80**
Ba	**473.86**	**63.94**	**85.11**	**1642.61**	**0.37**	**2022.44**	**78.19**	**163.64**	**6.33**	**266.18**
Sr	**473.15**	**92.98**	**17.45**	**534.75**	**21.17**	**480.70**	**9.61**	**15.12**	**3.04**	**1773.99**
Sc	**1.64**	**1.53**	**3.85**	**145.17**	**3.78**	**148.60**	**3.50**	**6.63**	**4.50**	**5.20**
V	**8.09**	**8.57**	**3.74**	**289.88**	**7.94**	**259.56**	**6.27**	**31.60**	**4.27**	**2.40**
Cr	**25.93**	**21.80**	**8.94**	**250.20**	**4.85**	**1629.57**	**6.22**	**7.21**	**7.14**	**5.40**
Co	**8.09**	**8.57**	**185.57**	**1269.42**	**160.50**	**1674.44**	**1628.24**	**986.68**	**27.65**	**1763.57**
Ni	**25.93**	**21.80**	**29.05**	**876.21**	**49.51**	**50.19**	**31.89**	**60.76**	**39.86**	**47.50**
Cu	**46.38**	**32.67**	**383.12**	**201.75**	**52.90**	**242.81**	**129.04**	**286.42**	**9.45**	**9.05**
Pb	**5.48**	**8.76**	**25.33**	**7244.30**	**2400.87**	**815.86**	**317.00**	**852.49**	**358.70**	**9.34**
Mo	**53.86**	**42.60**	**4.01**	**101.25**	**3.67**	**50.50**	**200.10**	**5.74**	**4.01**	**5.20**
Zn	**5.78**	**2.52**	**24.10**	**497.51**	**0.37**	**100.52**	**14.90**	**10.10**	**1.18**	**0.45**
Ce	**3.27**	**3.23**	**20.71**	**259.16**	**0.92**	**130.73**	**15.56**	**67.26**	**2.82**	**0.09**
Y	**5.82**	**5.54**	**23.47**	**577.50**	**1.90**	**62.06**	**4.39**	**13.38**	**2.59**	**0.16**
U	**0.53**	**0.34**	**0.47**	**19.26**	**0.35**	**3.85**	**1.55**	**1.85**	**0.07**	**0.07**

MTOt – Mamatwan-type low-grade Mn ore (upper layer)

MTOb – Mamatwan-type low-grade Mn ore (lower layer)

Table A2: ***Normalized hausmannite data against the assumed low-grade protore***

Element	MTOt	MTOb	T14	GH2	GH8	S1	S7	W136	W162	W162
Ba	**1.00**	**1.00**	**1.33**	**3.47**	**1.22**	**4.27**	**1.22**	**0.35**	**0.35**	**0.56**
Li	**1.00**	**1.00**	**1.28**	**11.00**	**0.71**	**53.79**	**2.95**	**9.51**	**0.31**	**2.76**
Sr	**1.00**	**1.00**	**0.19**	**1.13**	**0.10**	**1.02**	**0.10**	**0.03**	**0.03**	**3.75**
B	**1.00**	**1.00**	**0.41**	**3.09**	**0.02**	**2.73**	**0.01**	**0.11**	**0.10**	**0.03**
Sc	**1.00**	**1.00**	**2.52**	**88.30**	**2.29**	**90.38**	**2.29**	**4.03**	**4.03**	**3.16**
Mo	**1.00**	**1.00**	**0.09**	**1.88**	**4.70**	**0.94**	**4.70**	**0.11**	**0.11**	**0.10**
V	**1.00**	**1.00**	**0.44**	**35.84**	**0.73**	**32.09**	**0.73**	**3.91**	**3.91**	**0.30**
Cr	**1.00**	**1.00**	**0.41**	**9.65**	**0.29**	**62.84**	**0.29**	**0.28**	**0.28**	**0.21**
Co	**1.00**	**1.00**	**21.65**	**156.95**	**189.93**	**207.02**	**189.93**	**121.99**	**121.99**	**218.04**
Ni	**1.00**	**1.00**	**1.33**	**33.79**	**1.46**	**1.94**	**1.46**	**2.34**	**2.34**	**1.83**
Cu	**1.00**	**1.00**	**11.73**	**4.35**	**3.95**	**5.23**	**3.95**	**6.18**	**6.18**	**0.20**
Zn	**1.00**	**1.00**	**9.58**	**86.11**	**5.92**	**17.40**	**5.92**	**1.75**	**1.75**	**0.08**
Pb	**1.00**	**1.00**	**2.89**	**1321.73**	**36.19**	**148.85**	**36.19**	**155.54**	**155.54**	**1.70**
Ce	**1.00**	**1.00**	**6.41**	**79.21**	**4.82**	**39.96**	**4.82**	**20.56**	**20.56**	**0.03**
Y	**1.00**	**1.00**	**4.23**	**99.30**	**0.79**	**10.67**	**0.79**	**2.30**	**2.30**	**0.03**
U	**1.00**	**1.00**	**1.39**	**36.23**	**4.60**	**7.24**	**4.60**	**3.48**	**3.48**	**0.14**

MTOt – mamantwan-type low-grade Mn ore upper ore layer

MTOb – mamantwan-type low-grade Mn ore lower ore layer

Table A3: *Trace element data for braunite mineral grains*

Element	MTOt	MTOb	T4	T14	Mn15	D13	GH2	GH8	S1	S7	DB38	W162	W162
Li	13.00	4.67	54.21	6.36	71.53	4.52	311.80	523.54	18.63	4.14	4.97	16.61	45.63
W	0.00	0.00	2.66	1.63	0.24	1.63	170.89	207.42	0.85	0.70	8.26	2.94	0.31
Sn	0.00	0.00	1.73	0.95	0.55	0.65	179.50	63.11	1.16	1.00	2.02	3.78	2.10
B	622.00	1457.0	199.99	714.01	43.82	81.92	3030.75	2418.36	278.13	38.94	44.57	868.16	56.26
Ba	473.86	63.94	186.91	56.04	5.27	0.80	3726.18	692.27	1514.22	75.97	15.09	10.50	673.86
Sr	473.15	92.98	296.97	12.16	3.85	1.93	1185.22	282.10	33.71	8.00	38.55	57.32	3974.97
Sc	1.64	1.53	9.72	4.81	4.24	4.82	409.94	227.03	10.13	4.21	5.66	11.58	7.29
Mo	3.28	2.37	7.70	3.70	3.73	4.49	374.80	189.97	4.32	3.69	5.49	6.40	7.09
V	8.09	8.57	7.00	2.78	4.23	2.31	374.84	118.89	24.80	4.46	19.96	5.79	3.20
Cr	25.93	21.80	11.10	5.36	4.43	4.43	420.36	230.31	7.41	4.07	7.06	8.27	6.52
Co	46.38	32.67	293.36	169.53	26.89	17.26	2540.23	464.30	205.11	55.45	55.54	82.06	1572.28
Ni	20.71	18.45	79.49	38.64	32.37	34.78	3088.89	1817.83	38.69	32.95	40.62	49.13	53.08
Cu	5.48	8.76	697.43	342.25	38.49	9.86	898.76	435.84	202.05	82.63	44.68	23.17	19.84
Zn	53.86	42.60	201.20	97.95	42.25	1562.93	998.00	590.64	140.04	12.16	38.75	64.71	102.48
Pb	5.78	2.52	172.20	19.12	31.81	144.78	16503.49	5371.68	27.05	181.62	12.13	7.57	10.90
Ce	3.27	3.23	35.57	16.09	1.48	0.75	132.76	126.10	3.55	14.92	9.12	10.73	5.17
Y	5.82	5.54	162.74	17.36	1.34	1.29	362.97	68.87	9.90	3.63	11.22	13.02	25.31
Nb	0.53	0.34	2.31	1.08	1.18	1.13	105.27	55.14	1.23	1.27	1.38	1.77	1.92
La	3.10	3.66	16.92	21.66	0.70	0.89	1271.38	647.81	4.85	12.12	12.61	6.19	3.69
U	0.11	0.10	0.47	0.36	0.29	0.33	31.87	7.89	0.67	1.59	1.16	0.32	0.23

MTOt – Mamatwan-type low-grade Mn ore (upper ore layer)

MTOb – Mamatwan-type low-grade Mn ore (lower ore layer)

Table A4: *Normalized braunite data against the assumed low-grade protore*

Element	MTOt	MTOb	T4	T14	Mn15	D13	GH2	GH8	S1	S7	DB38	W162	W162
Ba	**1.00**	**1.00**	**0.39**	**0.88**	**0.01**	**0.01**	**7.86**	**10.83**	**3.20**	**1.19**	**0.03**	**1.42**	**0.02**
Li	**1.00**	**1.00**	**4.17**	**1.36**	**5.50**	**0.97**	**23.98**	**112.11**	**1.43**	**0.89**	**0.38**	**3.51**	**3.56**
Sr	**1.00**	**1.00**	**0.63**	**0.13**	**0.01**	**0.02**	**2.50**	**3.03**	**0.07**	**0.09**	**0.08**	**8.40**	**0.12**
B	**1.00**	**1.00**	**0.32**	**0.49**	**0.07**	**0.06**	**4.87**	**1.66**	**0.45**	**0.03**	**0.07**	**0.09**	**1.40**
Sc	**1.00**	**1.00**	**5.91**	**3.15**	**2.58**	**3.16**	**249.34**	**148.75**	**6.16**	**2.76**	**3.44**	**4.43**	**7.05**
Mo	**1.00**	**1.00**	**2.35**	**1.56**	**1.14**	**1.89**	**114.38**	**80.04**	**1.32**	**1.56**	**1.68**	**2.16**	**1.95**
V	**1.00**	**1.00**	**0.87**	**0.32**	**0.52**	**0.27**	**46.34**	**13.87**	**3.07**	**0.52**	**2.47**	**0.40**	**0.72**
Cr	**1.00**	**1.00**	**0.43**	**0.25**	**0.17**	**0.20**	**16.21**	**10.56**	**0.29**	**0.19**	**0.27**	**0.25**	**0.32**
Co	**1.00**	**1.00**	**6.32**	**5.19**	**0.58**	**0.53**	**54.77**	**14.21**	**4.42**	**1.70**	**1.20**	**33.90**	**1.77**
Ni	**1.00**	**1.00**	**3.84**	**2.09**	**1.56**	**1.89**	**149.16**	**98.55**	**1.87**	**1.79**	**1.96**	**2.56**	**2.37**
Cu	**1.00**	**1.00**	**127.25**	**39.07**	**7.02**	**1.13**	**163.98**	**49.76**	**36.86**	**9.43**	**8.15**	**3.62**	**4.23**
Zn	**1.00**	**1.00**	**3.74**	**2.30**	**0.78**	**36.69**	**18.53**	**13.86**	**2.60**	**0.29**	**0.72**	**1.90**	**1.20**
Pb	**1.00**	**1.00**	**29.80**	**7.60**	**5.51**	**57.54**	**2856.40**	**2134.80**	**4.68**	**72.18**	**2.10**	**1.89**	**1.31**
Ce	**1.00**	**1.00**	**10.87**	**4.98**	**0.45**	**0.23**	**40.58**	**39.05**	**1.09**	**4.62**	**2.79**	**1.58**	**3.28**
Y	**1.00**	**1.00**	**27.98**	**3.13**	**0.23**	**0.23**	**62.41**	**12.42**	**1.70**	**0.66**	**1.93**	**4.35**	**2.24**
Nb	**1.00**	**1.00**	**4.34**	**3.20**	**2.22**	**3.34**	**198.05**	**163.47**	**2.31**	**3.77**	**2.59**	**3.62**	**3.33**
La	**1.00**	**1.00**	**5.46**	**5.92**	**0.23**	**0.24**	**410.32**	**177.04**	**1.57**	**3.31**	**4.07**	**1.19**	**2.00**
U	**1.00**	**1.00**	**4.18**	**3.70**	**2.56**	**3.39**	**282.96**	**81.55**	**5.98**	**16.43**	**10.31**	**2.08**	**2.83**

MTOt – Mamatwan-type low-grade Mn ore (upper ore layer)

MTOb – Mamantwan-type low-grade Mn ore (lower ore layer)

3. *EPMA data for hausmannite*

Comment	MgO(Mass%)	Fe2O3(Mass%)	Mn3O4	CaO(Mass%)	BaO(Mass%)	Total(Mass%)
		DB50A				
		B20(Lower Body)				
"B20_7 "	0.06	11.40	86.29	0.02	0.03	97.79
"B20_7 "	0.01	5.02	92.25	0.02	0.00	97.30
"B20_8 "	0.06	10.10	86.65	0.03	0.00	96.84
"B20_9 "	0.06	9.14	88.15	0.01	0.00	97.36
"B20_10 "	0.05	8.89	89.20	0.08	0.00	98.21

Comment	MgO(Mass%)	Fe2O3(Mass%)	Mn3O4	CaO(Mass%)	BaO(Mass%)	Total(Mass%)
		DK21				
		L22(Upper Body)				
"L22_1 "	0.15	3.09	95.48	0.00	0.00	98.72
"L22_1 "	0.14	3.19	95.24	0.03	0.00	98.60
"L22_1 "	0.15	3.00	95.45	0.01	0.00	98.61
"L22_1 "	0.12	3.90	94.70	0.03	0.00	98.76
"L22_1 "	0.15	3.61	95.77	0.01	0.01	99.54
"L22_1 "	0.11	3.13	95.33	0.02	0.00	98.58
"L22_1 "	0.16	3.89	93.58	0.00	0.01	97.64
"L22_1 "	0.11	2.77	96.04	0.02	0.01	98.94
"L22_1 "	0.12	3.69	93.97	0.00	0.00	97.77
"L22_1 "	0.18	3.90	94.72	0.01	0.01	98.82
		L20 (upper Body)				
"L20_34 "	0.06	8.07	92.30	0.07	0.00	100.49
"L20_35 "	0.04	9.55	89.84	0.04	0.00	99.47
"L20_36 "	0.06	6.30	93.85	0.07	0.00	100.29
"L20_37 "	0.16	10.43	90.12	0.06	0.00	100.75
"L20_38 "	0.03	11.92	87.40	1.46	0.00	100.82
"L20_39 "	0.02	10.23	90.12	0.12	0.00	100.48
"L20_40 "	0.01	9.14	88.41	0.10	0.00	97.66
"L20_41 "	0.17	3.29	96.50	0.03	0.02	100.00
"L20_42 "	0.18	3.41	96.33	0.00	0.01	99.93
"L20_43 "	0.20	2.58	97.20	0.01	0.00	99.99
"L20_44 "	0.17	3.63	96.14	0.05	0.00	100.00
"L20_45 "	0.18	2.13	97.21	0.02	0.00	99.53
L20_1	0.11	3.23	95.18	0.00	0.00	98.52
L20_2	0.15	3.20	93.89	0.00	0.01	97.25
L20_3	0.08	4.07	93.51	0.01	0.00	97.68
L20_4	0.10	6.19	91.60	0.01	0.02	97.92
L20_5	0.13	5.73	92.21	0.00	0.00	98.06
L20_6	0.12	5.45	91.99	0.02	0.00	97.58
L20_7	0.05	5.46	91.91	0.00	0.04	97.46
L20_8	0.06	6.41	91.06	0.01	0.00	97.54
L20_9	0.06	5.96	92.00	0.00	0.00	98.02
L20_10	0.07	7.96	89.71	0.02	0.06	97.81
L23_3	0.03	6.72	90.03	0.05	0.00	96.83
L23_4	0.07	4.77	91.95	0.06	0.00	96.85
L23_5	0.08	4.88	91.90	0.02	0.00	96.88
L23_6	0.05	4.28	93.04	0.01	0.00	97.38
		L6(Lower Body)				
"L6_20 "	0.06	0.53	98.61	0.06	0.00	99.25
"L6_21 "	0.04	0.50	99.30	0.08	0.00	99.92
"L6_22 "	0.01	0.52	98.70	0.14	0.04	99.42
"L6_23 "	0.34	3.49	95.50	0.05	0.01	99.38
"L6_24 "	0.04	0.61	98.40	0.05	0.01	99.11
"L6_25 "	0.23	4.30	94.53	0.03	0.11	99.19
"L6_26 "	0.51	2.28	94.41	0.10	0.00	97.30
"L6_27 "	0.77	2.85	93.86	0.11	0.06	97.65
"L6_28 "	0.23	3.69	94.63	0.06	0.00	98.60
"L6_30 "	0.16	4.28	94.28	0.04	0.08	98.83

"L6_31 "	0.14	3.80	94.14	0.18	0.10	98.36
"L6_32 "	0.05	2.08	95.78	0.07	0.00	97.97
"L6_65 "	0.28	3.96	94.39	0.76	0.04	99.43
"L6_66 "	0.25	2.81	92.51	8.97	0.00	104.54
"L6_67 "	0.21	4.96	91.83	0.74	0.00	97.74
L6_26	0.06	1.90	96.52	0.06	0.00	98.54
L6_27	0.02	0.89	96.96	0.09	0.00	97.96
L6_28	0.09	3.68	93.34	0.04	0.00	97.15
L6_29	0.06	3.02	93.23	0.08	0.00	96.39
L6_30	0.07	1.99	93.78	0.11	0.00	95.95

Comment	MgO(Mass%)	Fe2O3(Mass%)	Mn3O4	CaO(Mass%)	BaO(Mass%)	Total(Mass%)
		W162				
		LB06				
"W162_3_6 "	0.10	8.10	87.89	0.18	0.32	96.58
"W162_3_6 "	0.05	2.87	93.90	0.15	0.14	97.10
"W162_3_8 "	0.07	9.07	87.92	0.27	0.08	97.41
"W162_3_9 "	0.03	4.29	91.89	0.20	0.12	96.54
"W162_3_8 "	0.07	9.07	87.92	0.27	0.08	97.41
		LB04				
"W162LB04_22 "	0.03	0.21	98.80	0.08	0.00	99.12
"W162LB04_23 "	0.03	0.20	98.87	0.27	0.07	99.44
"W162LB04_24 "	0.06	0.20	97.79	0.44	0.00	98.49
"W162LB04_27 "	0.00	0.30	98.66	0.18	0.01	99.14
"W162LB04_51 "	0.02	0.12	97.85	0.43	0.00	98.42
"W162LB04_53 "	0.00	0.27	97.93	0.09	0.00	98.30
"W162LB04_55 "	0.00	0.25	98.59	0.05	0.06	98.95
"W162LB04_56 "	0.00	0.17	98.44	0.00	0.06	98.66
"W162LB04_58 "	0.00	0.21	98.28	0.02	0.00	98.51
"W162LB04_37 "	0.12	0.28	95.95	1.55	0.00	97.90
"W162LB04_60 "	0.06	0.16	97.93	0.04	0.00	98.19
		UB04				
"W162_19	0.08	2.32	94.91	0.06	0.03	97.39
"W162_20	0.01	3.18	93.53	0.02	0.00	96.75
"W162_22	0.06	4.66	92.97	0.04	0.00	97.73
"W162_23	0.08	3.61	93.65	0.06	0.00	97.40
"W162UB04_54 "	0.08	1.92	95.70	0.11	0.02	97.83
"W162UB04_55 "	0.03	2.88	95.03	0.03	0.01	97.98
"W162UB04_56 "	0.12	3.73	94.43	0.07	0.00	98.35
"W162UB04_57 "	0.10	1.55	96.09	0.08	0.00	97.82
"W162UB04_58 "	0.12	2.62	94.66	0.08	0.00	97.49
"W162UB_3_19 "	0.13	12.43	77.92	0.76	0.00	91.24
"W162UB_3_20 "	0.10	9.95	81.56	0.88	0.00	92.49
"W162UB_3_22 "	0.13	12.03	80.82	0.65	0.00	93.63
"W162UB_3_19 "	0.13	12.43	77.92	0.76	0.00	91.24
"W162UB_3_20 "	0.10	9.95	81.56	0.88	0.00	92.49
"W162UB_3_22 "	0.13	12.03	80.82	0.65	0.00	93.63
		UB06				
"W162UB_4_4 "	0.02	12.81	82.10	0.04	0.00	94.98
"W162UB_4_6 "	0.09	15.65	77.69	0.32	0.01	93.77
"W162UB_4_7 "	0.11	14.42	76.92	0.33	0.12	91.90

"W162UB_4_9 "	0.02	9.63	83.20	0.21	0.00	93.06
"W162LB05_1 "	0.02	2.21	93.49	0.07	0.22	96.00
"W162LB05_2 "	0.06	13.01	87.34	0.11	0.01	100.52

Comment	MgO(Mass%)	Fe2O3(Mass%)	Mn3O4	CaO(Mass%)	BaO(Mass%)	Total(Mass%)
		DB38				
		UB01				
"DB38_24 "	0.02	0.29	98.50	0.02	0.01	98.84
"DB38_25 "	0.29	1.92	98.17	0.02	0.03	100.43
"DB38_33 "	0.07	1.28	95.55	0.01	0.01	96.92
		UB03				
"DB38UB_3_11 "	0.19	10.26	97.00	0.02	0.00	107.47
"DB38UB_3_12 "	0.14	12.02	87.63	0.01	0.00	99.80
"DB38UB_3_13 "	0.06	10.66	86.25	0.03	0.00	97.00
"DB38UB_3_20 "	0.17	8.19	80.75	0.04	0.00	89.15
"DB38UB_3_29 "	0.23	9.03	88.52	0.27	0.00	98.05
"DB38UB_3_30 "	0.25	9.73	87.52	0.44	0.00	97.94

Comment	MgO(Mass%)	Fe2O3(Mass%)	Mn3O4	CaO(Mass%)	BaO(Mass%)	Total(Mass%)
		W125				
		LB04				
"W125LB_1_4 "	0.30	0.98	93.91	0.03	0.00	95.22
"W125LB_1_5 "	0.33	2.42	95.50	0.04	0.00	98.28
"W125LB_1_6 "	0.30	1.03	93.95	0.04	0.00	95.32
"W125LB_1_7 "	0.98	6.07	95.15	0.01	0.00	102.21
"W125LB_1_8 "	0.99	4.68	89.95	0.00	0.00	95.62
"W125LB_1_9 "	0.80	4.40	91.87	0.03	0.01	97.10
"W125LB_1_10 "	1.06	4.93	91.39	0.01	0.00	97.39
"W125LB_1_11 "	0.94	3.62	91.40	0.00	0.00	95.96
"W125LB_1_12 "	0.93	3.82	93.32	0.00	0.00	98.07
"W125LB_1_13 "	1.03	4.48	92.61	0.02	0.00	98.14
"W125LB_1_15 "	0.24	1.81	95.72	0.06	0.00	97.84
"W125LB_1_16 "	0.26	1.62	95.08	0.05	0.05	97.05
		Upper body				
"W125UB_1_1 "	0.17	5.46	95.08	0.03	0.00	100.74
"W125UB_1_2 "	0.17	5.21	91.77	0.03	0.00	97.18
"W125UB_1_3 "	0.15	5.25	90.75	0.04	0.00	96.19
"W125UB_1_4 "	0.19	6.61	85.97	0.04	0.01	92.81
"W125UB_1_5 "	0.14	5.45	90.55	0.07	0.00	96.21
"W125UB_1_6 "	0.13	5.42	92.26	0.01	0.00	97.82
"W125UB_1_7 "	0.14	4.57	91.52	0.00	0.00	96.23
"W125UB_1_8 "	0.13	4.86	92.53	0.02	0.02	97.56
"W125UB_1_9 "	0.13	6.06	93.17	0.02	0.00	99.38
"W125UB_1_10 "	0.15	4.77	92.14	0.05	0.00	97.10

Comment	MgO(Mass%)	Fe2O3(Mass%)	Mn3O4	CaO(Mass%)	BaO(Mass%)	Total(Mass%)
		DB07				
		Lower body				
"DB7_2	0.07	2.53	94.90	0.02	0.00	97.52
"DB7_4	0.07	1.33	95.36	0.09	0.00	96.85
"DB7_5	0.04	0.94	94.55	0.03	0.00	95.57
"DB7_6	0.05	1.06	95.08	0.05	0.05	96.29
"DB7_7	0.03	0.53	95.52	0.10	0.00	96.18
"DB7_8	0.03	6.73	95.49	0.03	0.00	102.28
"DB07_2	0.03	8.46	89.77	0.01	0.00	98.28

		Upper body				
"DB7UB_1	0.13	10.23	85.09	0.20	0.00	95.64
"DB7UB_12	0.10	8.91	87.76	0.43	0.00	97.20
DB07_UB03_11	0.62	7.94	88.29	0.01	0.01	96.86
DB07_UB03_12	0.51	6.14	89.54	0.02	0.02	96.23
DB07_UB03_13	0.61	5.98	89.88	0.01	0.03	96.52
DB07_UB03_14	0.81	7.21	88.36	0.00	0.00	96.38
DB07_UB03_15	0.65	5.17	90.18	0.00	0.00	96.00
DB07_UB03_16	0.12	8.16	87.77	0.06	0.00	96.11
DB07_UB03_17	0.13	7.29	88.60	0.22	0.00	96.24
DB07_UB03_18	0.18	8.12	88.24	0.29	0.00	96.83
DB07_UB03_19	0.13	7.59	89.57	0.07	0.00	97.35
DB07_UB03_20	0.12	6.79	89.18	0.40	0.00	96.50

Comment	MgO(Mass%)	Fe2O3(Mass%)	Mn3O4	CaO(Mass%)	BaO(Mass%)	Total(Mass%)
		W136				
		LB01 (Lower body)				
"W136LB_1_1 "	0.22	4.43	88.35	0.10	0.00	93.10
"W136LB_1_2 "	0.29	6.38	93.72	0.08	0.00	100.48
"W136LB_1_3 "	0.35	1.67	91.18	0.13	0.01	93.34
"W136LB_1_4 "	0.59	0.65	95.90	0.25	0.00	97.38
"W136LB_1_5 "	0.21	4.69	96.82	0.03	0.00	101.74
"W136LB_1_7 "	0.21	1.16	93.34	0.26	0.00	94.97
		LB04 (Lower body)				
W136_LB04_7	0.10	8.14	90.26	0.09	0.00	98.58
W136_LB04_10	0.07	4.88	92.71	0.10	0.01	97.76
W136_LB04_12	0.16	6.53	90.40	0.11	0.00	97.20
W136_LB04_13	0.13	6.04	90.54	0.28	0.00	96.99
W136_LB04_14	0.09	4.25	93.01	0.47	0.00	97.82
W136_LB04_15	0.08	3.86	92.63	0.47	0.00	97.04
W136_LB04_31	0.09	3.05	93.81	0.25	0.00	97.20
W136_LB04_34	0.05	2.30	95.39	0.01	0.00	97.75
		LB05 (Lower body)				
W136_LB05_7	0.82	0.71	95.76	0.12	0.00	97.42
W136_LB05_8	0.75	0.92	96.24	0.19	0.00	98.10
W136_LB05_9	0.99	0.91	96.52	0.06	0.00	98.47
W136_LB05_10	0.83	0.95	95.72	0.07	0.00	97.57
W136_LB05_11	0.75	0.61	96.29	0.07	0.00	97.72
W136_UB05_12	0.64	0.52	96.71	0.08	0.00	97.95
W136_LB05_12	0.98	0.51	96.53	0.19	0.00	98.21
W136_LB05_13	1.07	0.43	95.96	0.13	0.00	97.59
W136_LB05_14	0.81	0.61	96.77	0.07	0.00	98.27
W136_LB05_15	1.12	0.54	95.14	0.13	0.00	96.93
		UB04 (Upper Body)				

W136_UB04_1	**1.02**	**5.50**	**89.82**	**0.04**	**0.00**	**96.38**
W136_UB04_3	**0.23**	**5.67**	**86.19**	**3.38**	**0.01**	**95.49**
W136_UB04_4	**1.24**	**4.83**	**90.03**	**0.19**	**0.00**	**96.28**
W136_UB04_5	**1.16**	**9.58**	**85.81**	**0.06**	**0.04**	**96.64**
W136_UB04_7	**1.00**	**6.70**	**87.97**	**0.15**	**0.02**	**95.83**
W136_UB04_8	**1.10**	**4.68**	**91.36**	**0.17**	**0.00**	**97.31**
W136_UB04_9	**0.68**	**6.72**	**87.93**	**0.09**	**0.02**	**95.43**
W136_UB04_10	**1.02**	**7.08**	**88.47**	**0.19**	**0.00**	**96.77**
W136_UB05_3	**0.25**	**15.24**	**80.98**	**0.02**	**0.00**	**96.50**
W136_UB05_5	**0.53**	**15.11**	**79.12**	**0.04**	**0.00**	**94.80**
W136_UB05_7	**0.28**	**14.67**	**81.27**	**0.00**	**0.02**	**96.24**
W136_UB05_9	**0.33**	**15.38**	**81.47**	**0.00**	**0.00**	**97.18**
W136_UB05_10	**0.47**	**14.31**	**82.30**	**0.13**	**0.00**	**97.20**
W136_UB04_2	**1.04**	**10.79**	**85.25**	**0.08**	**0.00**	**97.15**
W125_UB04_2	**1.09**	**11.12**	**85.59**	**0.07**	**0.00**	**97.86**

Comment	**MgO(Mass%)**	**Fe2O3(Mass%)**	**Mn3O4**	**CaO(Mass%)**	**BaO(Mass%)**	**Total(Mass%)**
		N95 A				
		T14(Lower Body)				
"T4lb_10 "	**0.22**	**4.03**	**96.01**	**0.16**	**0.00**	**100.41**
"T4lb_11 "	**0.18**	**2.84**	**94.60**	**0.16**	**0.00**	**97.78**
"T4lb_12 "	**0.01**	**2.27**	**94.16**	**0.13**	**0.01**	**96.57**
"T4lb_13 "	**0.21**	**3.25**	**95.13**	**0.88**	**0.01**	**99.47**
"T4lb_15 "	**0.04**	**6.26**	**95.81**	**0.24**	**0.00**	**102.36**
"T4lb_16 "	**0.46**	**6.89**	**92.80**	**0.07**	**0.00**	**100.22**
"T4lb_17 "	**0.06**	**4.41**	**90.94**	**0.15**	**0.00**	**95.56**
T14	**0.29**	**2.10**	**95.14**	**1.16**	**0.02**	**98.71**
T14	**0.27**	**2.40**	**95.38**	**0.26**	**0.00**	**98.32**
T14	**0.26**	**1.51**	**98.43**	**0.17**	**0.00**	**100.37**
T14	**0.09**	**2.94**	**96.89**	**0.12**	**0.00**	**100.04**
		T15				
T15	**0.57**	**5.67**	**93.63**	**0.37**	**0**	**100.24**
T15	**0.32**	**2.02**	**98.18**	**0.44**	**0.01**	**100.97**
T15	**0.29**	**2.11**	**97.89**	**0.48**	**0.03**	**100.80**
T15	**0.27**	**1.96**	**98.15**	**0.51**	**0**	**100.89**
T15	**0.52**	**5.62**	**93.72**	**0.34**	**0**	**100.20**
T15	**0.3**	**2.77**	**96.90**	**0.51**	**0.04**	**100.52**
T15	**0.31**	**5.84**	**94.37**	**0.44**	**0**	**100.96**
T15	**0.26**	**2.27**	**95.62**	**0.58**	**0**	**98.73**
T15	**0.03**	**5.86**	**94.00**	**0.7**	**0**	**100.59**
T15	**0.26**	**2.56**	**96.23**	**0.4**	**0.04**	**99.49**
T15	**0.3**	**2.35**	**97.86**	**0.28**	**0**	**100.78**
T15	**0.09**	**5.16**	**93.43**	**0.74**	**0.04**	**99.46**
T15	**0.23**	**2.53**	**97.43**	**0.42**	**0**	**100.60**
T15	**0.14**	**4.34**	**95.24**	**0.52**	**0**	**100.24**
T15	**0.03**	**8.31**	**91.21**	**0.91**	**0.02**	**100.48**
T15	**0.3**	**2.19**	**98.06**	**0.29**	**0**	**100.84**
T15	**0.06**	**6.04**	**93.44**	**0.76**	**0.03**	**100.33**

T15	**0.01**	**2.28**	**92.86**	**3.5**	**0.01**	**98.66**
T15	**0.26**	**1.62**	**98.47**	**0.45**	**0.04**	**100.84**
T15	**0.53**	**2.64**	**97.27**	**0.35**	**0.01**	**100.79**
T15	**0.06**	**8.39**	**90.40**	**0.78**	**0.13**	**99.75**
T15	**0.06**	**5.80**	**92.31**	**1.6**	**0**	**99.76**

Comment	**MgO(Mass%)**	**Fe2O3(Mass%)**	**Mn3O4**	**CaO(Mass%)**	**BaO(Mass%)**	**Total(Mass%)**
		N92 I				
		GH11				
GH11	**0.11**	**5.13**	**94.08**	**0.04**	**0.00**	**99.36**
GH11	**0.25**	**5.95**	**92.86**	**0.02**	**0.02**	**99.10**
GH11	**0.29**	**5.68**	**92.45**	**0.00**	**0.00**	**98.42**
GH11	**0.16**	**6.71**	**91.94**	**0.17**	**0.00**	**98.98**
GH11	**0.11**	**6.85**	**92.44**	**0.00**	**0.01**	**99.41**
GH11	**0.13**	**7.15**	**91.82**	**0.02**	**0.00**	**99.12**
GH11	**0.17**	**8.28**	**90.87**	**0.03**	**0.00**	**99.34**
GH11	**0.24**	**9.00**	**89.37**	**0.32**	**0.00**	**98.93**
GH11	**0.19**	**9.19**	**91.00**	**0.01**	**0.00**	**100.39**
		GH10				
GH10	**0.98**	**9.96**	**88.51**	**0.05**	**0.00**	**99.50**
GH10	**0.24**	**8.62**	**90.72**	**0.05**	**0.01**	**99.64**
GH10	**0.26**	**8.54**	**92.31**	**0.02**	**0.03**	**101.16**
GH10	**0.24**	**8.06**	**90.95**	**0.02**	**0.00**	**99.28**
GH10	**0.24**	**6.84**	**91.42**	**0.03**	**0.00**	**98.53**
GH10	**0.10**	**6.20**	**92.05**	**0.45**	**0.01**	**98.81**
GH10	**0.10**	**5.21**	**93.81**	**0.04**	**0.00**	**99.16**
Average	**0.31**	**7.63**	**91.40**	**0.09**	**0.01**	**99.44**
		GR8(Lower Body)				
"GH8lb_2 "	**0.09**	**7.20**	**93.22**	**0.00**	**0.00**	**100.52**
"GH8lb_3 "	**0.10**	**7.00**	**92.64**	**0.00**	**0.03**	**99.78**
"GH8lb_4 "	**0.13**	**7.48**	**92.09**	**0.00**	**0.00**	**99.70**
"GH8lb_5 "	**0.20**	**7.94**	**91.65**	**0.09**	**0.00**	**99.88**
"GH8lb_6 "	**0.31**	**0.38**	**98.43**	**0.11**	**0.03**	**99.26**
"GH8lb_7 "	**0.22**	**0.33**	**97.36**	**0.07**	**0.01**	**97.99**
"GH8lb_8 "	**0.25**	**1.59**	**98.48**	**0.08**	**0.00**	**100.40**
"GH8lb_9 "	**0.25**	**0.22**	**97.88**	**0.03**	**0.00**	**98.38**
"GH8lb_10 "	**0.16**	**0.19**	**98.68**	**0.00**	**0.00**	**99.04**
"GH8lb_11 "	**0.12**	**7.45**	**91.62**	**0.09**	**0.00**	**99.29**
"GH8lb_45 "	**0.23**	**6.00**	**93.38**	**0.03**	**0.00**	**99.63**
"GH8lb_49 "	**0.19**	**9.93**	**89.09**	**0.01**	**0.00**	**99.22**
"GH8lb_50 "	**0.23**	**8.46**	**91.54**	**0.03**	**0.00**	**100.26**
"GH8lb_12 "	**0.26**	**8.91**	**91.30**	**0.02**	**0.00**	**100.48**
Average	**0.20**	**5.22**	**94.10**	**0.04**	**0.01**	**99.56**
		GR2(Upper Body)				
"GHup_1 "	**0.10**	**6.05**	**92.19**	**0.03**	**0.00**	**98.37**
"GHup_15 "	**0.20**	**6.65**	**93.23**	**0.08**	**0.00**	**100.17**

"GHup_16 "	0.24	6.49	91.85	0.03	0.00	98.61
"GHup_18 "	0.16	7.93	91.21	0.01	0.00	99.31
"GHup_19 "	0.16	7.69	91.38	0.03	0.00	99.27
"GHup_20 "	0.13	6.31	93.07	0.09	0.00	99.60
"GHup_21 "	0.10	6.53	93.00	0.05	0.00	99.67
"GHup_22 "	0.11	5.69	93.74	0.02	0.09	99.64
"GHup_23 "	0.14	6.20	93.08	0.02	0.00	99.44
"GHup_24 "	0.13	6.44	92.47	0.03	0.03	99.09
"GHup_38 "	0.13	6.11	93.43	0.00	0.00	99.67
"GHup_46 "	0.15	6.88	93.32	0.02	0.00	100.38
"GHup_25 "	0.08	6.60	92.58	0.02	0.00	99.27
graben2_21	0.09	4.42	92.42	0.04	0.00	96.97
graben2_22	0.15	5.08	91.86	0.04	0.00	97.13
graben2_23	0.13	4.50	92.84	0.03	0.02	97.51
graben2_24	0.09	4.47	92.22	0.04	0.01	96.84
graben2_25	0.13	4.60	92.57	0.00	0.00	97.29
graben2_45	0.20	3.21	92.60	0.31	0.00	96.32
graben2_29	0.20	6.55	90.54	0.12	0.00	97.41
graben2_30	0.20	7.84	88.85	0.07	0.02	96.97
		GH3				
GH3	0.29	4.19	93.72	0.36	0.00	98.56
GH3	0.28	5.28	93.32	0.09	0.00	98.97
GH3	0.23	5.75	93.59	0.03	0.02	99.62
GH3	0.13	7.07	92.64	0.02	0.00	99.87
GH3	0.26	3.80	95.45	0.05	0.00	99.56
GH3	0.23	2.93	95.89	0.10	0.00	99.15
GH3	0.08	4.99	94.76	0.04	0.00	99.88
GH3	0.19	1.37	98.09	0.15	0.00	99.80
GH3	0.23	6.40	93.13	0.01	0.00	99.76
GH3	0.24	5.16	93.29	0.01	0.00	98.70
		GH4				
graben4_2	0.90	3.31	93.05	0.02	0.00	97.27
graben4_4	0.10	8.23	89.56	0.00	0.00	97.89
graben4_5	0.03	5.40	93.33	0.00	0.00	98.76
graben4_16	0.35	6.61	91.81	0.04	0.00	98.80
graben4_17	0.15	5.03	92.79	0.01	0.03	98.02
graben4_19	0.21	8.26	90.01	0.01	0.01	98.49
graben4_20	0.13	13.33	83.16	0.02	0.00	96.64

Comment	MgO(Mass%)	Fe2O3(Mass%)	Mn3O4	CaO(Mass%)	BaO(Mass%)	Total(Mass%)
		N94J				
		J28 (lower body)				
J28	0.05	0.31	98.66	0.00	0.01	99.03
J28	0.02	0.44	97.85	0.02	0.00	98.33
J28	0.02	0.56	97.58	0.01	0.00	98.16
J28	0.03	0.38	98.29	0.01	0.01	98.72
J28	0.06	0.44	98.90	0.02	0.01	99.43
J28	0.15	0.61	98.22	0.01	0.00	98.99

J28	**0.01**	**0.48**	**98.34**	**0.03**	**0.00**	**98.86**
J28	**0.02**	**0.36**	**98.20**	**0.00**	**0.02**	**98.60**
J28	**0.02**	**0.40**	**97.61**	**0.00**	**0.00**	**98.03**
J28	**0.03**	**1.56**	**95.58**	**0.02**	**0.04**	**97.23**
J28	**0.03**	**0.53**	**98.14**	**0.02**	**0.00**	**98.72**
J28	**0.02**	**0.73**	**97.94**	**0.02**	**0.02**	**98.74**
J28	**0.03**	**0.33**	**98.74**	**0.00**	**0.00**	**99.10**
J28	**0.04**	**0.69**	**99.00**	**0.01**	**0.02**	**99.76**
J28	**0.05**	**0.57**	**98.34**	**0.00**	**0.00**	**98.96**
J28	**0.01**	**0.66**	**98.67**	**0.02**	**0.01**	**99.37**
J28	**0.05**	**0.67**	**98.90**	**0.03**	**0.02**	**99.67**
J28	**0.02**	**0.60**	**98.46**	**0.00**	**0.00**	**99.08**
		J31 (Lower Body)				
"J31lb_2 "	**0.00**	**0.58**	**97.87**	**0.02**	**0.00**	**98.47**
"J31lb_3 "	**0.02**	**0.31**	**98.63**	**0.02**	**0.00**	**98.98**
"J31lb_4 "	**0.23**	**0.93**	**97.35**	**0.02**	**0.00**	**98.52**
"J31lb_6 "	**0.04**	**0.50**	**97.15**	**0.04**	**0.02**	**97.75**
"J31lb_7 "	**0.01**	**0.38**	**96.75**	**0.03**	**0.01**	**97.18**
"J31lb_8 "	**0.07**	**0.44**	**97.79**	**0.05**	**0.01**	**98.36**
"J31lb_9 "	**0.04**	**0.50**	**95.72**	**0.03**	**0.00**	**96.28**
"J31lb_10 "	**0.01**	**0.35**	**98.13**	**0.03**	**0.00**	**98.52**
"J31lb_20 "	**0.07**	**0.35**	**97.65**	**0.03**	**0.01**	**98.11**
"J31lb_21 "	**0.02**	**0.52**	**98.31**	**0.03**	**0.00**	**98.88**
"J31lb_29 "	**0.04**	**1.41**	**95.99**	**0.26**	**0.00**	**97.69**
"J31lb_30 "	**0.11**	**0.67**	**97.27**	**0.00**	**0.00**	**98.06**
"J31lb_36 "	**0.07**	**1.80**	**97.08**	**0.00**	**0.01**	**98.95**
"J31lb_22 "	**0.02**	**2.21**	**96.44**	**0.00**	**0.00**	**98.67**
		J4(Upper body)				
J4	**0.00**	**0.00**	**100.17**	**0.05**	**0.03**	**100.25**
J4	**0.00**	**0.00**	**101.28**	**0.05**	**0.00**	**101.33**
J4	**0.01**	**0.00**	**100.47**	**0.07**	**0.00**	**100.55**
J4	**0.01**	**0.00**	**99.96**	**0.09**	**0.00**	**100.06**
J4	**0.01**	**0.00**	**100.09**	**0.10**	**0.02**	**100.22**
J4	**0.02**	**0.00**	**99.99**	**0.17**	**0.00**	**100.18**
J4	**0.00**	**0.00**	**100.15**	**0.04**	**0.01**	**100.20**
J4	**0.00**	**0.00**	**99.65**	**0.10**	**0.00**	**99.75**
J4	**0.03**	**0.08**	**100.24**	**0.12**	**0.00**	**100.47**
J4	**0.08**	**0.00**	**99.95**	**0.11**	**0.00**	**100.14**
J4	**0.02**	**0.03**	**99.65**	**0.13**	**0.00**	**99.84**
J4	**0.01**	**0.00**	**99.84**	**0.14**	**0.02**	**100.01**
J4	**0.05**	**1.09**	**98.72**	**0.24**	**0.01**	**100.11**
J4	**0.01**	**0.00**	**100.00**	**0.05**	**0.00**	**100.06**
J4	**0.01**	**0.60**	**98.38**	**0.48**	**0.02**	**99.49**
J4	**0.00**	**0.02**	**99.43**	**0.56**	**0.00**	**100.01**
J4	**0.02**	**0.23**	**98.78**	**0.12**	**0.00**	**99.16**
J4	**0.08**	**0.27**	**98.14**	**0.03**	**0.00**	**98.51**
J4	**0.00**	**0.00**	**100.32**	**0.07**	**0.01**	**100.40**
J4	**0.01**	**0.00**	**99.60**	**0.09**	**0.00**	**99.70**
J4	**0.04**	**0.22**	**98.79**	**0.23**	**0.00**	**99.29**
J4	**0.01**	**0.00**	**99.28**	**0.14**	**0.00**	**99.43**
		J7(Upper Body)				

"J7up_22 "	0.05	1.81	96.50	0.05	0.00	98.40
"J7up_24 "	0.02	1.76	96.59	0.03	0.00	98.40
"J7up_25 "	0.04	1.52	96.81	0.01	0.00	98.38
"J7up_27 "	0.03	1.35	96.76	0.02	0.00	98.16
"J7up_28 "	0.04	1.10	96.80	0.02	0.00	97.95
"J7up_29 "	0.06	1.75	96.51	0.03	0.00	98.35
"J7up_33 "	0.00	0.80	97.39	0.00	0.01	98.20
"J7up_34 "	0.04	1.36	96.44	0.00	0.00	97.84
"J7up_35 "	0.02	1.47	97.15	0.01	0.00	98.66
"J7up_40 "	0.03	1.92	95.50	0.01	0.00	97.45
"J7up_65 "	0.00	0.31	97.31	0.01	0.00	97.63
"J7up_66 "	0.00	0.26	99.19	0.04	0.04	99.53
"J7up_67 "	0.00	0.71	98.96	0.04	0.00	99.71
"J7up_71 "	0.01	0.65	99.04	0.04	0.00	99.74
"J7up_72 "	0.00	0.26	99.02	0.04	0.01	99.33
"J7up_73 "	0.01	0.28	98.72	0.00	0.00	99.00
"J7up_74 "	0.00	0.28	98.39	0.01	0.00	98.68
"J7up_75 "	0.00	0.47	98.36	0.03	0.00	98.86
"J7up_77 "	0.10	0.21	98.45	0.06	0.02	98.85
J7	0.03	1.03	96.60	0.01	0.02	97.69
J7	0.05	1.71	96.47	0.03	0.00	98.26
J7	0.01	0.30	99.25	0.00	0.02	99.59
J7	0.01	0.00	98.02	0.02	0.00	98.05
J7	0.00	0.00	98.57	0.01	0.00	98.58
J7	0.00	0.00	98.04	0.03	0.01	98.08
J7	0.03	0.07	97.42	0.02	0.02	97.55
J7	0.00	0.00	98.61	0.01	0.05	98.67
J7	0.12	0.09	98.01	0.04	0.00	98.26
J7	0.00	0.00	98.96	0.00	0.00	98.96
J7	0.02	0.08	98.69	0.00	0.00	98.78
J7	0.04	0.88	98.75	0.05	0.00	99.72
J7	0.01	1.77	96.85	0.00	0.01	98.64

Comment	MgO(Mass%)	Fe2O3(Mass%)	Mn3O4	CaO(Mass%)	BaO(Mass%)	Total(Mass%)
		GL57				
		D10(Lower Body)				
"D10_13 "	0.26	1.27	96.25	0.20	0.00	97.98
"D10_15 "	0.57	0.54	97.25	0.55	0.04	98.95
D10	0.01	0.22	97.05	0.94	0.00	98.22
D10	0.21	0.22	97.80	0.74	0.00	98.98
D10	0.02	0.00	98.76	0.68	0.00	99.46
D10	0.01	0.00	98.39	0.23	0.01	98.64
D10	0.02	0.00	98.17	0.20	0.01	98.40
D10	0.01	0.00	99.10	0.13	0.08	99.32
D10	0.10	0.02	95.23	1.12	0.05	96.53
D10	0.00	0.12	99.30	0.15	0.00	99.57
		Upper body				
"Mn17_17 "	0.58	2.18	95.88	0.02	0.00	98.65
"Mn17_19 "	1.22	2.00	95.56	0.01	0.00	98.79

"Mn17_32 "	0.67	2.61	94.57	0.04	0.00	97.89
Mn17	0.66	2.11	97.16	0.36	0.00	100.29
Mn17	1.35	2.34	95.95	0.29	0.05	99.98
Mn17	0.83	2.08	96.16	0.25	0.00	99.32
Mn17	0.70	1.62	97.18	0.23	0.01	99.74
Mn17	0.81	2.38	94.72	1.19	0.02	99.12
Mn17	1.11	2.74	94.47	1.21	0.02	99.55
Mn17	1.51	1.69	96.02	0.52	0.00	99.74
Mn17	0.74	0.93	99.07	0.07	0.03	100.85
Mn17	0.81	2.20	97.37	0.11	0.04	100.54
Mn17	1.02	2.09	96.86	0.33	0.00	100.30
Mn17	1.51	2.70	95.72	0.31	0.00	100.24
Mn17	0.76	2.79	96.74	0.07	0.03	100.39
Mn17	0.54	2.61	96.45	0.38	0.01	99.99
		Mn18				
Mn18	0.29	2.66	94.40	0.48	0.00	97.82
Mn18	0.33	1.27	97.86	0.45	0.04	99.95
Mn18	0.28	2.77	95.76	0.42	0.00	99.23
Mn18	0.29	3.43	95.06	0.53	0.00	99.31
Mn18	0.52	2.80	96.09	0.12	0.00	99.54

Comment	MgO	Fe2O3	Mn3O4	CaO	BaO	Total
		N95 E				
		S7 (lower body)				
S7	0.28	4.46	93.15	0.06	0.01	97.96
S7	0.30	3.95	92.68	0.01	0.00	96.93
S7	0.16	4.58	92.12	0.06	0.00	96.92
		s8(Lower ore)				
S 8	0.16	3.20	91.58	2.15	0.00	97.08
S8	0.08	4.76	91.35	0.60	0.00	96.79
S8	0.07	7.40	89.64	0.51	0.00	97.62
S8	0.14	4.35	90.60	1.35	0.00	96.44
"S8_3 "	0.13	4.72	89.24	0.93	0.00	95.01
"S8_4 "	0.09	5.00	89.57	0.57	0.00	95.22
"S8_5 "	0.06	1.92	92.18	0.50	0.00	94.66
"S8_10 "	0.07	2.38	92.83	0.52	0.02	95.82
"S8_11 "	0.09	2.76	91.95	1.29	0.01	96.10
"S8_12 "	0.17	3.73	88.31	3.06	0.00	95.27
"S8_13 "	0.08	5.25	84.29	0.50	0.02	90.13
"S8_1 "	0.07	3.04	90.67	0.66	0.02	94.46
S9	0.01	19.50	76.22	0.03	0.04	95.79
S9	0.05	18.55	77.71	0.00	0.01	96.32
S9	0.01	15.65	80.27	0.03	0.03	95.99
S9	0.01	17.17	78.55	0.03	0.03	95.79
S9	0.05	17.33	77.94	0.35	0.00	95.67
S9	0.02	18.30	77.28	0.15	0.00	95.75
S9	0.09	12.54	79.33	2.05	0.00	94.01
S9	0.10	10.83	80.81	2.10	0.00	93.84
S9	0.09	11.77	81.07	1.43	0.04	94.40
S9	0.01	19.87	76.16	0.06	0.00	96.10
S9	0.04	18.02	78.02	0.04	0.00	96.12
S9	0.01	18.42	77.51	0.05	0.02	96.01
S9	0.00	18.65	77.75	0.05	0.01	96.47

S9	**0.02**	**18.43**	**77.67**	**0.07**	**0.00**	**96.19**
		Upper body				
"S2_29 "	**0.01**	**4.48**	**90.90**	**0.10**	**0.00**	**95.48**
"S2_42 "	**0.08**	**6.72**	**92.02**	**0.51**	**0.00**	**99.33**
"S2_43 "	**0.09**	**3.15**	**91.82**	**0.48**	**0.07**	**95.61**
"S2_44 "	**0.06**	**2.63**	**89.66**	**0.69**	**0.00**	**93.04**
"S2_45 "	**0.07**	**3.66**	**89.40**	**0.56**	**0.00**	**93.70**
"S2_41 "	**0.13**	**3.06**	**90.96**	**1.38**	**0.00**	**95.53**
"S2_30 "	**0.06**	**5.27**	**86.76**	**0.12**	**0.03**	**92.24**
"S2_31 "	**0.04**	**10.81**	**85.23**	**0.67**	**0.02**	**96.76**
"S2_32 "	**0.02**	**9.01**	**86.62**	**1.37**	**0.00**	**97.02**
"S2_33 "	**0.00**	**11.34**	**83.46**	**1.54**	**0.04**	**96.37**
S1	**0.02**	**6.15**	**92.65**	**0.05**	**0.05**	**98.92**
S1	**0.02**	**4.91**	**93.83**	**0.07**	**0.03**	**98.85**
S1	**0.02**	**6.36**	**92.85**	**0.05**	**0.10**	**99.38**
S1	**0.01**	**3.92**	**95.50**	**0.14**	**0.09**	**99.66**
S1	**0.02**	**6.71**	**92.33**	**0.07**	**0.05**	**99.18**

4. *EPMA data for braunite*

Comment	SiO2	Fe2O3	Mn2O3	CaO	Total
		N92 I			
		Lower body			
GH10	2.94	18.43	71.96	2.94	96.47
GH10	4.29	16.93	73.20	4.06	98.62
GH10	3.87	15.56	74.96	3.80	98.39
GH10	2.79	14.44	77.02	3.21	97.81
GH10	3.35	11.15	79.49	3.62	97.87
GH10	3.29	8.88	81.59	3.73	97.83
		Upper body			
graben2_34	4.19	11.40	76.39	4.74	97.01
graben2_35	4.57	10.79	75.90	4.81	96.23
graben2_11	5.25	10.26	75.42	5.38	96.40
graben2_12	4.58	10.24	77.04	4.70	96.67
graben2_13	4.40	10.70	77.47	4.64	97.40
graben2_14	4.55	10.40	77.42	4.77	97.25
graben2_15	4.52	10.41	76.93	4.80	96.79
graben2_16	4.51	11.06	77.15	4.75	97.56
graben2_17	4.38	11.15	75.65	4.78	96.18
graben2_18	2.80	10.89	79.10	3.76	97.19
graben2_19	3.55	10.52	77.84	4.41	96.46
graben2_20	4.03	11.83	76.19	4.58	96.99
"GHup_7 "	4.08	13.72	78.16	4.78	101.03
"GHup_8 "	4.48	16.33	74.81	4.83	100.56
"GHup_9 "	4.31	12.68	79.39	4.76	101.29
"GHup_10 "	4.19	12.96	77.84	4.82	99.92
"GHup_11 "	4.45	13.39	77.06	4.88	99.92
"GHup_12 "	4.28	13.11	77.67	4.83	100.10
"GHup_13 "	4.41	10.83	80.11	4.92	100.38
"GHup_14 "	4.37	13.98	77.78	4.80	101.12
"GHup_39 "	4.14	13.88	76.29	4.78	99.31
"GHup_40 "	4.08	14.50	75.85	4.77	99.47
"GHup_41 "	4.20	13.20	77.61	4.89	100.08
"GHup_42 "	4.29	12.63	78.39	4.90	100.28

Comment	SiO2	Fe2O3	Mn2O3	CaO	Total
		DK21			
		Lower body			
		L6			
L6_1	2.43	14.69	74.22	3.41	95.44
L6_2	2.65	10.07	79.96	3.61	96.85
L6_3	2.36	11.49	78.58	3.45	96.48
L6_4	2.34	10.33	79.55	3.41	96.03

L6_5	**2.71**	**11.30**	**78.53**	**3.58**	**96.45**
L6_23	**2.42**	**5.68**	**70.33**	**10.11**	**95.78**
L5_56	**2.41**	**8.75**	**82.48**	**3.37**	**97.28**
L5_57	**2.75**	**6.91**	**81.84**	**3.31**	**94.98**
L5_61	**2.97**	**8.88**	**80.91**	**3.89**	**96.78**
L5_62	**2.73**	**8.73**	**81.01**	**3.84**	**96.51**
L5_63	**2.50**	**9.08**	**80.86**	**3.66**	**96.60**
"L4_1 "	**4.86**	**17.06**	**72.15**	**4.83**	**99.12**
"L4_2 "	**5.04**	**16.31**	**72.50**	**5.06**	**99.11**
"L4_3 "	**5.82**	**13.61**	**72.85**	**5.89**	**98.62**
"L4_4 "	**4.75**	**14.46**	**74.85**	**4.65**	**98.89**
"L4_5 "	**4.67**	**18.11**	**71.96**	**4.70**	**99.69**
"L4_6 "	**6.28**	**13.46**	**73.08**	**6.12**	**99.06**
"L4_7 "	**4.74**	**17.50**	**72.42**	**4.62**	**99.54**
"L4_9 "	**6.05**	**11.26**	**74.84**	**5.61**	**98.12**
		Upper body			
L20_11	**4.67**	**13.59**	**74.80**	**4.52**	**97.70**
L20_12	**5.21**	**12.17**	**74.77**	**5.05**	**97.43**
L20_14	**4.77**	**14.11**	**73.49**	**4.67**	**97.15**
L20_15	**4.75**	**14.04**	**73.89**	**4.70**	**97.55**
L20_16	**4.73**	**14.05**	**73.37**	**4.70**	**97.33**
L20_17	**4.97**	**13.60**	**75.86**	**2.90**	**97.40**
L20_18	**4.71**	**12.16**	**74.72**	**4.47**	**96.16**
L20_19	**4.74**	**13.51**	**74.43**	**4.76**	**97.54**
L20_20	**4.77**	**12.50**	**76.14**	**3.89**	**97.36**
"L20_27 "	**4.46**	**13.42**	**77.39**	**4.57**	**99.90**
"L20_28 "	**4.49**	**16.78**	**73.79**	**4.54**	**99.69**
"L20_29 "	**4.55**	**16.75**	**74.13**	**4.57**	**100.17**
"L20_30 "	**4.50**	**16.04**	**75.79**	**4.61**	**101.05**
"L20_31 "	**4.47**	**15.20**	**77.25**	**4.58**	**101.58**
"L20_32 "	**4.40**	**14.70**	**76.46**	**4.60**	**100.24**
"L20_33 "	**4.48**	**15.85**	**74.89**	**4.64**	**99.92**
"L22_1 "	**8.88**	**4.21**	**85.15**	**0.55**	**98.91**
"L22_1 "	**9.01**	**4.64**	**84.46**	**0.74**	**99.00**
"L22_1 "	**9.05**	**4.25**	**84.66**	**0.77**	**98.84**
"L22_1 "	**9.12**	**4.45**	**83.19**	**0.86**	**97.76**
"L22_1 "	**9.02**	**4.95**	**81.95**	**0.79**	**96.86**
"L22	**9.27**	**4.47**	**84.88**	**0.69**	**99.44**
"L22_1	**9.15**	**4.37**	**83.13**	**0.74**	**97.53**
"L22_1	**9.33**	**4.56**	**84.61**	**0.70**	**99.34**
"L22_2	**9.41**	**4.22**	**84.82**	**1.11**	**99.65**
"L22_3	**9.10**	**3.84**	**85.31**	**0.65**	**98.99**
"L22_4	**8.92**	**4.08**	**84.46**	**0.50**	**98.11**
"L22_5	**9.07**	**4.26**	**85.58**	**0.58**	**99.63**
"L22_19	**9.22**	**4.46**	**84.22**	**1.05**	**99.08**
"L22_20	**9.05**	**4.62**	**84.29**	**0.65**	**98.80**
"L22_22	**9.18**	**4.17**	**85.91**	**0.26**	**99.99**
L23_26	**9.15**	**3.97**	**84.96**	**0.97**	**99.22**
L23_27	**9.10**	**3.94**	**84.82**	**0.95**	**98.97**
L23_29	**9.20**	**3.84**	**82.51**	**1.11**	**96.79**
L23_30	**8.41**	**5.96**	**82.32**	**1.37**	**98.21**

L23_31	9.24	4.31	83.13	0.90	97.70
L23_32	9.32	4.08	82.72	1.14	97.37
L23_33	9.34	3.97	83.17	0.84	97.56
L23_34	9.17	4.10	83.74	0.79	98.02

Comment	SiO2	Fe2O3	Mn2O3	CaO	Total
		DB50			
		Lower body			
B5_1	9.52	0.61	84.01	1.45	96.46
B5_2	9.25	3.63	81.69	0.98	95.76
B5_3	9.14	3.35	81.90	0.80	95.36
B5_5	9.39	2.64	81.94	1.13	95.35
B5_6	9.37	0.98	83.32	1.18	95.38
B5_8	9.33	3.80	81.34	0.87	95.74
"B6_4 "	9.59	4.21	80.68	0.78	95.52
"DB50A_1	9.54	5.49	81.80	1.11	98.19
"DB50A_2	9.62	5.36	82.88	1.07	99.26
"DB50A_3	9.57	4.66	83.06	1.37	100.16
"DB50A_4	9.37	5.83	82.63	0.77	98.78
"DB50A_5	9.43	5.25	82.88	0.96	98.80
"DB50A_6	9.34	7.74	79.38	0.95	97.72
"DB50A_7	9.55	5.81	82.54	0.96	99.04
		Upper body			
"B20_2 "	4.73	14.33	74.00	4.43	97.78
"B20_3 "	4.77	11.16	77.29	4.37	97.78
"B20_4 "	4.76	14.26	73.93	4.43	97.63
"B20_5 "	4.78	14.48	73.81	4.45	97.60
"DB50A_16	4.73	15.54	74.81	4.33	99.65
"DB50A_17	4.72	14.93	75.33	4.46	99.68
"DB50A_18	4.75	17.03	72.82	4.48	99.23
"DB50A_19	4.78	19.50	72.23	4.04	100.64
"DB50A_20	4.75	18.14	71.89	4.20	99.13
"DB50A_21	4.67	19.73	69.16	4.04	97.77
"DB50A_22	4.72	19.94	68.28	3.91	96.96
"DB50A_23	4.51	16.54	72.41	3.96	98.00

Comment	SiO2	Fe2O3	Mn2O3	CaO	Total
		GL57			
		Upper body			
Mn18	7.33	1.77	87.34	1.36	97.91
Mn18	7.58	2.67	85.98	1.37	97.70
Mn18	7.23	2.59	86.43	0.98	97.36
Mn18	6.78	2.19	86.45	1.04	96.51

Comment	SiO2	Fe2O3	Mn2O3	CaO	Total
		N95 E			
		Upper body			
S1	10.01	3.44	76.10	7.88	97.71
S1	10.97	4.89	74.37	7.26	97.79
S1	10.94	4.89	73.45	7.47	97.20

S1	**11.39**	**5.92**	**75.68**	**4.86**	**98.04**
S1	**11.49**	**5.94**	**73.55**	**5.51**	**96.67**
S1	**11.20**	**5.46**	**76.16**	**4.49**	**97.78**
S1	**11.14**	**2.68**	**77.87**	**5.04**	**97.21**
S1	**11.20**	**3.07**	**78.02**	**4.95**	**97.74**
S1	**10.82**	**5.97**	**74.81**	**5.56**	**97.4**
S1	**10.78**	**5.45**	**76.35**	**4.56**	**97.53**

Comment	SiO2	Fe2O3	Mn2O3	CaO	Total
			DB38		
			LB01(Lower Body)		
"DB38_LB_1 "	4.79	16.71	73.96	4.79	100.46
"DB38_LB_2 "	4.74	18.73	72.07	4.75	100.52
"DB38_LB_3 "	4.67	17.90	72.43	4.68	99.94
"DB38_LB_4 "	4.73	14.89	75.89	4.67	100.31
"DB38_LB_5 "	4.72	17.92	72.91	4.70	100.52
"DB38_LB_6 "	4.83	18.76	72.31	4.64	100.78
"DB38_LB_7 "	4.73	15.83	75.84	4.73	101.27
"DB38_LB_8 "	4.76	18.37	72.22	4.71	100.32
"DB38_LB_9 "	4.71	18.26	71.92	4.75	99.99
"DB38_LB_12 "	4.67	17.59	73.59	4.72	100.75
			UB01(Upper Body)		
"DB38_20 "	4.62	16.36	74.58	4.80	101.15
"DB38_21 "	4.75	16.86	74.94	4.77	101.47
"DB38_22 "	4.92	13.04	77.48	4.78	100.44
"DB38_23 "	4.63	17.07	74.92	4.70	101.96
"DB38_26 "	4.73	16.41	74.25	4.79	100.78
"DB38_31 "	4.84	17.18	74.07	4.65	100.86
"DB38_32 "	4.84	17.16	74.25	4.69	101.09
"DB38_34 "	4.76	16.53	74.94	4.67	101.07
"DB38_35 "	4.80	13.99	77.15	4.67	100.70
			Lower Body(LB03)		
"DB38LB_2_1 "	4.74	17.32	71.45	4.71	98.30
"DB38LB_2_2 "	4.70	17.34	73.14	4.58	99.88
"DB38LB_2_3 "	4.75	17.08	71.81	4.71	98.54
"DB38LB_2_4 "	4.63	17.15	71.39	4.63	97.88
"DB38LB_2_5 "	4.78	17.33	71.70	4.69	98.59
"db38LB03_1 "	4.72	17.19	70.78	4.51	97.36
"db38LB03_1 "	4.75	16.42	71.64	4.67	97.57
"db38LB03_1 "	4.73	14.94	73.35	4.66	97.74
"db38LB03_1 "	4.74	17.61	70.25	4.63	97.41
"db38LB03_1 "	4.69	17.35	71.16	4.60	97.92

			Upper Body		
"DB38UB_2_7 "	4.41	14.94	74.89	4.06	99.16
"DB38UB_2_8 "	4.70	19.15	70.06	4.55	98.70
"DB38UB_2_9 "	4.30	18.10	72.88	3.89	99.67
"DB38UB_2_11 "	3.89	16.46	73.37	3.72	98.06
"DB38UB_2_13 "	4.62	17.48	72.83	4.31	99.82
"db38UB_1 "	4.67	13.93	73.53	3.94	96.61
"db38UB_1 "	4.61	10.88	78.46	3.48	98.47
"db38UB_1 "	4.63	9.18	78.49	3.16	97.59
			Lower Body (LB03)		
"DB38LB_3_1 "	4.84	17.79	72.28	4.74	99.87
"DB38LB_3_1 "	4.77	18.10	72.11	4.73	99.92
"DB38LB_3_2 "	4.26	11.46	77.86	4.59	98.63
"DB38LB_3_3 "	3.52	10.31	80.48	3.94	98.54
"DB38LB_3_4 "	4.44	10.71	78.38	4.74	98.66
"DB38LB_3_6 "	4.22	12.17	76.74	4.60	98.54
"DB38LB_3_7 "	4.30	12.46	75.74	4.68	97.78
"DB38LB_3_8 "	4.73	16.04	73.45	4.72	99.09
"DB38LB_3_9 "	4.66	16.58	73.28	4.64	99.31
"DB38LB_3_10 "	4.21	10.41	79.40	4.62	98.91
"DB38LB_3_11 "	3.96	10.57	77.98	4.43	97.41
"DB38LB_3_12 "	4.68	10.17	78.32	4.62	98.01
"DB38LB_3_25 "	4.63	19.31	68.38	4.60	97.16
"DB38LB_3_29 "	4.20	12.00	77.75	4.64	99.14
			UB03		
"DB38UB_3_3 "	4.57	14.90	73.03	4.61	97.32
"DB38UB_3_5 "	4.81	13.67	74.81	4.77	98.24
"DB38UB_3_6 "	4.59	17.41	71.20	4.46	97.93
"DB38UB_3_7 "	4.55	17.70	71.55	4.46	98.48
"DB38UB_3_8 "	4.69	16.60	72.41	4.66	98.84
"DB38UB_3_9 "	4.66	13.67	74.54	4.71	97.76
"DB38UB_3_10 "	4.57	17.39	73.32	4.42	99.91
"DB38UB_3_28 "	4.32	14.60	74.67	4.14	98.68

Comment	SiO2	Fe2O3	Mn2O3	CaO	Total
		N95 A			
		Upper body			
T5	9.16	4.62	78.98	5.16	98.86
T5	9.14	4.23	79.64	4.99	98.93
T5	9.05	4.35	79.42	5.05	98.87
T5	9.11	4.16	79.67	5.21	99.01
T5	9.20	5.29	78.20	5.67	98.95
T5	8.90	4.43	78.84	5.16	98.10

T5		**8.41**	**4.42**	**79.65**	**5.04**	**98.44**
T5		**8.36**	**4.40**	**79.16**	**5.09**	**97.96**
T5		**8.35**	**5.78**	**77.20**	**5.60**	**97.32**
T5		**7.98**	**4.82**	**78.59**	**5.30**	**97.22**
T5		**9.25**	**6.92**	**77.54**	**5.36**	**99.59**
T5		**9.00**	**5.55**	**77.77**	**4.93**	**97.96**
T5		**9.30**	**5.44**	**77.79**	**5.85**	**98.79**
T5		**9.25**	**5.80**	**77.94**	**5.22**	**99.02**
T5		**9.23**	**5.95**	**78.22**	**5.25**	**99.32**
T5		**9.14**	**4.74**	**79.30**	**5.24**	**99.22**
T5		**8.48**	**8.12**	**76.11**	**4.85**	**98.25**
T5		**8.72**	**6.01**	**77.82**	**5.20**	**98.43**
T5		**10.41**	**3.80**	**76.84**	**4.53**	**98.86**
T5		**9.82**	**3.66**	**79.55**	**4.74**	**99.23**
T5		**10.11**	**3.64**	**78.10**	**4.67**	**99.33**
T5		**9.13**	**5.03**	**79.38**	**4.99**	**99.38**
T4		**10.69**	**8.89**	**71.39**	**5.39**	**96.45**
T4		**10.80**	**7.14**	**73.33**	**5.10**	**96.51**
T4		**10.91**	**8.14**	**71.83**	**5.41**	**96.43**
T4		**11.77**	**6.38**	**72.84**	**5.93**	**97.13**
T4		**10.75**	**6.26**	**72.65**	**6.56**	**96.36**
T4		**11.76**	**5.90**	**68.45**	**5.73**	**91.95**
"T4up_2	**"**	**9.19**	**7.23**	**72.70**	**6.79**	**96.16**
"T4up_3	**"**	**8.85**	**7.92**	**74.22**	**6.89**	**98.11**
"T4up_3	**"**	**8.90**	**7.71**	**74.60**	**6.86**	**98.23**
"T4up_2	**"**	**9.13**	**7.83**	**72.65**	**6.85**	**96.68**
"T4up_2b	**"**	**9.54**	**7.53**	**73.06**	**6.86**	**97.24**
"T4up_2b	**"**	**9.57**	**7.75**	**73.35**	**6.96**	**97.89**
"T4up_2b	**"**	**9.48**	**7.73**	**73.89**	**7.20**	**98.85**
"T4up_2b	**"**	**8.99**	**7.21**	**75.11**	**7.36**	**98.83**
"T4up_2b	**"**	**9.54**	**7.54**	**73.37**	**6.83**	**97.49**
"T4up_4	**"**	**8.56**	**6.65**	**74.66**	**6.84**	**96.91**
"T4up_5	**"**	**8.55**	**5.15**	**74.65**	**6.85**	**95.66**
"T4up_6	**"**	**8.72**	**7.29**	**73.06**	**6.86**	**96.15**
"T4up_7	**"**	**9.36**	**7.43**	**74.16**	**6.89**	**98.04**
"T4up_10	**"**	**9.72**	**6.46**	**73.95**	**7.01**	**97.30**
			Lower body			
T14		**10.14**	**0.46**	**85.14**	**2.79**	**98.98**
T14		**10.00**	**0.38**	**84.72**	**2.98**	**98.72**
T14		**10.28**	**0.20**	**85.15**	**2.98**	**99.21**
T14		**10.17**	**0.04**	**84.92**	**3.02**	**98.75**
T14		**9.99**	**0.21**	**85.74**	**2.47**	**99.01**
"T4lb_1	**"**	**9.14**	**4.14**	**81.27**	**3.23**	**98.26**
"T4lb_2	**"**	**9.40**	**1.15**	**83.02**	**3.79**	**97.75**
"T4lb_3	**"**	**9.12**	**2.41**	**82.83**	**3.33**	**98.12**
"T4lb_4	**"**	**8.83**	**3.77**	**81.48**	**3.16**	**97.73**
"T4lb_5	**"**	**8.95**	**3.63**	**81.52**	**3.30**	**97.85**
"T4lb_7	**"**	**8.88**	**3.82**	**82.27**	**3.19**	**98.57**
"T4lb_8	**"**	**9.06**	**0.86**	**83.12**	**3.68**	**97.16**
"T4lb_9	**"**	**9.11**	**0.85**	**83.27**	**3.62**	**97.28**

Comment	SiO2	Fe2O3	Mn2O3	CaO	Total
		W162			
		Lower Body (LB06)			
"W162_3_2 "	9.50	5.88	81.00	1.01	97.66
"W162_3_3 "	9.51	5.27	80.22	1.64	96.87
"W162_3_4 "	9.29	4.85	81.43	1.15	97.05
"W162_3_5 "	9.50	5.48	80.65	1.08	96.94
"W162LB06_1 "	9.17	5.69	76.21	3.33	95.65
"W162LB06_1 "	9.49	6.63	78.64	1.18	96.13
"W162LB06_1 "	9.54	6.71	78.50	1.21	96.12
"W162LB06_1 "	9.75	7.06	78.89	1.22	97.14
"W162LB06_1 "	9.72	6.11	78.17	2.34	96.61
"W162LB06_1 "	9.25	4.56	79.54	2.36	96.65
		Lower Body (LB05)			
"W162LB_4_6 "	9.69	7.32	78.22	1.11	96.78
"W162LB_4_7 "	9.13	8.40	77.08	1.01	95.95
"W162LB_4_11 "	9.47	8.90	77.43	1.01	97.11
"W162LB_4_12 "	9.65	7.17	78.35	0.97	96.62
		Upper Body			
"W162UB_4_11 "	8.86	6.81	78.56	3.71	98.07
"W162UB_4_12 "	9.44	5.94	78.61	3.25	97.49
"W162UB_4_13 "	9.42	5.09	80.57	3.34	98.63
"W162UB_4_14 "	9.39	5.18	79.64	3.39	97.80
"W162UB_4_15 "	9.23	6.57	77.73	3.55	97.30
"W162UB_4_16 "	9.59	8.25	77.31	3.37	98.79
"W162UB_4_17 "	9.74	4.67	74.14	5.04	94.29
"W162UB_4_18 "	9.85	5.81	75.21	4.76	95.82
"W162UB_4_19 "	10.96	6.36	74.16	6.02	97.78
		LB04(Lower Body)			
"W162LB04_1 "	8.91	1.99	86.45	1.08	98.83
"W162LB04_3 "	8.82	2.65	86.45	1.25	99.53
"W162LB04_4 "	8.82	2.22	86.48	1.19	99.47
"W162LB04_6 "	8.96	2.03	87.05	1.20	99.74
"W162LB04_7 "	8.77	2.41	86.73	1.13	99.33
"W162LB04_8 "	9.76	2.08	84.43	0.97	99.02
"W162LB04_10 "	8.86	2.05	86.19	1.19	99.01
"W162LB04_12 "	8.55	0.68	88.92	1.12	99.73
"W162LB04_13 "	7.78	2.84	82.88	1.14	96.10
"W162LB04_16 "	8.80	1.41	86.86	1.40	99.14
"W162LB04_18 "	8.14	1.47	87.32	1.31	98.75
"W162LB04_19 "	8.77	0.75	89.44	1.11	100.59
		UB04(Upper Body)			
"W162UB04_34 "	0.12	3.04	99.20	0.01	102.40
"W162UB04_35 "	0.19	2.52	100.67	0.02	103.40
"W162UB04_36 "	0.12	3.24	98.95	0.02	102.35
"W162UB04_37 "	0.14	4.10	98.20	0.00	102.48
"W162UB04_38 "	0.19	3.91	98.49	0.00	102.62
"W162UB04_39 "	0.04	3.40	97.92	0.06	101.63
"W162UB04_40 "	1.86	5.64	94.04	0.35	102.08
"W162UB04_41 "	0.05	3.06	98.77	0.01	102.10
"W162UB04_43 "	0.02	2.62	99.69	0.04	102.60
"W162UB04_44 "	0.04	0.93	100.26	0.06	101.58
"W162UB04_45 "	0.02	1.35	101.14	0.10	102.88

"W162UB04_46	"	0.04	7.50	90.37	0.03	98.09
"W162UB04_47	"	0.05	7.64	96.32	0.06	104.32
"W162UB04_48	"	0.05	3.42	98.60	0.03	102.29
"W162UB04_49	"	0.04	2.71	98.84	0.03	101.85
			LB03(Lower Body)			
"W162LB03_10	"	8.38	5.80	79.82	2.54	96.98
"W162LB03_11	"	8.38	6.50	78.82	2.84	97.03
"W162LB03_12	"	8.31	5.57	79.54	2.97	96.91
"W162LB03_13	"	8.32	5.68	79.60	2.89	97.03
"W162LB03_14	"	8.29	5.87	79.77	2.71	97.17
"W162LB03_17	"	8.17	7.49	79.32	2.47	98.00
"W162LB03_11	"	8.54	5.70	80.55	2.78	98.01
			UB03(Upper Body)			
"W162UB03_21	"	9.05	6.93	81.71	1.46	99.81
"W162UB03_23	"	9.07	5.18	82.25	1.54	98.25
"W162UB03_25	"	8.53	4.74	83.65	1.58	98.83
"W162UB03_26	"	8.99	4.61	83.54	1.46	98.94
"W162UB03_27	"	8.93	4.45	82.86	1.78	98.29
"W162UB03_29	"	8.85	6.04	81.98	1.55	98.70
"W162UB03_30	"	8.99	5.48	82.83	1.42	99.08
"W162UB03_31	"	9.45	6.48	82.02	1.04	99.33
"W162UB03_32	"	8.98	5.81	83.67	1.24	99.89
"W162UB03_34	"	9.01	4.81	83.42	1.39	98.88
"W162UB03_35	"	8.89	4.56	83.76	1.17	98.62
"W162UB03_36	"	9.05	4.58	83.03	1.76	98.66
"W162UB03_38	"	9.03	4.95	83.89	1.35	99.41
"W162UB03_39	"	9.25	5.60	82.08	1.33	98.65

Comment		SiO2	Fe2O3	Mn2O3	CaO	Total
				N 94 J		
				J31 (Lower Body)		
"J31lb_23	"	8.80	6.47	82.78	0.65	98.91
"J31lb_24	"	8.74	6.52	79.61	0.56	95.69
"J31lb_25	"	8.55	5.83	79.87	0.45	94.92
"J31lb_26	"	9.13	5.71	79.99	0.50	95.67